TIME-TEMPERATURE RESPONSE OF MULTI-PHASE VISCOELASTIC SOLIDS THROUGH NUMERICAL ANALYSIS

Thesis by
Lynda Catherine Brinson

In Partial Fulfillment of the Requirements for the Degree of Doctor of Philosophy

California Institute of Technology
Pasadena, California

1990
(submitted February 2, 1990)

to my parents, my first and best teachers, and to Warren, my inspiration

ACKNOWLEDGMENTS

There are, of course, not nearly enough words or paper to properly thank all of those who have helped along my way through graduate school and during the writing of this thesis. I am perhaps the most indebted to my advisor, Prof. Wolfgang Knauss, who has continually helped to guide me through the various stages of my research. He has imparted to me a great deal of his knowledge of the field, and more importantly, helped me to define a framework within which new problems can be conceived, motivated, evaluated, and solved. I would like to thank him for his support and encouragement during all the stages of my work: the slow as well as the productive times. Prof. Ravichandran was also a source of inspiration and understanding for me; many times he patiently discussed the ins and outs of finite elements and the FEAP program with me. Prof. Brian Moran, during his stay at Caltech as a postdoc, helped greatly in the special modifications I needed for FEAP. I am grateful to Prof. Ben Freund for his aid in the shear modulus section. Prof. N. W. Tschoegl must be thanked for his guidance at the beginning and end of this project and for graciously allowing access to the data obtained by himself and Prof. R. E. Cohen. Of course, I also wish to thank my committee members for patiently reading this thesis and for the helpful comments during and after my defense: W. G. Knauss, N. W. Tschoegl, G. Ravichandran, J. F. Hall, J. K. Knowles. In addition, the Office of Naval Research, specifically Dr. L. Peebles, is to be thanked for the grant which supported this work.

As for non-professor types, there are a great many to be thanked. Some of the most important people in my life at Caltech have been my women friends. I cannot possibly thank all of them by name or employ nearly enough adjectives to begin to impart the true importance and relevance of their support through the years to my scientific endeavors. I must, however, name a few of these women in particular: To Jennifer Kolden I am indebted for making it through the infamous "first year" at Caltech; she was my roommate, my classmate, my homework partner, and my buddy; without her, I may have survived my first year, but I would not have enjoyed it. Dr. Erica Harvey has

been a challenging source of support throughout my years here; she helped me to better define myself and my role through example, discussion and friendship. And to the soon-to-be-Doctor Suzanne Paulson, I am eternally grateful for our never-a-dull-moment friendship and camaraderie; the mutual support and encouragement received through many hours-long conversations and through our myriad endeavors to improve Caltech through the Graduate Student Council, the Affirmative Action Committee, the Red Door Café, etc. was essential to the eventual production of this thesis. I would also like to thank Betty Wood, my office-mate since first year, for her tolerance and encouragement of a sometimes talkative, sometimes rude, always frustrated graduate student; she was an unwavering constant throughout my stay at Caltech and actively, vocally helped me through any number of minor traumas. Marta Goodman, during my first two years, and Theresa Thalken, during the last year and a half, each individually helped me to keep perspective in the otherwise completely male research group; their willingness to talk, and let me talk, to discuss everything from scientific difficulties, to the status of my cats, to the latest in fashion was crucial to my progress in research.

On a different level, I must thank Dr. Warren Kibbe for our life together outside of research, without whom my life would not be nearly as rich. On the technical side, I greatly appreciate his ability with his Chemistry background to patiently help me through several minor crises in my research and, of course, his willingness to cheerfully read portions of this document.

And last, but definitely not least, I am most appreciative of all the students in the Solid Mechanics research group throughout my years here. I am notably aware that the friendship and genuine concern for each other and each other's research that pervades the SM group is markedly unusual. I am happy to have been a part of the SM research family and although I cannot mention the students by name for fear of omitting even one, I thank them all for our scientific discussions and their support as friends.

ABSTRACT

A numerical model has been constructed for the study of the properties of multi-phase viscoelastic composites. The model utilizes the dynamic correspondence principle of viscoelasticity in a finite element program to solve boundary value problems simulating uniaxial tension or simple shear and obtains the global complex Young's or shear moduli of the composite.

Each phase of the composite is considered to be thermorheologically simple. The resulting modulus properties of the composite however, are thermorheologically complex and this investigation examines the nature of time-temperature behavior of multi-phase composite materials. The specific composite considered throughout this study contains viscoelastic inclusions embedded in a different viscoelastic matrix material. The deviation of the composite moduli from thermorheologically simple behavior of the matrix material is shown to occur at frequencies and temperatures where the glass-to-rubber transition of the included phases are reached.

Properties of polystyrene and polybutadiene are used to investigate the thermorheological complexity (non-shiftability) of a Styrene-Butadiene-Styrene (SBS) block copolymer. To achieve congruence of the results with experimental data, it is necessary to consider a transition phase of properties "intermediate" to those of styrene and butadiene. Using accurate physical information on the individual phase properties and on the interphase region, it is possible to utilize the numerical model to predict long term properties of multi-phase composites from short term laboratory data. Lacking detailed information on the properties of a particular phase (*e.g.*, the interphase), but knowing the time dependent properties for the composite material at a broad range of temperatures, it is also possible to use the numerical tool to solve an inverse problem and determine the unknown properties of the phase in question.

TIME-TEMPERATURE RESPONSE OF MULTI-PHASE VISCOELASTIC SOLIDS THROUGH NUMERICAL ANALYSIS

TABLE OF CONTENTS

TIME-TEMPERATURE RESPONSE OF SOLIDS CONTAINING MULTIPLE VISCOELASTIC PHASES BY NUMERICAL ANALYSIS

I. INTRODUCTION

Viscoelastic composites usually consist of a "stiff" material and a "softer" viscoelastic material arranged together with one phase distributed as an array inside of the other phase. This type of composite material has many advantages over either phase alone, due in particular to the increased strength of the composite from the stiff phase and the increased toughness of the composite derived from the soft phase. The best known examples of this type of composite are fibrous composites, where the "stiff" phase is usually not a viscoelastic material but instead long thin fibers of graphite, glass, or boron. However, many other common materials are composites in which both phases are viscoelastic such as Styrene-Butadiene Rubber, used in automotive tires; many forms of adhesives, such as American Cyanamide's FM 73 and 3M's AF153; and polyethylene fiber composites used, for example, in tennis rackets.

It is well known that all homogeneous, viscoelastic materials possess mechanical properties which are sensitive to time, temperature, and moisture. The material property defining the mechanical behavior of a viscoelastic material is the modulus function, which relates stress to strain in the material as a function of these variables. Since viscoelastic structures usually have to sustain loading over time, it is especially important to understand how the behavior of these materials varies with time. Also, because of the possibly very long time scales that can be involved for engineering applications, it is

necessary to resort to a time-acceleration scheme when determining the modulus functions of viscoelastic materials in laboratory experiments. Such a time acceleration scheme is well established for thermorheologically simple (TRS) materials, which involves a time-temperature equivalence as described below. This scheme is based on a relationship between the relaxation mechanisms of the viscoelastic material with respect to temperature and with respect to time. It enables the calculation of long time modulus properties for the material based on short time, multi-temperature data.

Many types of viscoelastic materials, however, are not thermorheologically simple. The relaxation mechanisms as functions of temperature and time do not relate in a straightforward fashion, and therefore the simple time acceleration scheme for determination of moduli cannot be employed. Materials that are not thermorheologically simple are called thermorheologically complex (TRC). Examples of TRC materials include many crystalline polymers and all composite materials containing multiple TRS viscoelastic phases. In the case of crystalline polymers, the internal structure, and therefore the relaxation mechanisms, change markedly with decreasing temperature, making a single relationship between the time and temperature behavior of the material infeasible. For multi-phase viscoelastic composites, there are two or more sets of relaxation mechanisms active in the material at all times and temperatures, and the manner of coupling between the two phases and their respective TRS behaviors is unknown. For all such TRC materials a simple time acceleration scheme is not available and the need to develop an understanding of the long time behavior and the time-temperature behavior of this class of materials is what motivates this study. The latter is limited, however, to the investigation of the time-temperature behavior of a special class of multi-

phase viscoelastic composites and does not address the very different TRC behavior of other types of materials.

Tobolsky[1] and Leaderman[2] in 1943, and later Ferry in 1950[3], noted that the effects of temperature and time on most homogeneous viscoelastic materials are related in a simple and convenient way.[4] This relationship states that for a given loading, increasing the temperature produces a material response that is equivalent to increasing the time. Specifically, temperature effects are experienced primarily through a temperature dependent factor multiplying the time scale. Materials for which this is true are called thermorheologically simple materials. Several empirical equations represent the multiplicative factor that relates time and temperature in TRS materials, the most noted being the Arrhenius, the Doolittle, and the WLF equations.[4, 5] These equations each define the temperature dependent "shift factor", a_T, which relates the relaxation or creep response data at one temperature to that at another temperature.

The shiftability of a modulus curve at one temperature through time via a_T to represent the modulus at another temperature for TRS materials is the way in which temperature is commonly used as an accelerator in determining viscoelastic modulus functions for long term applications. Tests measuring modulus as a function of time for a material are performed in the laboratory at many different temperatures in a short time frame "window"; then, choosing a single temperature as the reference temperature, each isothermal modulus curve segment is shifted through time to the reference temperature such that overlapping portions of curve segments superpose. This process yields one continuous curve of viscoelastic modulus response at a single temperature T_{ref}, spanning a large range of times. Such a single curve is called a

"master curve" of the viscoelastic modulus function and the procedure to obtain this master curve determines the shift factor for the material. With the shift factor empirically determined in this manner, one can fit, for example, the WLF equation to the a_T data and thus have the shift factor defined continuously for all temperatures above the glass transition temperature*. Then the shift factor may be used to shift the master curve itself from T_{ref} to another temperature.

As an example, data measured by Plazeck is presented in Figure 1.1 for low molecular weight polystyrene, a component of the SBS material considered later in this paper.[6] The resultant master curve at 85°C in Figure 1.2 is obtained by shifting the data in Figure 1.1 along the logarithmic time axis as described above. This shifting operation determines the corresponding shift factor given in Figure 1.3, where the squares represent the empirically determined shift factor and the solid line is the curve fit to these points by the WLF equation, which is discussed more fully in Section VI.

* The glass transition temperature (T_g) is the temperature at which the properties of a polymer change from glassy to rubbery behavior; it is frequently defined as the temperature at which the coefficient of thermal expansion experiences a discontinuity. Homogeneous polymers still maintain a time-temperature superposability below this temperature. However, the character of the material behavior is sufficiently different that the shift factor above and below the T_g cannot be represented by the same "standard" equation. The WLF equation is valid only above the T_g of polymers.

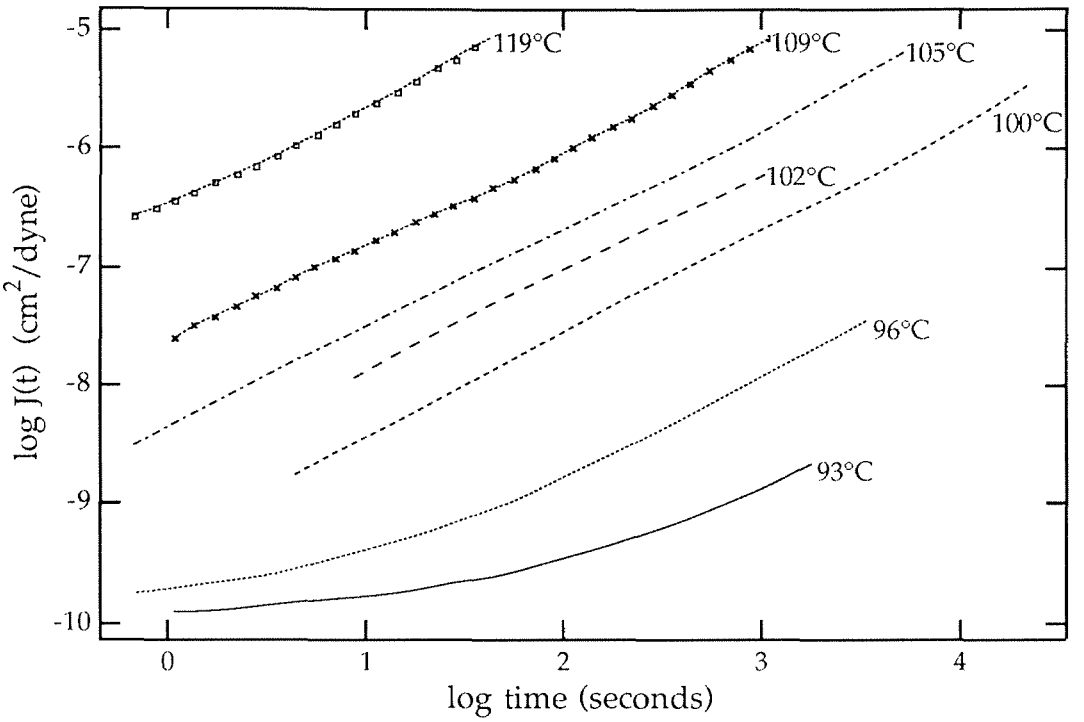

Figure 1.1: Shear creep compliance of low molecular weight polystyrene[6]

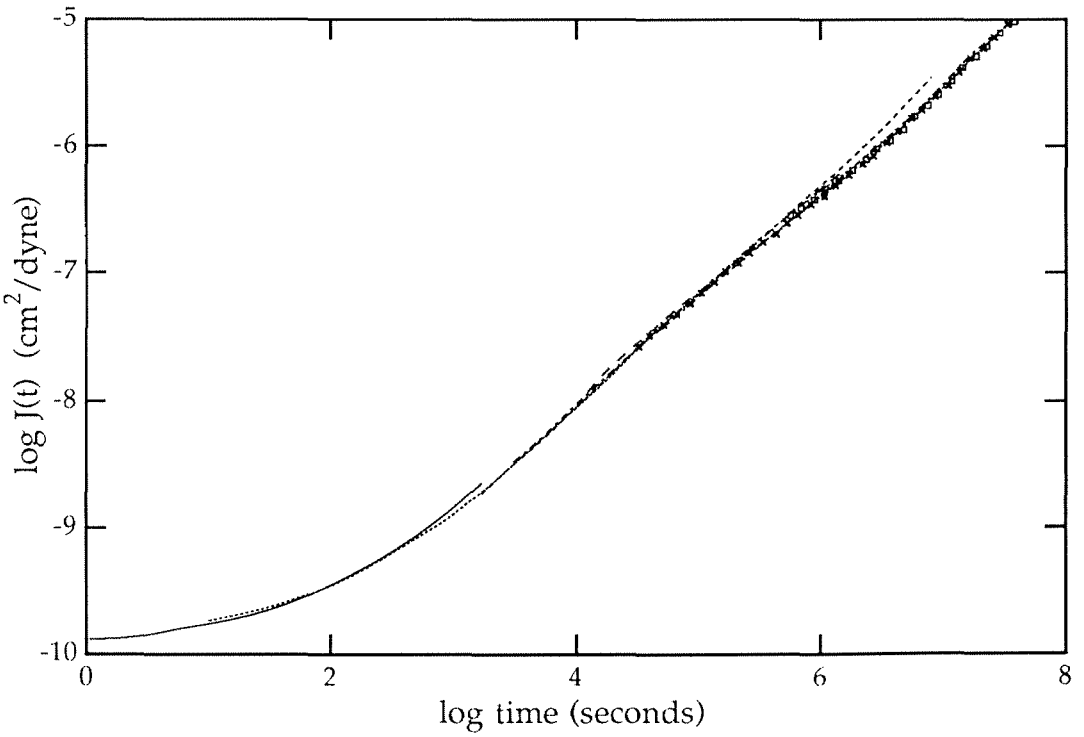

Figure 1.2: Polystyrene data "shifted" and reduced to a master curve at 93°C[6] Same legend as Figure 1.1.

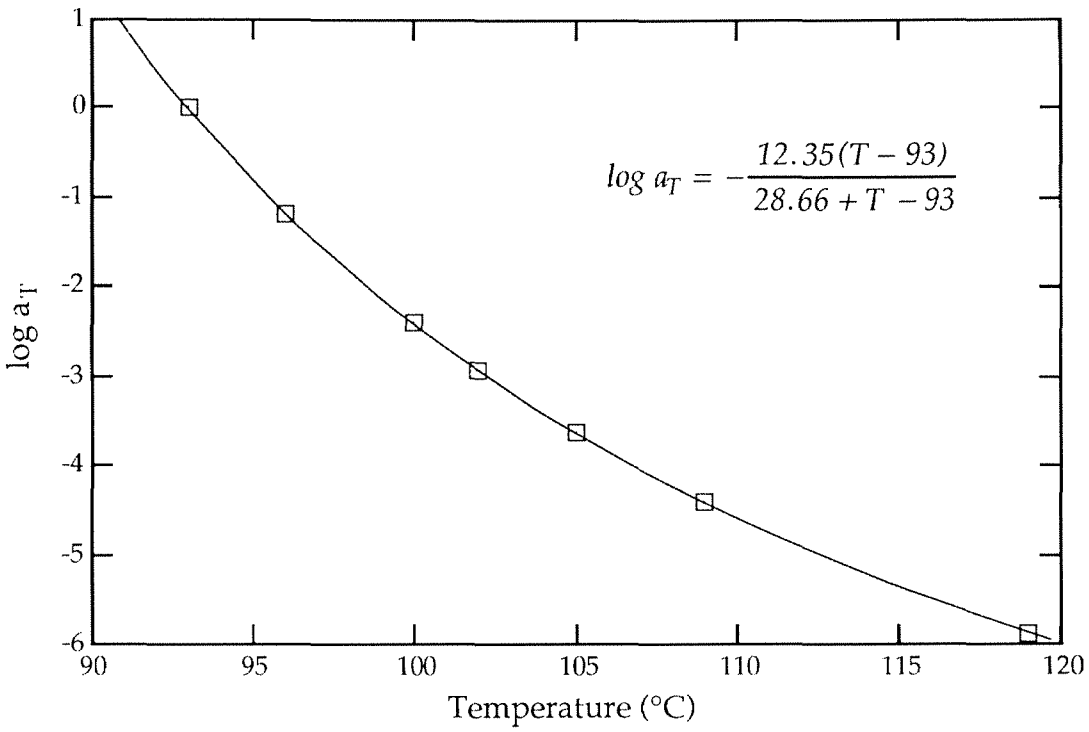

Figure 1.3: Shift factor for the polystyrene of Figures 1.1 and 1.2 at T_{ref}=93°C

This work examines the behavior of a viscoelastic composite consisting of several thermorheologically simple phases. Such viscoelastic composites are thermorheologically complex and the time-temperature equivalence of TRS materials does not apply. Because the composite consists of two or more materials, each with its own time-temperature and relaxation behavior, a single master curve cannot be attained by shifting isothermal segments of mechanical property curves; in fact such a master curve does not exist. Consequently, simple time-temperature shifting can no longer be utilized to relate data at one temperature to that at another temperature and determination of long term properties of these materials is quite difficult.

The particular type of viscoelastic composite studied contains uniformly sized parallel rods of one phase in a matrix of a second phase. These rods are regu-

larly distributed and small compared to any macroscopic dimension of the material, such that the composite can be considered to be homogeneous on a global scale. Such materials are frequently defined using representative volume elements, with dimensions that are large compared to the dimensions of the individual phases, such that all global geometrical characteristics are the same in any representative volume element regardless of position within the material.[7] Thus it is possible to speak of global effective modulus functions for these composites, which will apply to any sufficiently large volume of the material, and which will relate spatial averages of stress and strain in the material. The multi-phase composites or viscoelastic composites referred to throughout this work are constrained to this class of globally homogeneous composites.

Two phase composites in which the distributed phase is in the form of cylindrical or spherical inclusions arranged in a regular array embedded in a different viscoelastic matrix have been studied in a variety of ways. In such studies the common objective is the determination or estimation of the physical properties of the composite from those of the individual phases. The simplest method suggested to achieve this goal is the "Rule of Mixtures," in which the value of the composite modulus functions at any time is a simple combination of the magnitudes of the moduli of the phases and their volume fractions in the composite.[8] The rule of mixtures, however, does not account for coupling in the deformations of the multiple phases and is applicable at best only as a limit case when one phase dominates the material behavior. Christensen and Hill have explored the usefulness of the "self-consistent model," in which a single inclusion is examined as being embedded in an infinite solid of a "matrix material" representing the global effective proper-

ties of the composite.[9, 10] Their work was carried out analytically first for elastic materials using Eshelby's inclusion analysis[11] and was then extended to viscoelastic materials using the correspondence principle (discussed later). Hashin has investigated the so-called method of "composite spheres assembly" (likewise, the "composite cylinders assembly"), which considers the change in strain energy in a loaded homogeneous body due to the insertion of inhomogeneities and yields upper and lower bounds for the properties of particulate viscoelastic composites with low volume fractions of inclusions.[12, 13] Hashin and Shtrikman have also presented variational methods to bound the strain energy, which again yield bounds on the effective composite moduli, but not subject to the restriction of low inclusion volume fraction.[14] The variational and the composite assembly methods are also derived for elastic materials and the composite assembly method is extended to viscoelastic material descriptions through the correspondence principle. A thorough review of the various analyses of composite materials for prediction of effective composite moduli has been compiled by Hashin in 1983.[7]

As mentioned, the limitations of these previous studies have been that they avoid the coupled interactive deformation of the multiple phases and can therefore provide only approximations to the actual viscoelastic properties of multi-phase composites; the effect of the deformation compatibility of the phases contributing to the instantaneous moduli has been neglected at the local level; the existence of a substantial transition region between the two phases has not been included (in some cases, a transition region cannot be accommodated); often simplifying assumptions regarding the geometry of the microstructure were made in order to derive the theories; frequently expressions could be found for only one or two of the composite effective moduli;[7]

and the thermorheologically complex behavior, demonstrated by non-shiftability‡ of the resulting composite moduli, has in some cases been completely neglected. Experimental studies on viscoelastic composites have indeed demonstrated thermorheologically complex response,[15, 16, 17, 18, 19] but only few have attempted to model the anomalous behavior.[17, 20, 21] In spite of the variety of investigations into the mechanical properties of multi-phase composites, the nature of the viscoelastic properties and the interdependence of time and temperature remain incompletely understood.

The purpose of the present endeavor is to model the behavior of a specific type of two-phase viscoelastic material in terms of the linear field theory of viscoelasticity and to determine the mechanical response behavior as a function of time and temperature. A model is made of the microstructure of the particular composite to be studied, and a boundary value problem is formulated to extract a global effective modulus. The task of determining the solution is executed numerically because the elastic analogue to the requisite mixed boundary value problem described in Section II is not available. In addition, if the solution to the elastic analogue were available and the commonly employed viscoelastic-elastic correspondence principle using integral transforms could be employed to attain a closed form analytical solution, there is still considerable question as to the reliability of current approximate transform inversion methods. (See Cost for a thorough review of methods.[22]) The numerical method used here is an adaption of the finite element code FEAP[23] that is summarized in Section III. The problem is formulated in terms of the "dynamic" boundary value problem which evokes frequency

‡ "Non-shiftability" refers to the failure of isothermal moduli curves to form smooth master curves upon shifting and will be used throughout this paper as the definitive measure of the thermorheological complexity of a material.

dependent complex modulus data for the viscoelastic material characterization. Given the properties of the individual phases, one is able to solve the boundary problem numerically and examine the multi-phase material properties at long times and varying temperatures, where in every case the mechanics of the problem have been addressed exactly, except for numerical approximations.

It is in this regard that this work differs from previous investigations. The numerical tool developed here may be applied to numerous models of multi-phase viscoelastic composites under few restrictions to determine the global composite moduli at any time or temperature within finite element approximations. The accuracy of this method is dependent only upon the accuracy with which one knows the properties of the constituent phases of the composite and how precisely one knows and is able to model the microstructural geometry of the composite. Conversely, if the properties of one of the constituent phases are unknown, the numerical procedure may also be used in conjunction with extensive experimental data on the composite properties to make a reasonable estimation of the properties of the unknown phase. The investigation contained in this paper centers on a specific composite model described in Section II, but the tool itself is extremely flexible and potential uses extend well beyond what is covered here.

In the following pages, the model of the composite material examined is first described in Section II; then the derivation of the numerical tool for the purpose of obtaining composite Young's moduli is explained in Section III. Section IV contains some interesting preliminary results on the modulus of the composite before any temperature effects are considered and also offers comparisons with elementary models. Then Section V briefly presents the

transverse shear modulus case including consideration of the relationship between Young's modulus, Poisson's ratio and the shear modulus. Effects of temperature are added and discussed in Section VI, prior to comparison of the numerical results with experimental data on a Styrene-Butadiene-Styrene block copolymer in Section VII. One measure of anisotropy and the effect of anisotropy on composite properties is mentioned in Section VIII and finally the effect of the properties of an interlayer (a transition phase between the two main constituent phases found to be necessary for some composites) on the composite behavior is presented in Section IX, before the conclusion in Section X.

II. THE MODEL

Physical Aspects

The material model examined is that of regularly distributed cylindrical inclusions of one viscoelastic material embedded in a matrix possessing different viscoelastic properties. The cylindrical inclusions are arranged in square or hexagonal arrays such that repeating units of microstructure can be found. To determine the modulus of the composite in a direction perpendicular to the axes of the cylinders for this microstructure, one formulates a two-dimensional boundary value problem in plane-strain in which the cylinders are represented by circular domains, because the length of the cylinders is much larger than their diameter. As mentioned in the Introduction Section, the size of the inclusions and the inclusion spacing relative to the size of a structural member made from this material is such that the material can be viewed as being globally homogeneous on the macroscopic level, while actually being heterogeneous on the microscopic scale. For example, in the copolymer examined in Section VII the cylinders are on the order of 200Å in diameter.

A diagram of a portion of such a material array is shown in Figure 2.1. To determine the global properties of this material, one applies boundary conditions to the composite that if applied to a truly homogeneous body would produce homogeneous stress-strain states. The resulting non-uniform stress and strain states across the microstructure of the composite are then averaged to obtain the average global moduli. In this section, only (plane-strain) simple tension behavior is explored; the corresponding in-plane shear case is considered in Section V. The choice of the x-y directions in Figure 2.1 is convenient to the subsequent analysis; the global material properties will be

slightly different in other coordinate orientations and this effect is discussed later. Consider uniform displacements applied to the material in Figure 2.1 at the upper and lower boundaries simulating uniaxial extension; the dashed lines then represent lines of symmetry of the geometry and of the loading. These lines remain straight and parallel during the deformation. The resultant average force in the x-direction, $\sigma_x|_{avg}$, along the lines of $x=constant$ will be zero if there is no net force acting on the body in this direction.

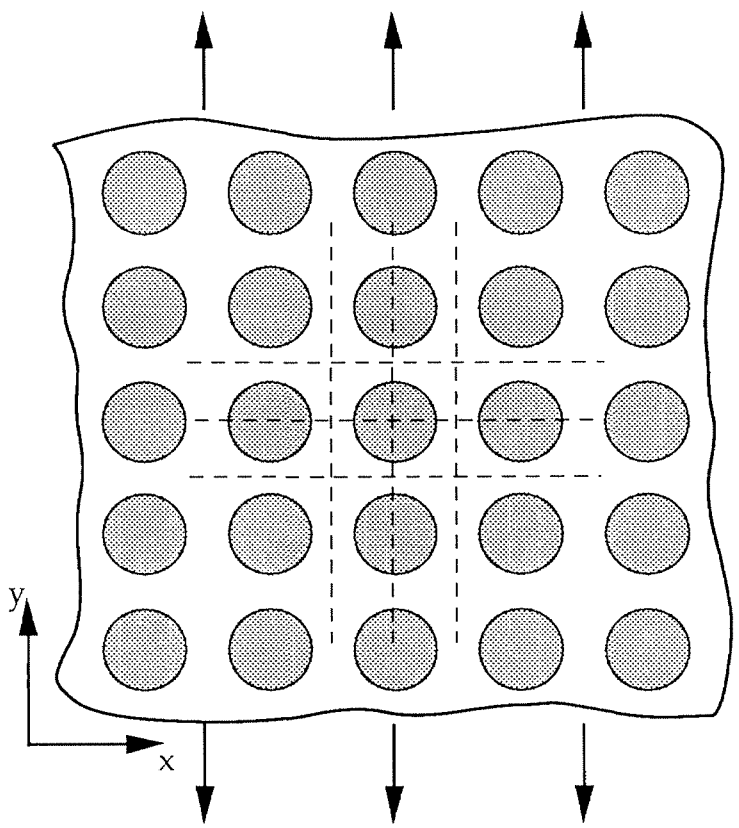

Figure 2.1: The global material

Thus the smallest symmetrically repeating unit, shown in Figure 2.2a, subject to the following boundary conditions is equivalent to study of the entire body under uniaxial tension:

on $y=\pm L$: uniform displacement $u_y=u_0=constant$
Shear traction $T_x \equiv 0$

on $x=\pm L$: $u_x=constant$, where the *constant* is determined such that $\sigma_x|_{avg}=0$
Shear traction $T_y \equiv 0$

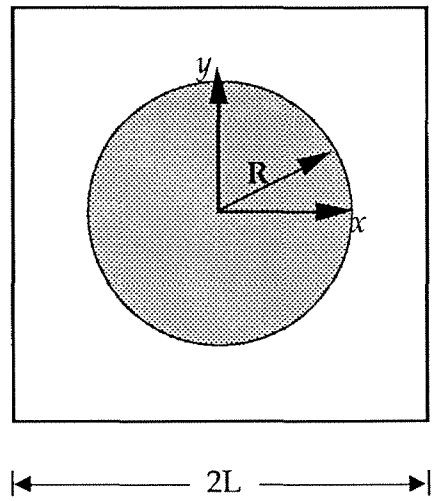

Figure 2.2a: The smallest repeating unit

Further symmetry of the geometry and of this loading allows us to consider one fourth of the smallest repeating unit as the unit cell shown in Figure 2.2b subject to the boundary conditions listed below as representative of the case of uniaxial tension from Figure 2.1.

Boundary conditions for unit cell in Figure 2.2b:

on $x=0$:	$u_x=0$	$T_y=0$	
on $y=0$:	$u_y=0$	$T_x=0$	(2.1)
on $x=L$:	$u_x=-b$	$T_y=0$	
on $y=L$:	$u_y=u_0$	$T_x=0$	

This unit cell is then discretized with a mesh and studied with the finite element procedure described in Section III. The value b in the displacement boundary condition $u_x=-b$ applied on $x=L$ is determined by linear interpolation of the resulting $\sigma_x|_{avg}$ along $x=L$ from two finite element solutions with

prescribed values of b; the interpolation is accomplished such that $\int_0^L T_x dy = 0$. This process is described in greater detail in Section III.†

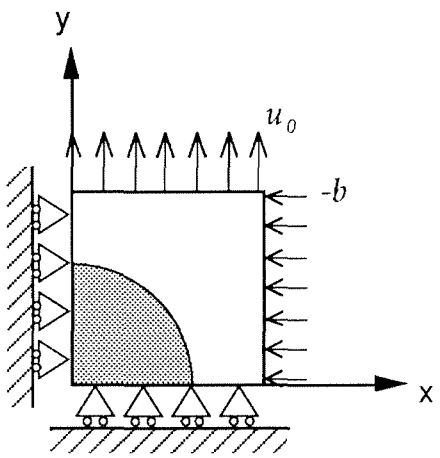

Figure 2.2b: Boundary conditions applied to unit cell

It is important to emphasize here that while the material may be considered globally homogeneous because of the regularity of the inclusions, it may not be considered isotropic. Even on the global scale a material such as that shown in Figure 2.1 is anisotropic. However, one can assert on the basis of studies, some of which are shown in Section VIII, that the effect of the anisotropy on the global properties, in particular on the thermorheology of these properties, is relatively small. In Section VIII the results for the global effective viscoelastic uniaxial response of this material are compared for two different orientations. The actual difference in the values of the modulus functions at various frequencies and temperatures is relatively minor and the degree of thermorheological complexity shown for the two cases is almost identical. Therefore, this study is limited to addressing the particular case illustrated in Figures 2.1 and 2.2 throughout this work.

---

† After completion of this work, it was discovered that using a particular finite element technique, the interpolation to determine the $x=L$ displacement could be avoided. This technique is described in more detail in a footnote in Section III.

Interlayer Aspects for Multi-phase Composites

The model was originally implemented in this work such that the inclusion and the matrix phases were distinctly separated and perfectly bonded at the interfaces. For later reference it will be of interest to note that the computational scheme addresses with nearly equal ease situations involving more than two viscoelastic phases. Indeed, it turns out that typical composites of two viscoelastic phases require an additional transition phase or property gradient, at the interfaces, which is composed of a molecular mixture of the two phases.[24, 25, 26, 27] This transition phase is also referred to as a transition region, an interfacial region or an interphase. In fact, even research on metal matrix composites and fibrous composites has discovered interphases in those materials that significantly influence the overall properties, although the interphase is generally much smaller for these materials than for composites of two polymeric phases.[28, 29, 30]

The size and properties of this transition region vary with different constituent phase materials, solvent type used in material synthesis, rate of solvent evaporation, etc.,[31] but there appears to be no firm data on the geometry and distinct properties of the transition region for any viscoelastic composite. In fact, there appears to exist a specific need for methods with which to determine these interphase properties. It turns out that the method of analysis presented here provides a possible tool, when joined by sufficiently refined experimental measurements, to estimate these interphase parameters more closely than has been possible to date. As will be seen in Section VII dealing with a particular block copolymer, lack of information on the actual transition region between phases in the composite compels the use of the numeri-

cal method to essentially solve an inverse problem: together with a reasonably broad set of experimental data on the composite properties, the numerical scheme is used iteratively to "back out" a set of properties for the interlayer included in the model.

For two-constituent polymeric materials, the results of the present work confirm the suggestions of Meier and Kaelble that the interphase can be quite large, can occupy a significant percentage of the volume fraction[25, 26] and thus strongly affect the properties of the composite. In the model for this study, the transition region has been incorporated as an interlayer between the two phases with one set of material properties. Fesko has attempted to construct a model of an interphase with multiple concentric rings (see also Figure 7.10a), each of slightly differing properties, but given the limited amount of experimental information on properties and size of the interphase it is not felt that the data justifies attempting this kind of refinement at this stage. Figure 2.3 shows a diagram of the unit cell including an interlayer that is used for the later comparison with experimental results; the size chosen for the interlayer will be discussed in that section.

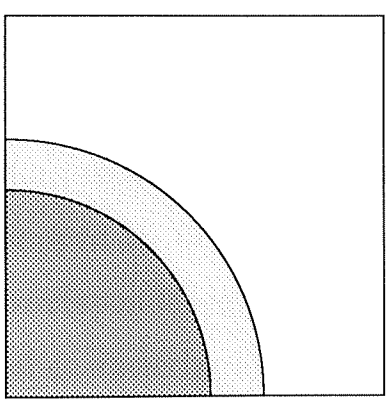

Figure 2.3: Unit cell with single interlayer

III. COMPLEX FINITE ELEMENT MODIFICATION

The finite element code used, Finite Element Analysis Program (FEAP) developed originally at Berkeley[23] then further modified at Brown University, was chosen for its segmented structure, which allows relatively easy modification of the subroutines of numerical procedure (*e.g.*, constitutive behavior, formation of the stiffness matrix, data input, matrix inversion routine...) without requiring interdependent changes scattered throughout the entire program. The base code of FEAP contains element subroutines to accommodate linear elastic constitutive behavior as well as plasticity behavior. In order to address viscoelastic boundary value problems, it was necessary to expand the code's function. The modifications to FEAP are discussed briefly in two sections: first the viscoelastic material behavior and the specific relationships that are best suited to solving this inclusion problem numerically are described; then the method in which this material behavior was incorporated into the FEAP program is explained.

Viscoelastic Material Behavior and the Dynamic Correspondence Principle

Due to the convolution form of the constitutive laws, numerical calculations for viscoelastic problems are usually computation-time intensive, requiring iteration over each time-step and retention of records of the history of the field variables at the previous time-step. Issues dealing explicitly with time dependence can be side-stepped by formulating the problem in the Fourier domain via the dynamic correspondence principle;[32] the traditional connotation in viscoelastic material characterization for this formulation relates to a dynamic or complex material description. Although the dynamic correspon-

dence principle is presented here, an entirely analogous correspondence principle may be formulated with Laplace transforms.[33]

For an isotropic linearly viscoelastic material, the constitutive law can be written in general as,

$$\begin{aligned} s_{nj}(\underset{\sim}{x},t) &= \int_{-\infty}^{t} 2G(t-\tau)\frac{de_{nj}(\underset{\sim}{x},t)}{d\tau}d\tau \\ \sigma_{kk}(\underset{\sim}{x},t) &= \int_{-\infty}^{t} 3K(t-\tau)\frac{d\varepsilon_{kk}(\underset{\sim}{x},t)}{d\tau}d\tau \end{aligned}, \tag{3.1}$$

where s_{nj} and σ_{kk} are the deviatoric and dilatational components of the stress tensor, e_{nj} and ε_{kk} are the deviatoric and dilatational components of the strain tensor, and $G(t)$ and $K(t)$ are, respectively, the time dependent shear and bulk moduli of the material. If the deformation history is harmonic

$$\varepsilon_{nj}(\underset{\sim}{x},t) = \bar{\varepsilon}_{nj}(\underset{\sim}{x},\omega)e^{i\omega t}, \tag{3.2}$$

then (3.1) reduces to

$$\begin{aligned} \bar{s}_{nj}(\underset{\sim}{x},\omega) &= 2i\omega\bar{G}(\omega)\bar{e}_{nj}(\underset{\sim}{x},\omega) \\ \bar{\sigma}_{kk}(\underset{\sim}{x},\omega) &= 3i\omega\bar{K}(\omega)\bar{\varepsilon}_{kk}(\underset{\sim}{x},\omega) \end{aligned} \tag{3.3}$$

where $\bar{\bullet}(\cdot)$ denotes complex quantities and $\bar{G}(\omega)$ and $\bar{K}(\omega)$ are the half-sided Fourier transforms of the shear and bulk moduli respectively, defined by*

$$\begin{aligned} \bar{G}(\omega) &= \int_0^{\infty} G(t)e^{-i\omega t}dt \\ \bar{K}(\omega) &= \int_0^{\infty} K(t)e^{-i\omega t}dt \end{aligned}. \tag{3.4}$$

The functions $i\omega\bar{G}(\omega)$ and $i\omega\bar{K}(\omega)$ are referred to as the complex moduli of the viscoelastic material and are described in terms of their real and imagi-

---

* The usual factor $\frac{1}{2\pi}$ appearing in the Fourier transform is contained in the inverse transform.

nary parts, which are called the storage moduli and the loss moduli respectively:

$$\begin{aligned} i\omega\bar{G}(\omega) &\equiv G^{*}(\omega) = G'(\omega) + iG''(\omega) \\ i\omega\bar{K}(\omega) &\equiv K^{*}(\omega) = K'(\omega) + iK''(\omega) \end{aligned} \quad . \tag{3.5}$$

Dynamic testing, which determines the storage and loss moduli, is a common means of assessing viscoelastic material behavior in the laboratory.

Based on the preceding relations, the dynamic correspondence principle[32] is applicable to situations in which the boundary conditions vary in a time harmonic fashion, and in which tractions and/or displacements are prescribed as separable functions in time and the coordinate along the surface of the domain of interest (proportional loading). For example, if only displacements are prescribed, one has

$$u_j(s,t) = \bar{u}_j(s)e^{i\omega t} \quad , \tag{3.6}$$

where s is the coordinate along the boundary and $\bar{u}_j$ is a complex quantity and a function of s only. If all boundary conditions are written in this form, with the same frequency ω, then the stress and strain states of the material are expected to be expressible in harmonic form. For example, knowing the displacement boundary conditions to be (3.6), the displacement-strain relation implies

$$\begin{aligned} e_{nj}(\underset{\sim}{x},t) &= \bar{e}_{nj}(\underset{\sim}{x},\omega)e^{i\omega t} \\ \varepsilon_{kk}(\underset{\sim}{x},t) &= \bar{\varepsilon}_{kk}(\underset{\sim}{x},\omega)e^{i\omega t} \end{aligned} \quad , \tag{3.7}$$

where the overbar again denotes a complex quantity, and a function of the frequency ω.

Thus in the case of harmonically varying boundary conditions on a viscoelastic solid, the constitutive equations in the form of convolution integrals

reduce to the form given in (3.3). Note that the explicit time-dependence has vanished from the constitutive equations in favor of the frequency ω, resulting in equations in the Fourier (frequency) domain that are analogous to the equations of elasticity. Equations (3.3) are valid for any fixed value of ω, independent of other frequencies, analogous to the corresponding elasticity problem, but here each field quantity has both real and imaginary parts.

Finite Element Modifications

The theory of finite elements has been used extensively for many years to solve numerous difficult mechanics problems for which analytical solutions cannot be derived. The basis of finite element theory as applied to solving static solid mechanics problems is briefly mentioned here. For an excellent, thorough derivation and explanation, see Zienkiewicz[34] or Reddy.[35] It should be noted that this study employs exclusively infinitesimal deformation analysis with strains and displacements such that the linear theory of elasticity and viscoelasticity hold; consequently there is no distinction between the deformed and the reference configurations.

In the context of the theory of finite elements for linear elasticity, upon using variational methods on the equilibrium equation and discretizing a body into a mesh of elements, one can relate the nodal displacements to the external forces through the element stiffness matrix, $[K]^e$ (dependent upon the constitutive behavior of the material):

$$[K]^e \underset{\sim}{u} + \underset{\sim}{f} = 0 \tag{3.8}$$

Here $\underset{\sim}{u}$ is a vector containing nodal displacements and $\underset{\sim}{f}$ is a vector containing the external nodal forces. The strain in the elements is related to the

nodal displacements through a matrix $[B]$, which contains essentially the derivatives of the shape functions for the element:

$$\underset{\sim}{\varepsilon} = [B]\underset{\sim}{u}, \tag{3.9}$$

where $\underset{\sim}{\varepsilon}$ contains the strains in the element in the form of:

$$\underset{\sim}{\varepsilon} = \begin{Bmatrix} \varepsilon_{11} \\ \varepsilon_{22} \\ \varepsilon_{33} \\ \varepsilon_{12} \end{Bmatrix} \tag{3.10}$$

and where shape functions are the interpolation functions used to approximate the relationship between nodal and interior displacements for an element. The constitutive relation between stress and strain is expressed at the element level by

$$\underset{\sim}{\sigma} = [D]\underset{\sim}{\varepsilon}, \tag{3.11}$$

where the stress vector contains the stresses in the element in the same form as the strains, and the matrix $[D]$ contains the constitutive law, which in the case of isotropic elasticity is written:

$$[D] = \frac{E}{1-\nu^2}\begin{bmatrix} 1 & \nu & \nu & 0 \\ \nu & 1 & \nu & 0 \\ \nu & \nu & 1 & 0 \\ 0 & 0 & 0 & \frac{1-\nu}{2} \end{bmatrix} \tag{3.12}$$

where E is Young's modulus of elasticity and ν is Poisson's ratio. The stiffness matrix for an element is related to both $[B]$ and $[D]$ by

$$[K]^e = \int_{V^e} [B]^T[D][B]dV^e \tag{3.13}$$

As explained in the previous section, for the case of harmonic boundary conditions on a viscoelastic structure, one obtains field equations that are analogous to elasticity equations. The field quantities, however, become complex variables; therefore to be able to utilize the Dynamic Correspondence principle to study a structure via the method of finite elements, the finite element procedure must be modified to allow for complex field quantities and stiffness matrices. This modification can be accomplished in one of two ways: 1) The numerical procedure could be changed to utilize complex variables for every quantity that would become complex and any intrinsic functions that the code uses with these complex quantities would have to be altered in all subroutines; or 2) the degrees of freedom at each node could be doubled, allowing for real and imaginary displacements in all directions and then necessary changes could be made to the element subroutine. In light of FEAP's substructure and that FEAP allows many degrees of freedom, the change was implemented in the latter form. This method required a major modification of one subroutine of the code, but left all other portions of numerical procedure untouched.

To outline the changes made, first consider equation (3.3) in reduced notation for simplicity, omitting the arguments of $\bar{\sigma}_{nj}$ and $\bar{\varepsilon}_{nj}$

$$\begin{aligned} \bar{s}_{nj} &= 2i\omega\bar{G}(\omega)\bar{e}_{nj} \\ \bar{\sigma}_{kk} &= 3i\omega\bar{K}(\omega)\bar{\varepsilon}_{kk}. \end{aligned} \tag{3.14}$$

Recombining the separated dilatational and deviatoric parts of both stress and strain into $\bar{\sigma}_{nj}$ and $\bar{\varepsilon}_{nj}$, respectively, and using the definitions

$$\begin{aligned}\bar{\sigma}_{nj} &= \bar{s}_{nj} + \tfrac{1}{3}\bar{\sigma}_{kk}\delta_{nj} \\ \bar{\varepsilon}_{nj} &= \bar{e}_{nj} + \tfrac{1}{3}\bar{\varepsilon}_{kk}\delta_{nj}\end{aligned}, \tag{3.15}$$

there follows

$$\bar{\sigma}_{nj} = 2i\omega\bar{G}(\omega)\bar{\varepsilon}_{nj} + i\omega(\bar{K}(\omega) - \tfrac{2}{3}\bar{G}(\omega))\bar{\varepsilon}_{kk}\delta_{nj}. \tag{3.16}$$

Equation (3.11) can now be used to develop the complex constitutive relation in matrix form

$$\begin{Bmatrix}\bar{\sigma}_{11}\\ \bar{\sigma}_{22}\\ \bar{\sigma}_{33}\\ \bar{\sigma}_{12}\end{Bmatrix} = \begin{bmatrix} i\omega(\frac{4}{3}\bar{G}+\bar{K}) & i\omega(-\frac{2}{3}\bar{G}+\bar{K}) & i\omega(-\frac{2}{3}\bar{G}+\bar{K}) & 0 \\ i\omega(-\frac{2}{3}\bar{G}+\bar{K}) & i\omega(\frac{4}{3}\bar{G}+\bar{K}) & i\omega(-\frac{2}{3}\bar{G}+\bar{K}) & 0 \\ i\omega(-\frac{2}{3}\bar{G}+\bar{K}) & i\omega(-\frac{2}{3}\bar{G}+\bar{K}) & i\omega(\frac{4}{3}\bar{G}+\bar{K}) & 0 \\ 0 & 0 & 0 & 2i\omega\bar{G} \end{bmatrix} \begin{Bmatrix}\bar{\varepsilon}_{11}\\ \bar{\varepsilon}_{22}\\ \bar{\varepsilon}_{33}\\ \bar{\varepsilon}_{12}\end{Bmatrix}, \tag{3.17}$$

where the 4x4 matrix is referred to below as $[\bar{D}]$. For ease of implementation with the standard properties known for viscoelastic materials, this D-matrix can be separated into real and imaginary parts

$$[\bar{D}] = [D]_{Re} + i[D]_{Im}. \tag{3.18}$$

Viscoelastic modulus functions are frequently represented in terms of a Prony series, *e.g.*,

$$G(t) = G_\infty + \sum_{j=1}^{N} G_j e^{-t/\xi_j} \tag{3.19}$$

where G_j and ξ_j are the relaxation spectra and relaxation times respectively and G_∞ is the rubbery asymptotic modulus. Taking the half-sided Fourier transform of (3.19) to obtain the complex modulus and separating into real and imaginary parts yields

$$
\begin{aligned}
i\omega\bar{G}(\omega) &= G_\infty + \sum_{j=1}^{N} \frac{i\omega G_j}{\frac{1}{\xi_j} + i\omega} \\
&= G_\infty + \sum_{j=1}^{N} \frac{G_j \omega^2}{\frac{1}{\xi_j^2} + \omega^2} + i \sum_{j=1}^{N} \frac{\frac{G_j}{\xi_j}\omega}{\frac{1}{\xi_j^2} + \omega^2} \\
&= G_{Re} + iG_{Im} \\
&\equiv G' + iG''
\end{aligned}
\tag{3.20}
$$

Thus, the $\bar{D}_{11}$ term, for example, of $[\bar{D}]$ is given by

$$
\begin{aligned}
\bar{D}_{11} &= \tfrac{4}{3} i\omega\bar{G}(\omega) + i\omega\bar{K}(\omega) \\
&= (\tfrac{4}{3} G_{Re} + K_{Re}) + i(\tfrac{4}{3} G_{Im} + K_{Im}) \\
&= (D_{11})_{Re} + i(D_{11})_{Im}
\end{aligned}
\tag{3.21}
$$

From (3.21) the stiffness matrix, (3.13), will also have real and imaginary parts,

$$
\begin{aligned}
[\bar{K}]^e &= \int_{V^e} [B]^T [\bar{D}][B] dV^e \\
&= \int_{V^e} [B]^T \{[D]_{Re} + i[D]_{Im}\}[B] dV^e \\
&= [K^e]_{Re} + i[K^e]_{Im}
\end{aligned}
\tag{3.22}
$$

Returning to the equilibrium equation (3.8), one obtains upon substituting complex quantities and splitting into real and imaginary parts

$$
\begin{gathered}
[\bar{K}]^e \underset{\sim}{\bar{u}} + \underset{\sim}{\bar{f}} = \underset{\sim}{0} \\
[[K^e]_{Re} + i[K^e]_{Im}]\{\underset{\sim}{u}_{Re} + i\underset{\sim}{u}_{Im}\} + \{\underset{\sim}{f}_{Re} + i\underset{\sim}{f}_{Im}\} = \underset{\sim}{0}
\end{gathered}
\tag{3.23}
$$

After equating real and imaginary parts of both sides of the equation (3.23), then recombining in matrix form, one obtains a matrix equation that is analogous to the elasticity form, but with double the degrees of freedom

$$\begin{bmatrix} [K^e]_{Re} & -[K^e]_{Im} \\ -[K^e]_{Im} & -[K^e]_{Re} \end{bmatrix} \begin{Bmatrix} \underset{\sim}{u}_{Re} \\ \underset{\sim}{u}_{Im} \end{Bmatrix} + \begin{Bmatrix} \underset{\sim}{f}_{Re} \\ -\underset{\sim}{f}_{Im} \end{Bmatrix} = \begin{Bmatrix} \underset{\sim}{0} \\ \underset{\sim}{0} \end{Bmatrix}. \tag{3.24}$$

Note that the second row in matrix (3.24) has been multiplied by -1 in order to obtain a symmetric stiffness matrix.

The B-matrix relating strain and displacement, which contains the derivatives of the shape functions, does not contain complex quantities; however it must be reformed to handle the extra degrees of freedom properly.

Through these modifications to the element subroutine of FEAP and other related changes in the same subroutine that ensure the proper interface of the modified matrices in calculations of the stress and strain fields etc., the elasticity finite element code was enlarged to accommodate the special case of viscoelastic materials subject to harmonic boundary conditions. The input section to FEAP was also modified to allow input of viscoelastic properties and parameters. The modified code, given the viscoelastic properties of the material(s) involved, can solve problems that could normally be handled by finite element analysis in the elasticity case, as long as the boundary conditions are harmonic. The real and imaginary parts of the boundary conditions are the required input.

Application of modified finite element analysis to inclusion problem

For the particular boundary value problem formulated earlier, represented by equations (2.1), to determine the global moduli of a particular multi-phase viscoelastic composite via a unit cell analysis, one can consider a corresponding harmonic boundary value problem: Replacing the displacement boundary conditions $u_y=u_0$ and $u_y=-b$ in Figure 2.2b with $u_y = \bar{u}_0 e^{i\omega t}$ and $u_x = -\bar{b}e^{i\omega t}$,

the uniaxial tension unit cell problem can be solved numerically in the Fourier domain for each value of ω independently as a complex elasticity-type problem. The new complex boundary value problem in the transformed domain is

$$\begin{array}{lll} \text{on } x=0: & \bar{u}_x = 0 + i0 & \bar{T}_y = 0 + i0 \\ \text{on } y=0: & \bar{u}_y = 0 + i0 & \bar{T}_x = 0 + i0 \\ \text{on } x=L: & \bar{u}_x = -\bar{b} & \bar{T}_y = 0 + i0 \\ \text{on } y=L: & \bar{u}_y = u_0 + i0 & \bar{T}_x = 0 + i0 \end{array} \tag{3.25}$$

The interpolation procedure to obtain the necessary x-displacement $\bar{b}$ such that $\int_0^L T_x^{Re} dy = 0$ and $\int_0^L T_x^{Im} dy = 0$ in Figure 2.2b, where T_x^{Re} and T_x^{Im} are the real and imaginary parts of $\bar{T}_x$ respectively, is based on the fact that the model is of a globally homogeneous material and the boundary conditions for the unit cell are constrained by this feature of the material. To obtain the proper interpolation procedure, it is simplest to think in terms of a square, with side length L, of purely homogeneous material. Consider such a homogeneous material subject to the conditions (in the transformed Fourier domain)

$$\begin{array}{lll} \text{on } x=0: & u_x=0 & T_y=0 \\ \text{on } y=0: & u_y=0 & T_x=0 \\ \text{on } x=L: & u_x=-\bar{d} & T_y=0 \\ \text{on } y=L: & u_y=u_0 & T_x=0 \end{array} \tag{3.26}$$

where $\bar{d}$ is arbitrarily chosen. Then the homogeneous strains in the body can be written

$$\begin{aligned} \bar{\varepsilon}_{22} &= \varepsilon_0 + 0i \\ \bar{\varepsilon}_{11} &= \varepsilon_{Re} + i\varepsilon_{Im} \end{aligned} \tag{3.27}$$

where $\varepsilon_0 = \frac{u_0}{L}$, and $\varepsilon_{Re} = \frac{d_{Re}}{L}$ and $\varepsilon_{Im} = \frac{d_{Im}}{L}$. One can then show that σ_{Re} and σ_{Im} (from $\bar{\sigma}_{11} = \sigma_{Re} + i\sigma_{Im}$) are related to ε_0, ε_{Re}, and ε_{Im} by four constants.

$$\begin{aligned} \bar{\sigma}_{11} &= \bar{A}\bar{\varepsilon}_{11} + \bar{C}\bar{\varepsilon}_{22} \\ &= (A + iB)(\varepsilon_{Re} + i\varepsilon_{Im}) + (C + iD)(\varepsilon_0) \end{aligned} \tag{3.28}$$

These four constants can be determined from two solutions of the numerical program with different values of $\bar{u}_x(x = L) = \bar{d}$, since the real and imaginary parts will yield essentially two equations for each solution.

$$\begin{aligned} \sigma_{Re} &= A\varepsilon_{Re} + C\varepsilon_0 - B\varepsilon_{Im} \\ \sigma_{Im} &= B\varepsilon_{Re} + A\varepsilon_{Im} + D\varepsilon_0 \end{aligned} \tag{3.29}$$

Once the constants are determined in this manner, one interpolates to determine the necessary values of ε_{Re} and ε_{Im}, and therefore of the $\bar{u}_x(x = L)$ displacement, to result in $\bar{\sigma}_{11} \equiv 0$ ($\sigma_{Re} = 0$ and $\sigma_{Im} = 0$). This procedure applies also to the *average* stress and strain values along the edge x=L in the unit cell of the globally homogeneous material. The average ε_0 value along y=L is the same as the point by point value in this particular case. One notes that in the homogeneous case the four constants can be determined analytically as functions of $\bar{E}(\omega)$ and $\bar{\nu}(\omega)$ without iteration. However, in the case of the two-phase material studied here, the global moduli of the material are to be determined from the analysis and are obviously not available for determining the boundary conditions necessary to carry out the analysis.§

From the results of the finite element analysis on the unit cell subjected to the described complex boundary conditions, the complex plane-strain

---

§ After completion of this work, a discussion with J. F. Hall determined that using a special finite element technique, the interpolation to determine the x=L displacement could be avoided. Two potential methods are are known at this time by the author: One method would be to add two-noded "shear beam elements" superposed on the boundary edge of the four-noded elements along x=L. These elements are very stiff to resist rotation, but have no stiffness in the y-direction. Use of the shear beam elements would thus ensure that all nodes on x=L are displaced by a constant amount. A second method would be to assign the same equation number to the horizontal degrees of freedom for the nodes along x=L in the assembly process. This procedure is equivalent to treating the entire x=L boundary as having one real and one imaginary degree of freedom in the x-direction. This method then ensures that the boundary displaces as a unit and, by specifying in the input that the real and imaginary forces in the x-direction be zero, also ensures that the resultant average x-forces are zero along that boundary. This second method will be implemented into the numerical procedure in the future: it will reduce computation time by a factor of three.

Young's Modulus of the global composite material was determined. By combining the "average" resulting normal stress, $\bar{\sigma}_y\big|_{avg}$ obtained by a simple nodal average on $y=L$, along with the applied average normal strain, $\bar{\varepsilon}_y = \frac{u_0}{L}$, the complex moduli, $E^*(\omega) = E'(\omega) + iE''(\omega)$, were extracted for the two-phase composite by

$$\frac{\bar{\sigma}_y\big|_{avg}(\omega)}{\bar{\varepsilon}_y(\omega)} \equiv i\omega\bar{E}(\omega) = E^*(\omega) \tag{3.30}$$

Note that the moduli determined are the plane-strain moduli since the basis of the numerical analysis performed is two-dimensional plane-strain. Figure 3.2 shows the unit cell discretized into a finite element mesh. This is the mesh used for the unit cell of the SBS material studied in Section VII. All other meshes are similar with a graded and finer mesh at the boundaries of any two phases. The meshes for each different geometry case studied were refined until the point at which the results for $\bar{E}(\omega)$ from a mesh with the number of elements increased by a factor of $1\frac{1}{2}$ could not be distinguished from the results of the previous mesh within plotting accuracy.

An assumption underlying this application of the correspondence principle to a non-homogeneous solid pertains to the issue of uniqueness. For homogeneous elastic and viscoelastic materials, there exists a uniqueness proof which guarantees that if one obtains a solution that satisfies the field equations and the boundary conditions, then that solution is unique.[36] There is no immediate such proof for inhomogeneous materials. In the formulation of the inclusion problem with the unit cell, it is assumed that the frequency of every point in the body is the same — in particular, that the frequency in the inclusion and in the matrix is the same frequency as applied in the boundary

conditions. Although through this assumption, a solution is obtained to the problem which satisfies the boundary conditions and the field equations, lacking a uniqueness theorem one cannot from this solution conclude that the frequency is indeed uniform throughout the body. In homogeneous materials, however, it is known that there is only one frequency throughout the body, and in this work it is assumed that the same is true for the globally homogeneous, although microscopically inhomogeneous material. This assumption is supported by the fact that the body as studied in this procedure undergoes instantaneous deformations, which would not account for a frequency in the interior to be different from that on the boundary.

More definitively, one can argue this point with superposition of two homogeneous sub-problems. See Figure 3.1. Consider the first sub-problem to be a square homogeneous body of the matrix material subject to the same $u_y=u_0$, and $u_x = -\bar{b}$ displacements with a void the size of the inclusion and with displacements u_s and tractions T_s on the boundary of the circular void. This first sub-problem possesses a unique solution by virtue of the theorem in Gurtin and Sternberg.[36] Then consider the second sub-problem of a circular homogeneous body of the inclusion material subject to displacements u_s and tractions $-T_s$ on the boundary. This second sub-problem, too, has a unique solution by the same theorem. Then by the theory of superposition, the solution to the inclusion unit cell problem is the addition of sub-problems one and two. Because the solutions to the sub-problems are unique, the superposed solution may be unique as well, as long as the interface boundary conditions are exactly matched. The superposed solution is at least a solution to the nonhomogeneous problem.

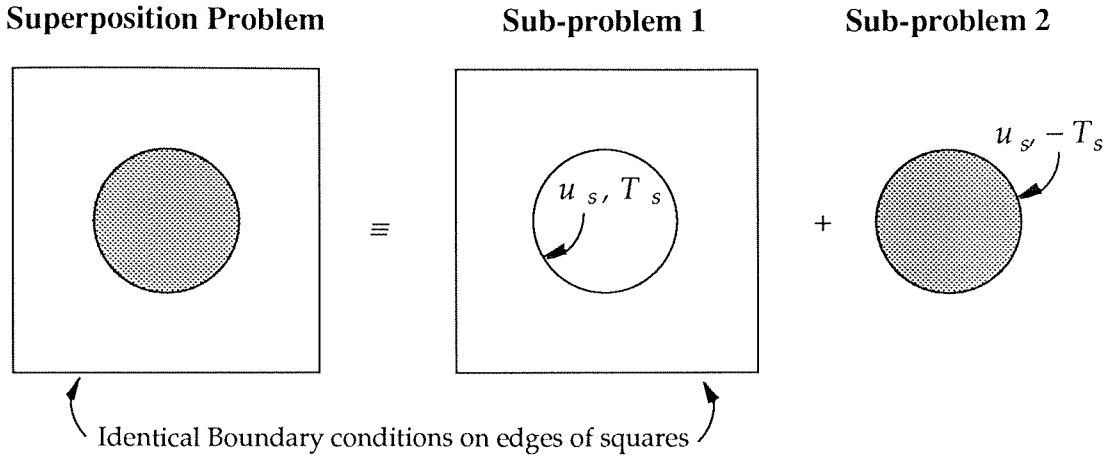

Figure 3.1: Superposition of two sub-problems to attain unit cell inclusion problem

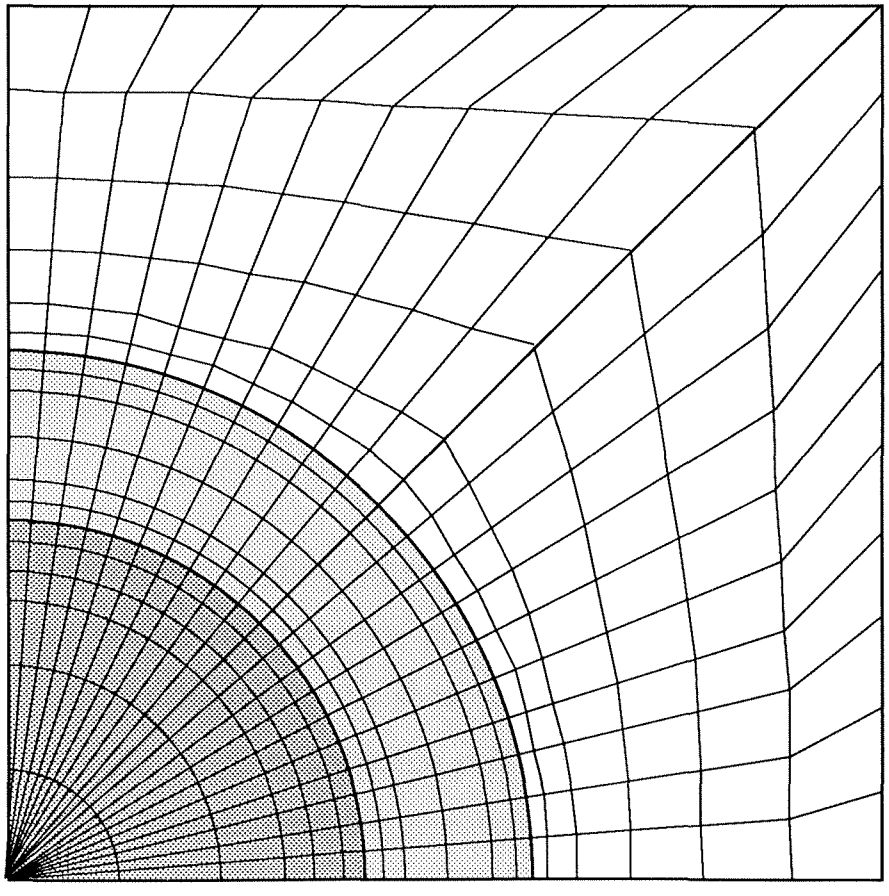

Figure 3.2: Finite element mesh used for unit cell with interlayer in later study of SBS copolymer (see Section VII)

Extremes Accounted for in Computations

There are special cases for which the numerical procedure fails to render solutions without specific attention. One of these situations occurs at high frequencies for the boundary value problem. Since viscoelastic material properties change over a large range of time (or frequency), the investigation of the global composite modulus properties of the multi-phase material frequently extend to very large values of frequency. The numerical difficulty with this occurs in the situation of large frequency values (*e.g.*, on the order of 10^8) in a viscoelastic material for which the Prony series characterization also involves large relaxation times (*e.g.*, on the order of 10^{14}). Referring back to equation (3.20), one notes that calculation of the complex modulus involves multiplication of relaxation times with the square of the frequency in the denominator of the imaginary part. This multiplication generates numbers (with this example) on the order of 10^{30} and causes a numerical overflow error. However, since this large number is in the denominator, the resultant value for the imaginary part is zero. Therefore, a procedure was placed in the finite element program to check for the conditions that lead to this error situation and bypass the calculation of the denominator in those cases.

A second consideration for the numerical analysis arises in the study of composites where one of the materials possesses a shear modulus without an asymptotic rubbery limit, *i.e.*, the shear modulus decreases to zero with increasing time, $G_\infty \equiv 0$. In the inclusion problem at low frequencies where the situation of "zero" shear modulus occurs, a specific numerical difficulty is encountered in which the element stiffness matrix is not calculated correctly because the incompressibility places too severe of a restraint on the possible

element deformation modes. The issue of modifying finite element procedures to correctly address the limit cases of incompressibility has been thoroughly addressed by Nagtegaal and Rice *et al.*[37, 38] In essence, the problem is that in a standard formulation of the tangent stiffness matrix for finite element analysis, incompressibility places too many constraints on the elements such that the individual components of the dilatational strain are forced to be constant. This restriction then gives the illusion of "stiffness" in the result for the material — the finite element results indicate that the material is stiffer than it actually is.

Summarizing Nagtegaal, Parks, and Rice, in the continuum for plane-strain problems, each point in the material has two degrees of freedom, and therefore in the case of incompressibility only one constraint can be valid at each point (in addition to the incompressibility constraint). Thus, to have a finite element code that accurately allows for incompressibility, the number of constraints on the dilatation for each element type must be related to the average degrees of freedom for the element in the mesh by a factor of two.[37] (For the four noded isoparametric elements used in FEAP for the inclusion problem, the ratio of degrees of freedom to constraints is 2/3, instead of the desired 2.) One method to reduce the parameters which govern dilatation to account for the limit case of incompressibility is to alter the variational principle through which the stiffness matrix for an element is derived. The simplest way in which to implement this method is by changing the B-matrix containing the derivatives of the shape functions. By splitting the B-matrix into its deviatoric and dilatational components, then calculating the dilatational portion of the B-matrix at a reduced number of quadrature points (in the case of four noded isoparametric elements, at one quadrature point), the constraints on

the element deformation are reduced and the correct dilatational strain is calculated. The calculation of the deviatoric strains are still correct with this method. Therefore, this method known as the B-Bar method was employed throughout the analysis.

IV. CIRCULAR INCLUSION PROBLEM

In this section (and in other sections prior to the specific example of the SBS composite) an "ideal" composite consisting of two phases is considered. The individual phase properties are chosen as idealized viscoelastic properties such that the modulus functions of each phase have distinct long-term and glassy asymptotic values and one phase is "stiffer" at all times than the other, "softer" phase. Figure 4.1 shows the Bulk and Shear moduli as functions of time chosen for these phases. Examination of the effective properties of a composite with phases of these idealized properties with simple relaxation characteristics and definitive glassy and rubbery moduli allows for easier interpretation of preliminary results before attempting the modelling of a real material.

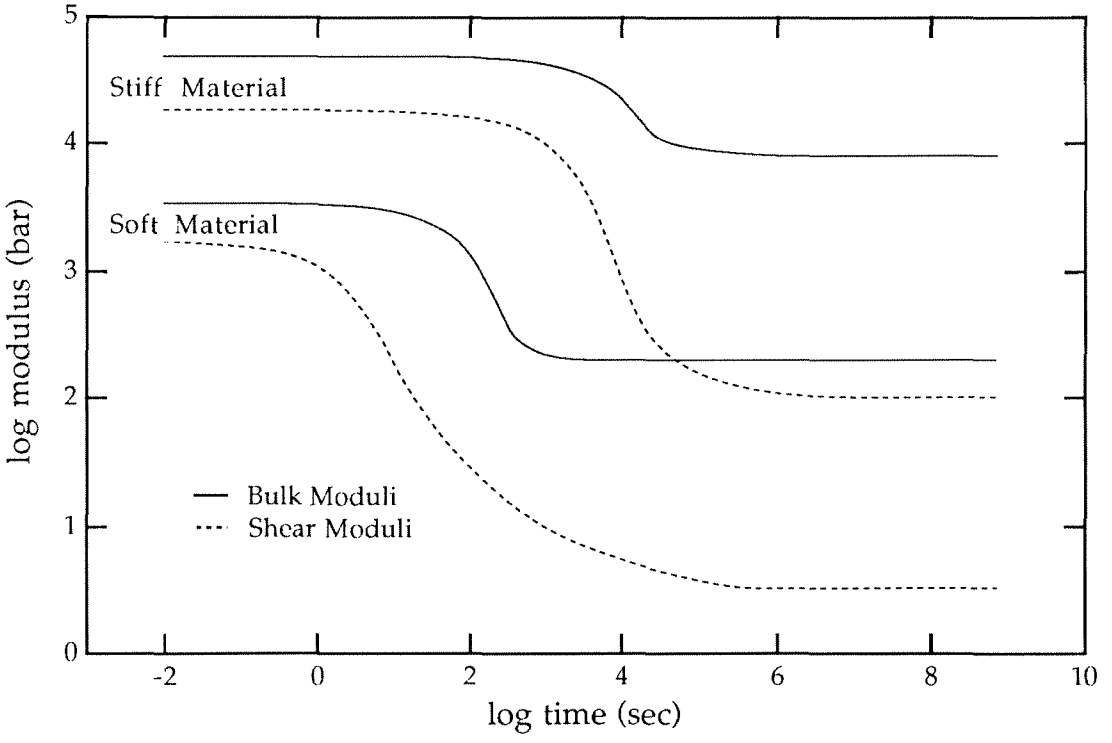

Figure 4.1: Modulus data for individual phases used in initial analysis

Effect of Varying Volume Fractions on Composite Properties

The first set of results presented in this section examines the behavior of the Young's modulus of the composite material of Figure 2.1 with increasing volume fractions of inclusion relative to the volume fraction of the matrix and involves no temperature changes of the material. Three separate cases of Young's modulus were studied for which the volume fraction of inclusion was chosen as 25%, 36%, or 64% of the total composite volume (or unit cell volume). Each case was also calculated for both the arrangement of a soft matrix material with stiff inclusions (as in the case of Styrene-Butadiene rubber) and for the case of a matrix of the stiff material with soft inclusions (like rubber reinforced adhesives).

Figure 4.2 shows the Young's modulus calculated from the numerical procedure for a composite of the soft material with stiff inclusions; the results are presented as the storage and loss moduli separately. Also shown on these plots are the Young's moduli for each phase as a homogeneous material. It is clear from these figures that the behavior of the composite is dominated by the behavior of the matrix material, even when the volume fraction of the inclusion exceeds 50% of the total volume. This is sensible since the continuous phase, as opposed to the dispersed phase, should govern the response of the composite. The magnitude of the storage modulus increases with increasing volume fraction of the stiff inclusion, but the character of the glass-to-rubber transition (shape, length, location) remains dominated by the soft matrix material. As one would intuitively expect, for nearly all frequencies the values of the composite moduli (storage and loss) lie between the values of the moduli of the soft material and the stiff material. However, there is an

exception to this guideline at high frequencies of the loss modulus. At high frequencies where the loss modulus of the stiff material is lower than the loss modulus of the soft material, the composite's loss modulus is completely dominated by the soft material, nearly independent of volume fraction. Before explaining this phenomenon, it is instructive to examine the inverse composite where the matrix is that of the stiff material and contains soft inclusions.

Figure 4.3 shows the complex Young's moduli results for increasing volume fractions of inclusion where the stiff material is the matrix and the soft material is the inclusion phase. The results here are quite similar to the inverse case shown in Figure 4.2. Once again the composite properties are governed by the matrix properties and the magnitudes of the moduli are between the magnitudes of the stiff and soft phase homogeneous moduli except for the high frequency loss modulus. As before, the high frequency loss modulus for the composite, where the stiff loss modulus is lower than the soft loss modulus, is almost equal in magnitude to the soft material's loss modulus, nearly independent of volume fraction. This occurrence can be most easily understood by the following physical argument: the energy dissipation, which is proportional to the loss modulus, must be expected to be absorbed by the softer material, even if there is a larger volume fraction of stiff material or if the stiff material surrounds the soft material. At high frequencies, the stiff material "does not have time" to react or prohibit dissipation.

Also worth noting in comparing the soft matrix and the stiff matrix cases is the relative influence of the included phase on the composite properties. When the stiff material is in the matrix, the magnitude of the resulting composite modulus is decreased by the presence of the soft material inclusion less

percentagewise than the magnitude of the composite modulus increases due to the presence of stiff material inclusion when the soft material is in the matrix. In other words, for a set volume fraction of inclusion, the magnitude of its effect on the properties of the composite depends greatly on whether the matrix phase is "stiffer" or "softer" than the inclusion phase. Physically this is reasonable because (except for the high frequency loss modulus for reasons mentioned earlier) one would expect a stiff material in the matrix to "shield" or block the influence of a softer inclusion material more than a soft material would be able to block the influence of a stiff material. Likewise, one would expect a stiff material inclusion to constrain the deformation of a softer matrix more than visa versa.

It is noted that the loss modulus of the composite with the stiff continuous phase shown in Figure 4.3 shows very clearly two distinct loss peaks, a main one due to the stiff matrix and a smaller one as the contribution from the soft inclusion. The loss modulus of the composite with the soft continuous phase (Figure 4.2) also shows two loss peaks; however, while the loss peak due to the soft matrix is distinct, the contribution from the stiff inclusion loss peak is somewhat obscured due to the fact that the loss modulus of the soft material itself has a slight second rise at approximately the same frequency as the stiff material. Later it will be shown that when the loss peaks of the stiff material and the soft material are separated farther in frequency than in this example, the second loss peak from the stiff inclusion is quite clear.

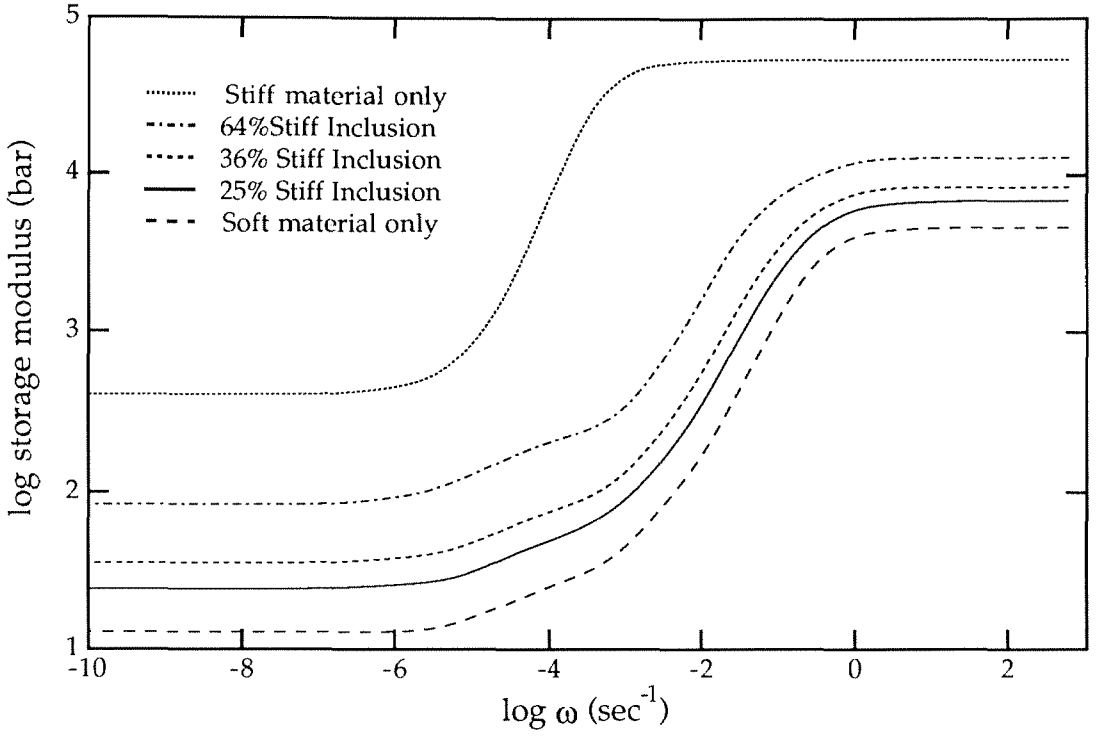

Figure 4.2a: Storage modulus of composite with soft (low modulus) matrix and stiff (high modulus) inclusions, at varying volume fractions

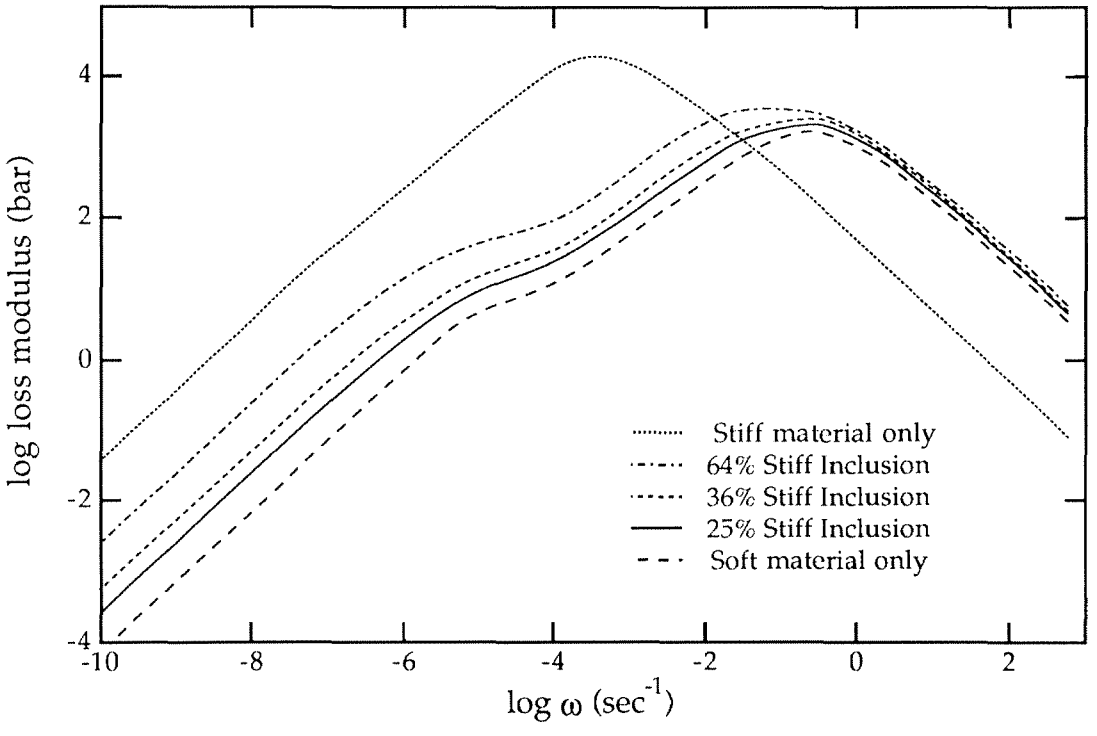

Figure 4.2b: Loss modulus of composite with soft (low modulus) matrix and stiff (high modulus) inclusions, at varying volume fractions

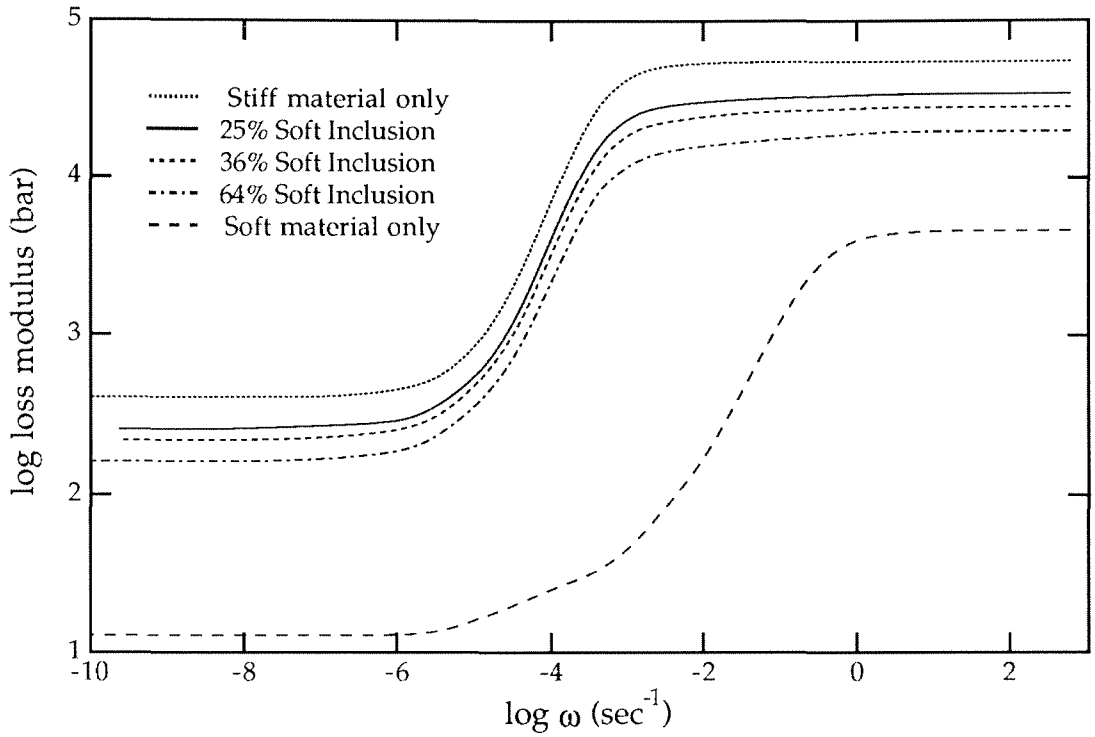

Figure 4.3a: Storage modulus of composite with stiff (high modulus) matrix and soft (low modulus) inclusions, at varying volume fractions

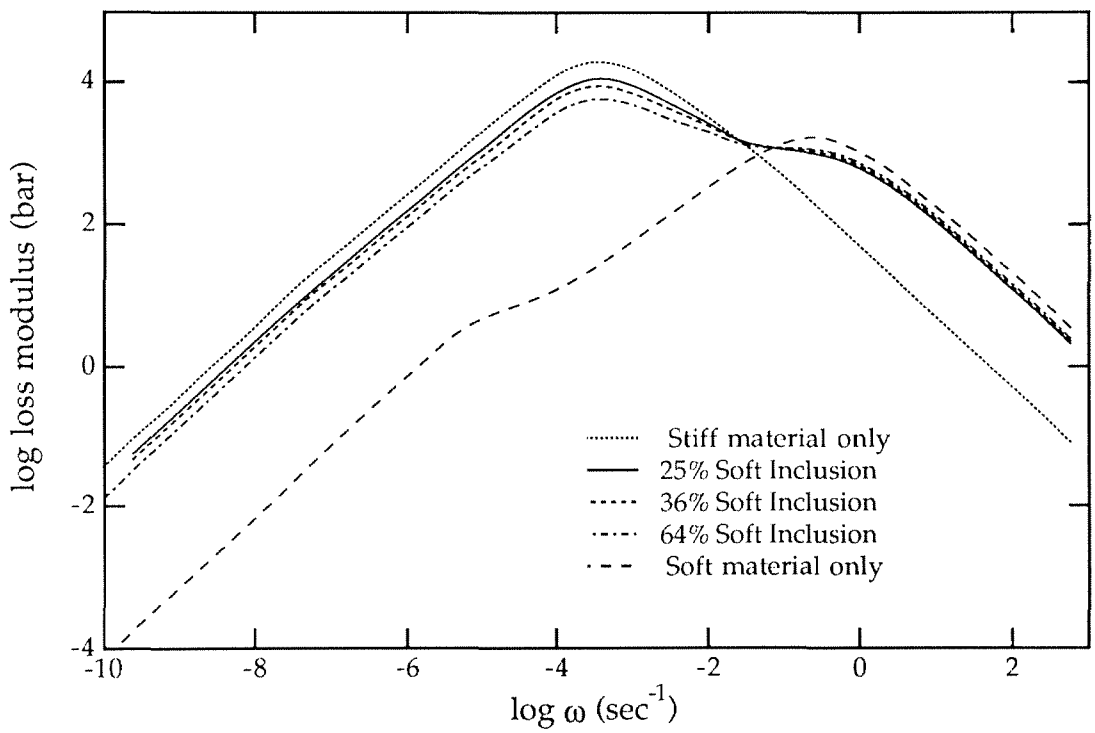

Figure 4.3b: Loss modulus of composite with stiff (high modulus) matrix and soft (low modulus) inclusions, at varying volume fractions

Unit Cells of the Same Volume Fraction: Comparison of Computational Results to Rule of Mixtures

The Rule of Mixtures commonly used to estimate the material properties of composite materials is based purely on the volume fractions and the material properties of the respective phases. For example, the Rule of Mixtures for the transverse modulus for unidirectional cylindrical inclusions in a matrix (which is the representation of the model in Figure 2.1) is given by[8]

$$\frac{1}{E_{comp}} = \frac{V_I}{E_I} + \frac{V_{II}}{E_{II}}, \tag{4.1}$$

where V_j and E_j are the volume fraction and modulus of phase j, and E_{comp} is the predicted modulus of the composite. Applying the correspondence principle, this is equivalent to

$$\begin{aligned} \frac{1}{E^*} &= \frac{V_I}{E_I^*} + \frac{V_{II}}{E_{II}^*} \\ \frac{1}{E' + iE''} &= \frac{V_I}{E_I' + iE_I''} + \frac{V_{II}}{E_{II}' + iE_{II}''}, \end{aligned} \tag{4.2}$$

which when solved for E' and E'' of the composite, yields formulas involving the products of quantities for the two phases. The formula for E' is shown here as an example:

$$E' = \frac{(E_I' E_{II}' - E_I'' E_{II}'')(V_1 E_{II}' + V_2 E_I') + (E_I' E_{II}'' + E_I'' E_{II}')(V_1 E_{II}'' + V_2 E_I'')}{(V_1 E_{II}' + V_2 E_I')^2 + (V_1 E_{II}'' + V_2 E_I'')^2} \tag{4.3}$$

From (4.1), and upon closer inspection also from (4.3) as well as the corresponding formula for the loss modulus of the composite, it is apparent that the Rule of Mixtures does not distinguish between which phase is in the inclusions or in the matrix for the same volume fraction of materials. Thus,

the Rule of Mixtures predicts the same composite moduli for stiff matrix/soft inclusions as for soft matrix/stiff inclusions for fixed volume fractions.

As an example, consider the case of 36% stiff material and 64% soft material in the composite of Figure 2.1. The complex Young's moduli calculated from the numerical procedure for both the composite with the 36% stiff material in the inclusion and the composite with the 36% stiff material in the matrix are given in Figure 4.4. Note that there is actually a great difference between the moduli of these two cases, greater than a 50% difference at some frequencies on the scale of the plots and upon conversion to the real modulus from the log modulus, the difference exceeds 90%. As illustrated earlier, the composite with the 36% stiff material in the matrix has moduli dominated in magnitude and form by the stiff material, whereas the composite with the 36% stiff material in the inclusion has moduli dominated in magnitude and form by the soft matrix material. Figure 4.5 shows the Rule of Mixtures result, which is the same for these two cases, along with the numerical results. From this comparison, it is evident that the Rule of Mixtures is inadequate for general prediction of multi-phase viscoelastic composite properties. The Rule of Mixtures best approximates the modulus for the stiff inclusions in a soft matrix (both in magnitude and shape), for the particular properties used here, although the magnitude of the modulus is underestimated in both cases.

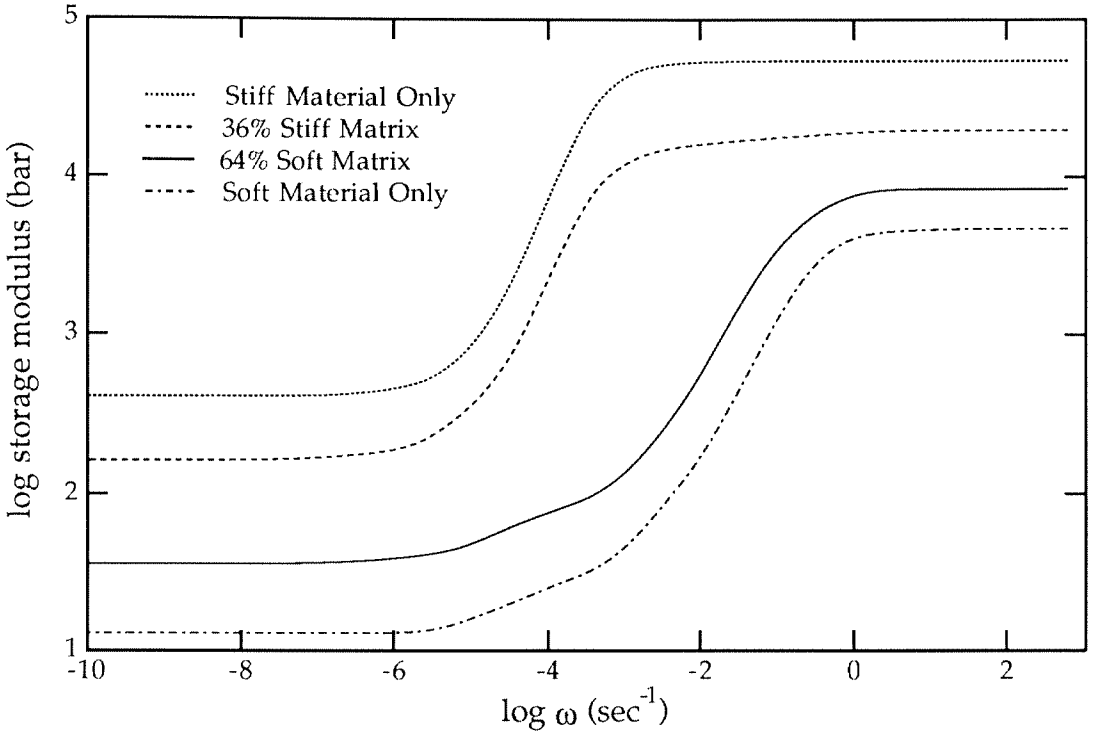

Figure 4.4a: Comparison of storage moduli for same volume fractions of materials: 36% Stiff, 64% Soft

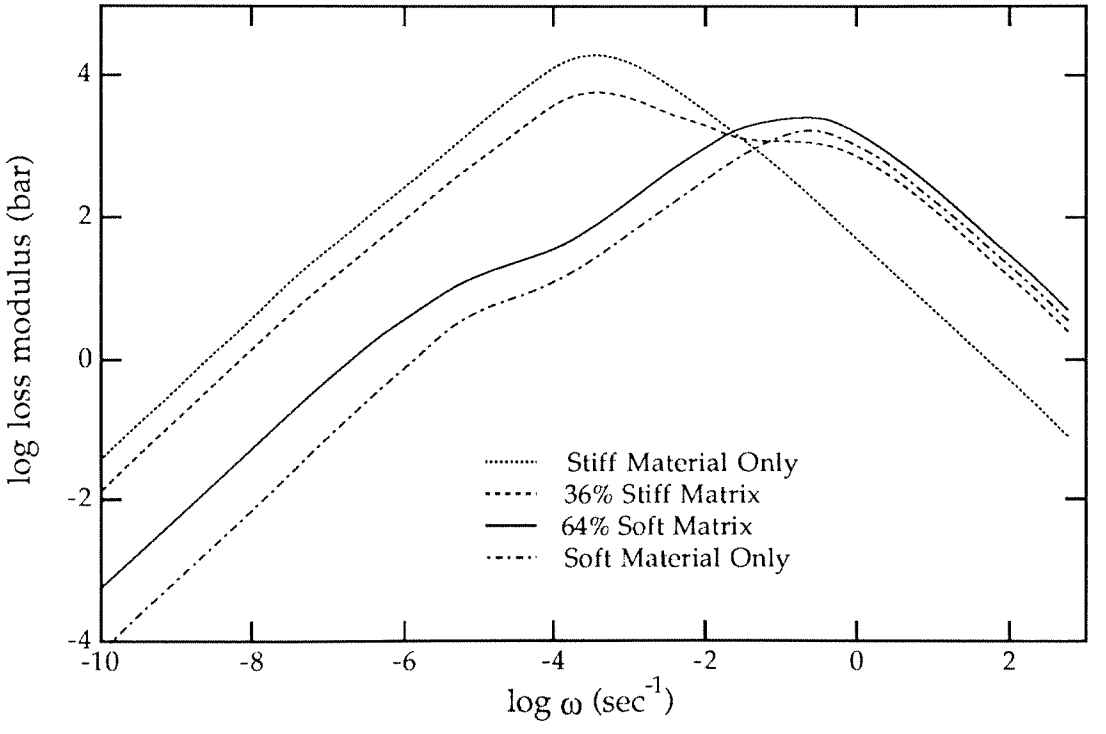

Figure 4.4b: Comparison of loss moduli for same volume fractions of materials: 36% Stiff, 64% Soft

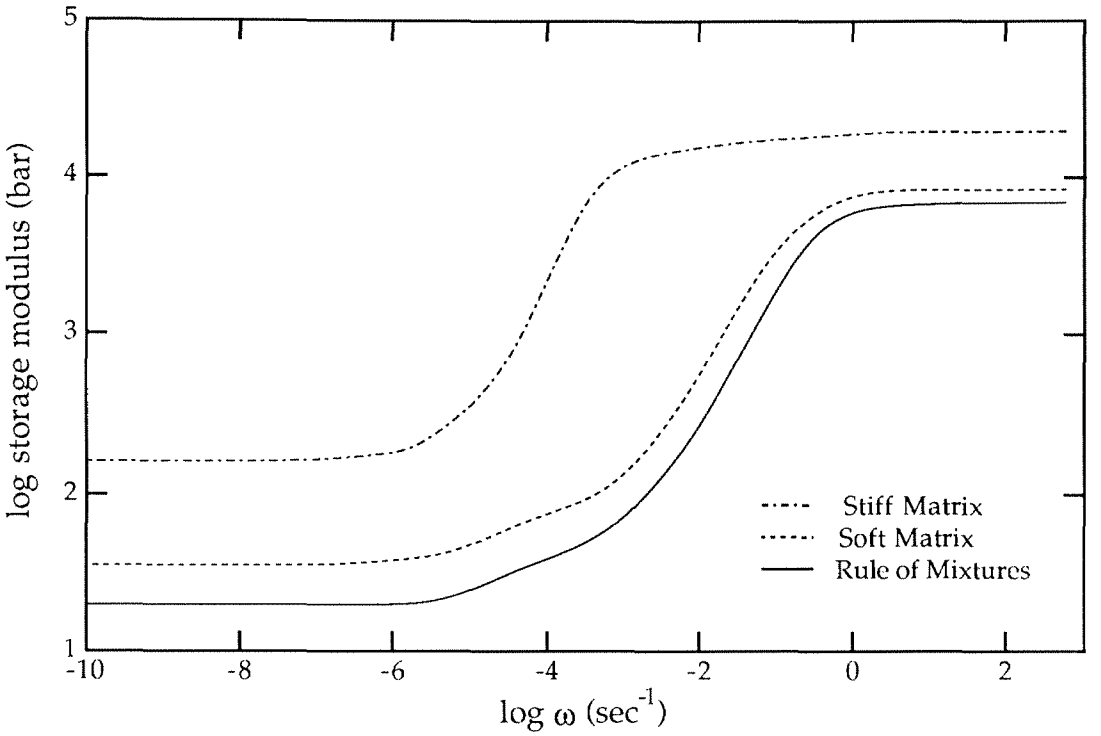

Figure 4.5a: Comparison of storage moduli of composite with 36% stiff material with rule of mixtures

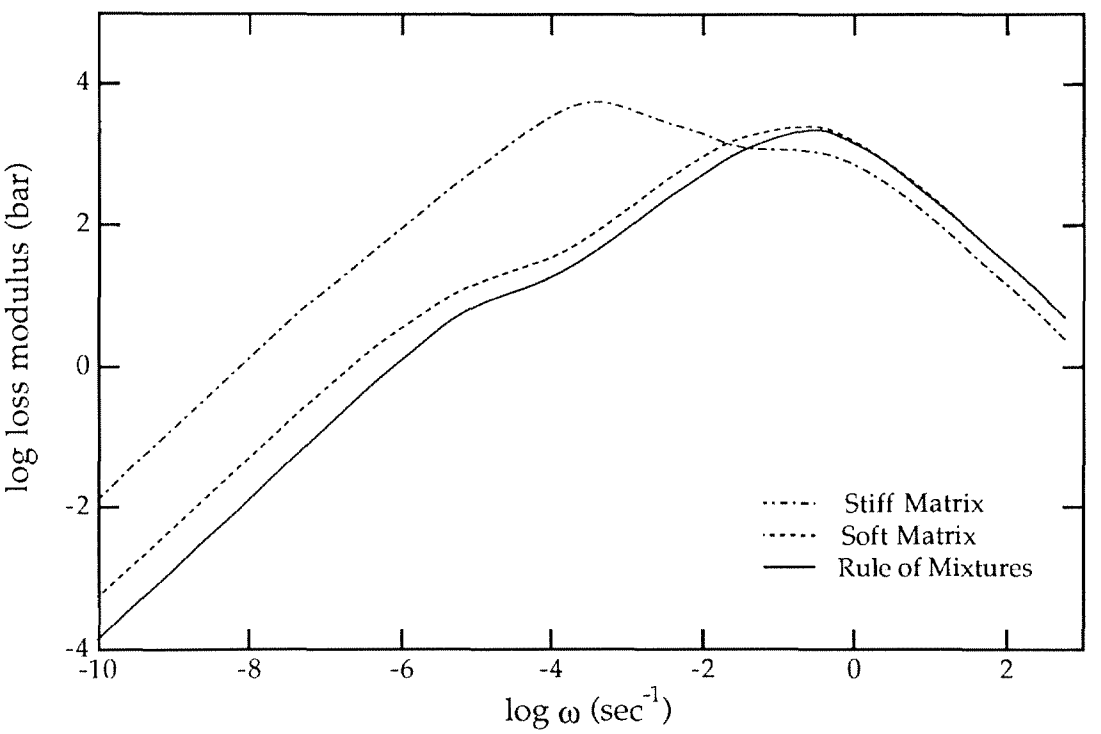

Figure 4.5b: Comparison of loss moduli of composite with 36% stiff material with rule of mixtures

V. SIMPLE SHEAR DEFORMATIONS

Derivation of boundary conditions

The procedure for determining the global moduli of a viscoelastic composite material comprised of an array of inclusions was developed in earlier sections for the case of uniaxial tension, to produce a global Young's modulus for the material. The same computational procedure is applicable to the determination of any modulus, under the following limitations: 1) The boundary value problem to obtain the effective modulus from the global material must be describable in two-dimensional plane-strain. 2) An appropriate set of boundary conditions must be derivable for the unit cell, which simulates the action of the boundaries of the unit cell when the global material is subjected to the boundary value problem to attain the modulus.

The boundary value problem for the unit cell in the case of a uniaxial extension to determine Young's modulus on the global material was formulated in Section II. The in-plane shear modulus for the composite material can be determined in a somewhat different fashion. Simply considering the global material from Figure 2.1 subjected to simple shear does not intuitively lead to boundary conditions for the unit cell as in the uniaxial tension case. It is not clear *a priori* what the deformations are or what tractions act along the boundaries of a unit cell.

To determine the proper boundary conditions for the unit cell under shear deformation, it is necessary to recall that the material being considered is globally homogeneous and that there exists an alternative representation for pure shear. In homogeneous materials, the state of stress at any point obtained by applying shear tractions to all four boundaries as in Figure 5.1a is

equivalent to the state of stress of any point in Figure 5.1b in a 45° rotated reference frame (x'-y'), where tension is applied in the y-direction and compression in the x-direction.

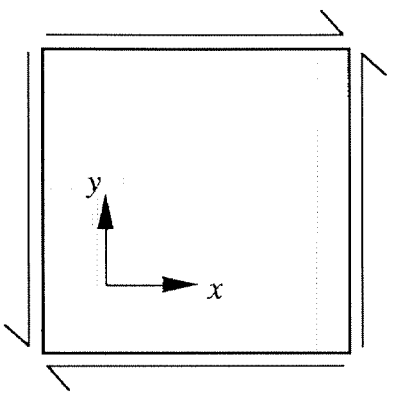

Figure 5.1a: Pure Shear, shear tractions applied

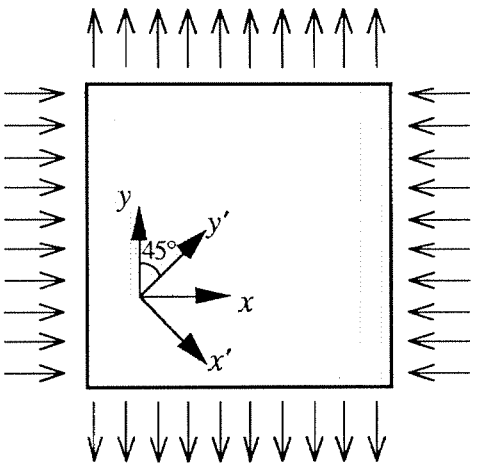

Figure 5.1b: Pure Shear, tensile and compressive tractions applied

Therefore, for the globally homogeneous material considered in this study, a state of pure shear (Figure 5.2) may also be attained by applying orthogonal tensile and compressive tractions. When considering the situation depicted in Figure 5.3, it is clear that by viewing a rotated unit cell at the angle of the loading, the boundary conditions on that unit cell are quite similar to those for uniaxial tension. The boundary conditions on the rotated unit cell (Figure 5.4) that are equivalent to studying the entire body in a state of pure shear are:

$$
\begin{aligned}
&\text{on } y'=L1: && \text{uniform displacement } \bar{u}_{y'} = u_0 \\
& && \text{Shear traction } \bar{T}_{x'} = 0 \\
&\text{on } x'=L1: && \text{uniform displacement } \bar{u}_{x'} = -u_0 \\
& && \text{Shear traction } \bar{T}_{y'} = 0 \\
&\text{on } y'=0: && \text{uniform displacement } \bar{u}_{y'} = 0 \\
& && \text{Shear traction } \bar{T}_{x'} = 0 \\
&\text{on } x'=0: && \text{uniform displacement } \bar{u}_{x'} = 0 \\
& && \text{Shear traction } \bar{T}_{y'} = 0
\end{aligned}
\qquad (5.1)
$$

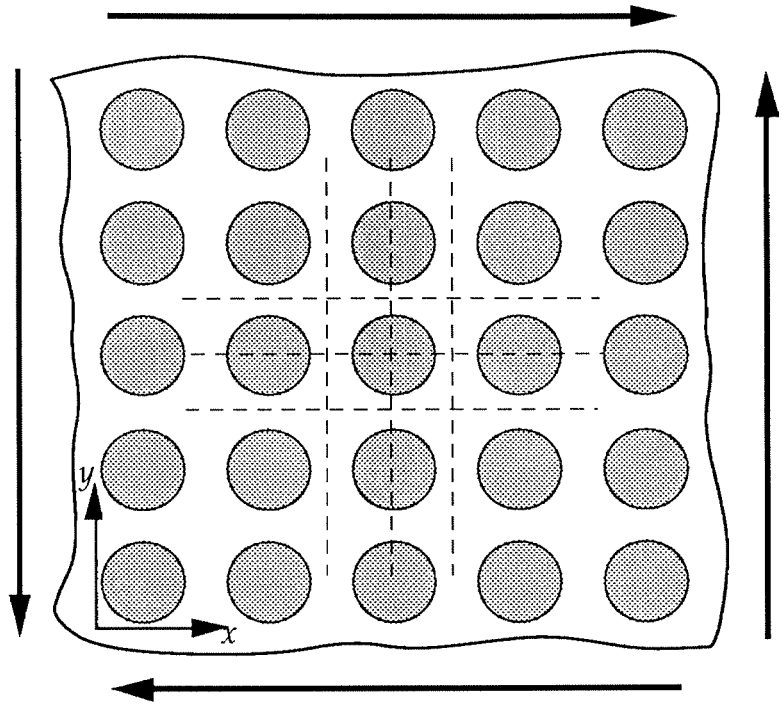

Figure 5.2: Pure Shear on Composite Material, shear displacements applied

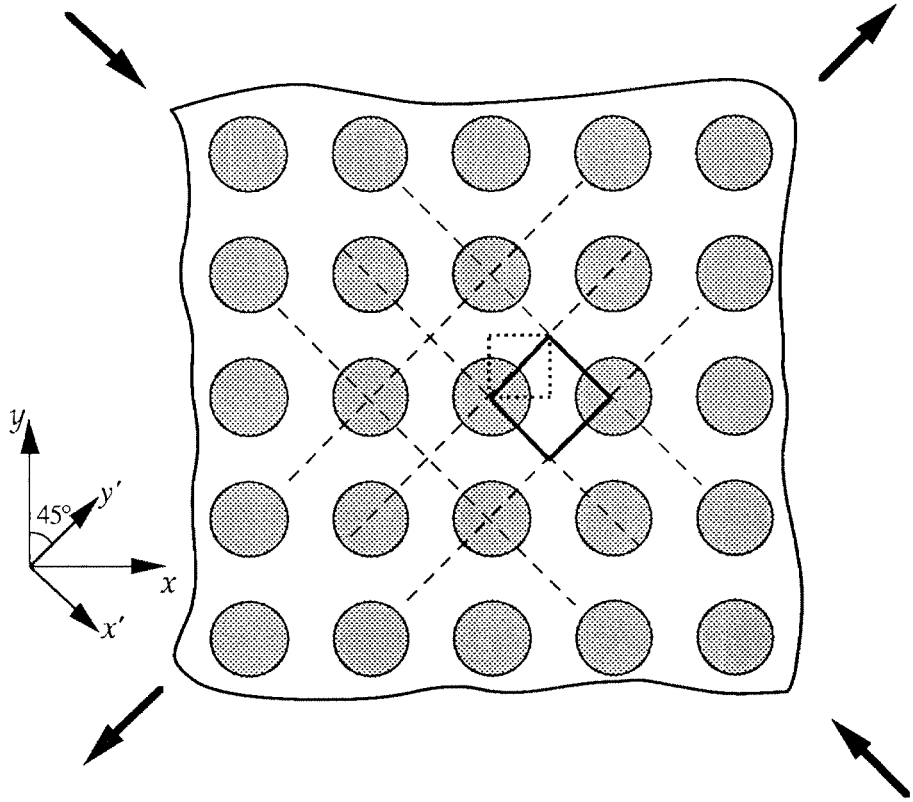

Figure 5.3: Pure Shear on Composite Material, tensile and compressive displacements applied. Repeating rotated unit cell is in bold. Original unit cell in dotted lines.

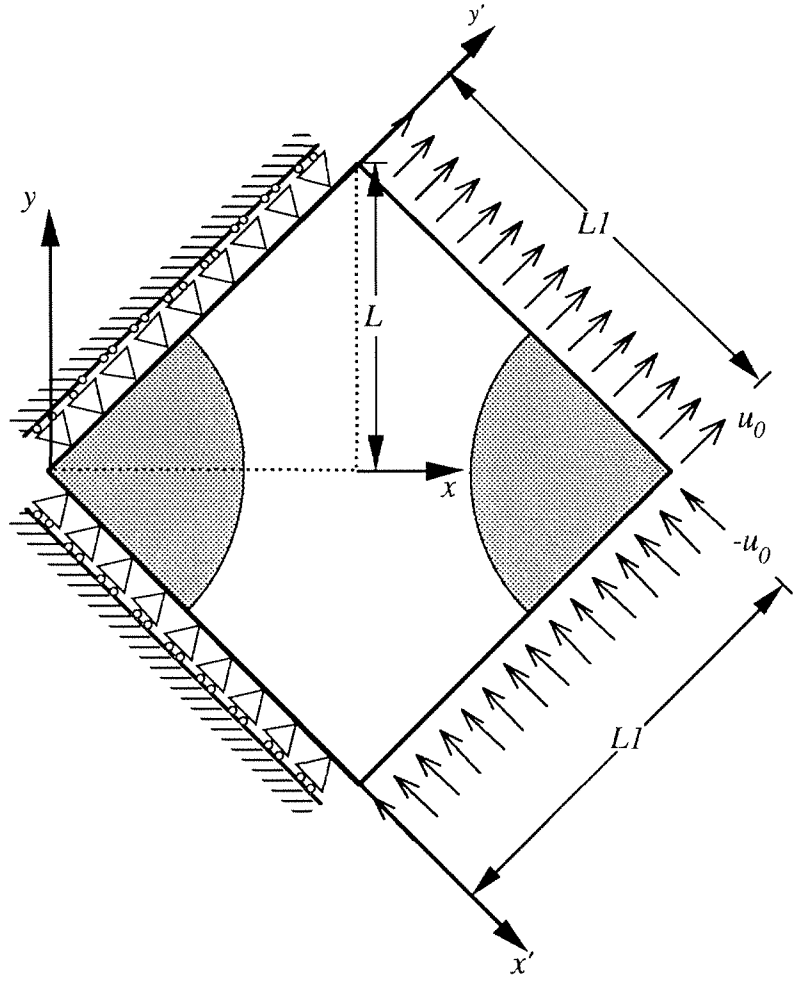

Figure 5.4: Rotated Unit Cell from Figure 5.2. Original unit cell boundaries in dotted lines.

It would now be possible to use this rotated unit cell to determine the global shear modulus for the composite. However, by examining the deformations and the nodal reaction forces along the dashed boundaries in Figure 5.4, which correspond to the boundaries of the original (un-rotated) unit cell, a clear set of boundary conditions for the original unit cell appear. After subtracting a rigid rotation from the pure shear results (and neglecting small second order effects), the boundary conditions for the original unit cell (Figure 5.5) corresponding to the global material in simple shear are determined to be:

$$
\begin{aligned}
&\text{on } y{=}L: && \text{uniform displacement } \bar{u}_x = u_0 \\
& && \text{Normal traction } \bar{T}_y = 0 \\
&\text{on } x{=}L: && \text{uniform displacement } \bar{u}_y = 0 \\
& && \text{Normal traction } \bar{T}_x = 0 \\
&\text{on } y{=}0: && \text{uniform displacement } \bar{u}_x = 0 \\
& && \text{Normal traction } \bar{T}_y = 0 \\
&\text{on } x{=}0: && \text{uniform displacement } \bar{u}_y = 0 \\
& && \text{Normal traction } \bar{T}_x = 0
\end{aligned}
\tag{5.2}
$$

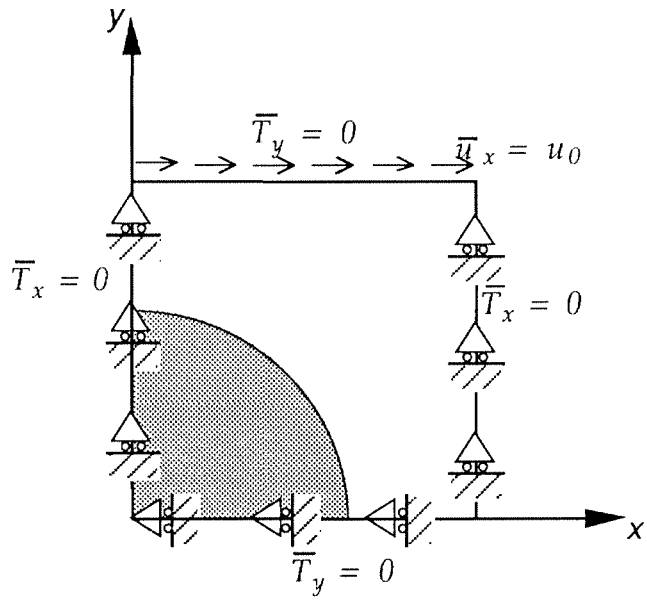

Figure 5.5: Boundary conditions for original unit cell in simple shear

The original unit cell subject to the determined boundary conditions in equation (5.2) was then used in the subsequent analysis to determine the shear modulus of the composite. Analogous to the methods described for uniaxial tension, the global composite shear modulus can be determined from the average resulting deformations of the unit cell subjected to (5.2) via

$$
\frac{\bar{\sigma}_{xy}\big|_{avg}(\omega)}{\gamma} \equiv i\omega\bar{G}(\omega) = G^*(\omega) \tag{5.3}
$$

Here, γ is defined to be the average applied change of angle that the global material experiences, $\gamma \equiv \frac{u_0}{L}$, and $\bar{\sigma}_{xy}\big|_{avg}(\omega)$ is the resulting nodal average shearing stress in the unit cell along $y=L$.

Shear modulus: Results

The shear modulus of the composite material with the individual phase properties again defined by Figure 4.1 was determined by the procedure of the preceding sub-section. The results for the shear modulus are consistent with those for the Young's modulus and therefore only one set of results are shown here. Figure 5.6 contains the values of the storage and loss components of the shear modulus for the composite with a 25% volume fraction of the stiff material in the inclusion. Also shown on the figures are the storage and loss components of the shear moduli for the individual phases. As in the case with Young's modulus, the matrix behavior dominates the behavior of the composite although the change in shear modulus due to the presence of another phase is less dramatic.

The deformation of the boundaries of the unit cell is of interest in the shear case, since the normal displacement on each boundary is not completely known *a priori*. Figure 5.7 contains the real displacements of the deformed mesh, exaggerated for presentation purposes. These results show that the boundaries of the unit cell do not remain straight in the case of shear.

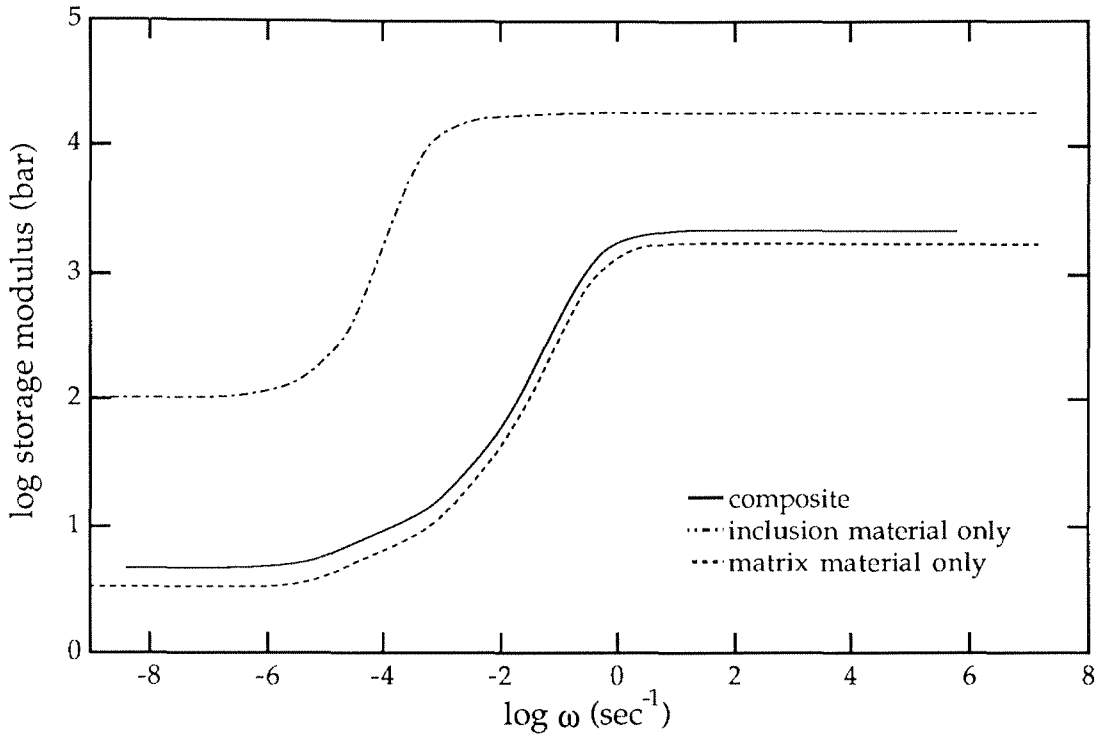

Figure 5.6a: Shear storage moduli for composite material and constituent phases

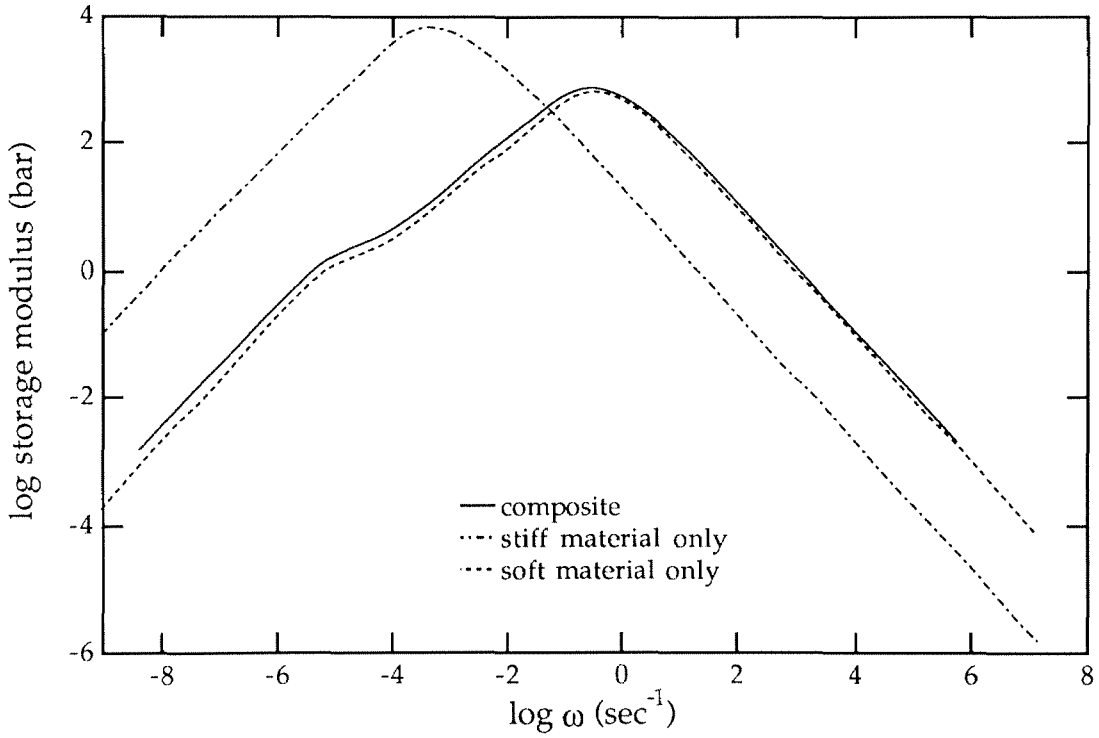

Figure 5.6b: Shear loss moduli for composite material and constituent phases

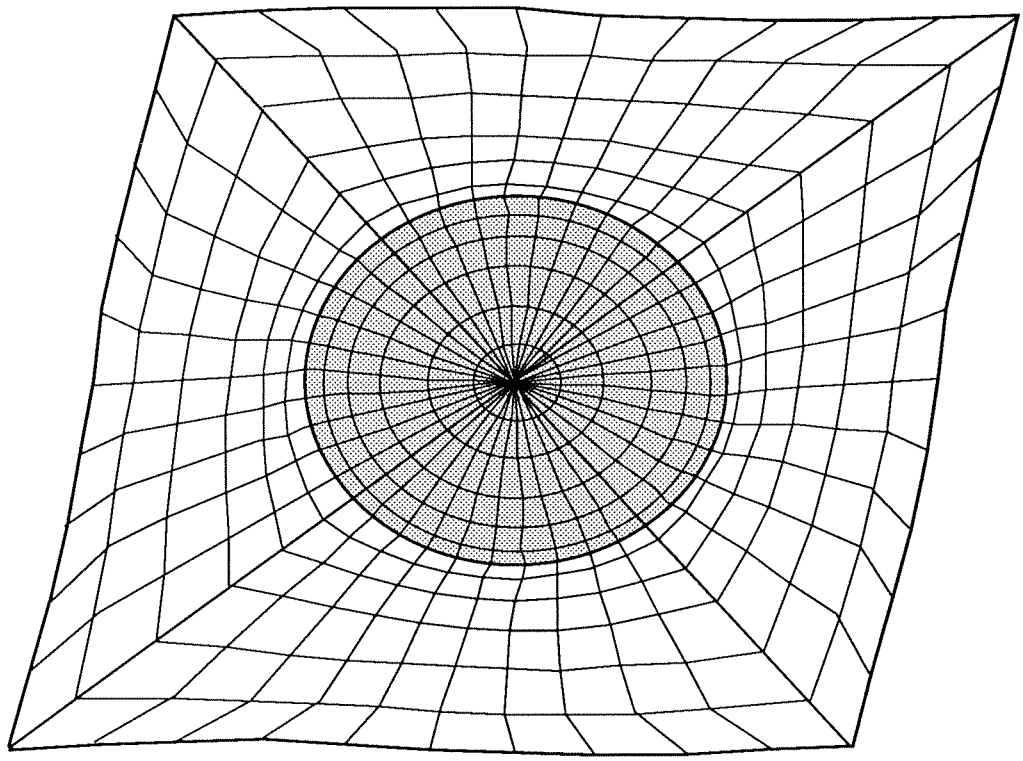

Figure 5.7: Deformed mesh for unit cell showing real components of displacements

A Measure of Anisotropy

As mentioned in Section II the composite material under consideration is globally homogeneous, but not globally isotropic. The anisotropy is also apparent from the necessity to examine a different unit cell in x'-y' reference frame than in the x-y frame. What is not obvious, however, is the degree of anisotropy of the material. One method by which to ascertain the extent of influence of the anisotropy on the composite properties is to compare the shear modulus obtained from the boundary value problem described in this section with the shear modulus obtained from the isotropic relation of Young's modulus and Poisson's ratio, where these two quantities are determined from the results obtained for uniaxial tension.

The definition of Poisson's ratio for an orthotropic material, in the Fourier domain, is

$$\bar{\nu}_{yx} = -\frac{\bar{\varepsilon}_x}{\bar{\varepsilon}_y} \tag{5.4}$$

where $\bar{\varepsilon}_x$ and $\bar{\varepsilon}_y$ are the strains resulting from a uniaxial tension test. Poisson's ratio may be determined for the composite material from the uniaxial tension results via (5.4) simply by calculating the ratio of the average x-strain along the x=L boundary, $\bar{\varepsilon}_x = \frac{\bar{b}}{L}$, and the average y-strain along the y=L boundary $\bar{\varepsilon}_y = \frac{u_0}{L}$.

Thus, for the composite material of the same phase properties as before, the Young's modulus was determined from the boundary value problem for uniaxial tension, the Poisson's ratio was determined in the manner just described, and the Shear modulus was determined from the solution to the

shear boundary value problem and equation (5.3). Then, the "isotropic shear modulus", $\bar{G}^i$, was determined via the isotropic relation:

$$\bar{G}^i = \frac{\bar{E}}{2(1+\bar{\nu})} \tag{5.5}$$

The example was performed on a composite with an inclusion volume fraction of 25% and the results for the Young's modulus and shear modulus are contained in Figure 4.2 and Figure 5.6 respectively. The Poisson's ratio is shown in Figure 5.8. Note that as with all other calculations, the Poisson's ratio determined is the plane-strain Poisson's ratio; with this consideration, the limit values for the glassy and rubbery response regions are as expected. The non-plane-strain Poisson's ratio, $\bar{\nu}$, is calculated from $\bar{\nu} = \frac{\bar{\nu}_{pl-\varepsilon}}{\bar{\nu}_{pl-\varepsilon}+1}$, where $\bar{\nu}_{pl-\varepsilon}$ is the plane-strain Poisson's ratio; this equation for conversion of plane-strain and non-plane-strain quantities is the same for isotropic materials and the square-symmetric material considered here. The non-plane-strain Poisson's ratio is shown on the plot with the plane-strain values for comparison. Again, the glassy and rubbery responses are reasonable, approaching unity low frequencies. The comparison of the shear modulus and its isotropic approximation is shown in Figure 5.9. There is a clear difference between the two, the isotropic approximation overpredicting the actual value at all frequencies. However, the magnitude of the difference between the shear modulus and the isotropic shear modulus is only about 20% at the worst case for this particular example. While 20% is certainly significant, this observation indicates still that anisotropic effects are not overwhelming and that isotropic approximations could be made as rough estimates for this composite material. Another measure of anisotropy is presented in Section VIII and the effect of anisotropy on the TRC behavior of the composite is discussed at that time.

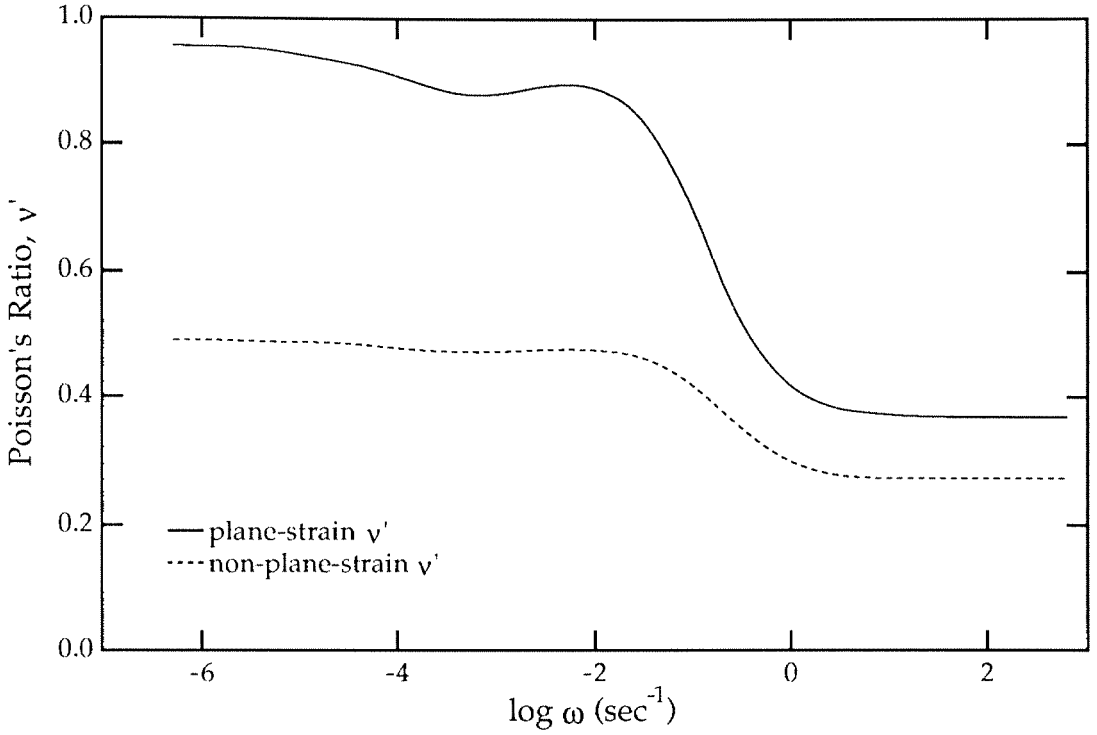

Figure 5.8a: Real part of complex Poisson's Ratio, plane-strain and non-plane-strain values

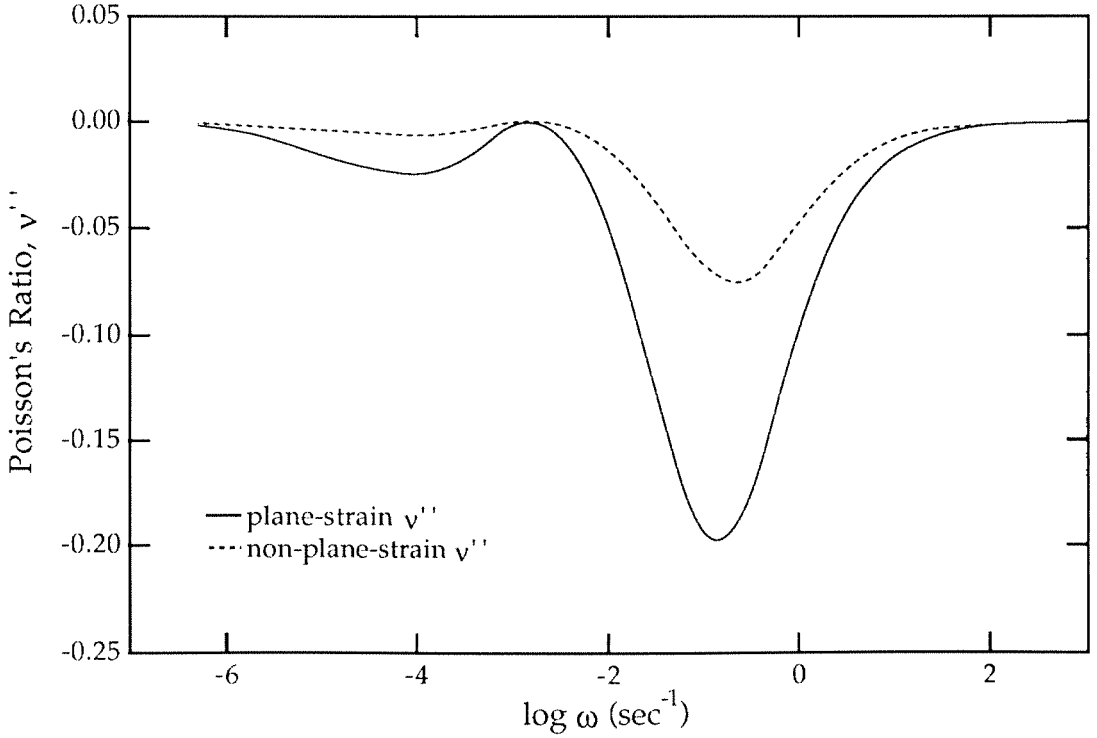

Figure 5.8b: Imaginary part of complex Poisson's Ratio, plane-strain and non-plane-strain values

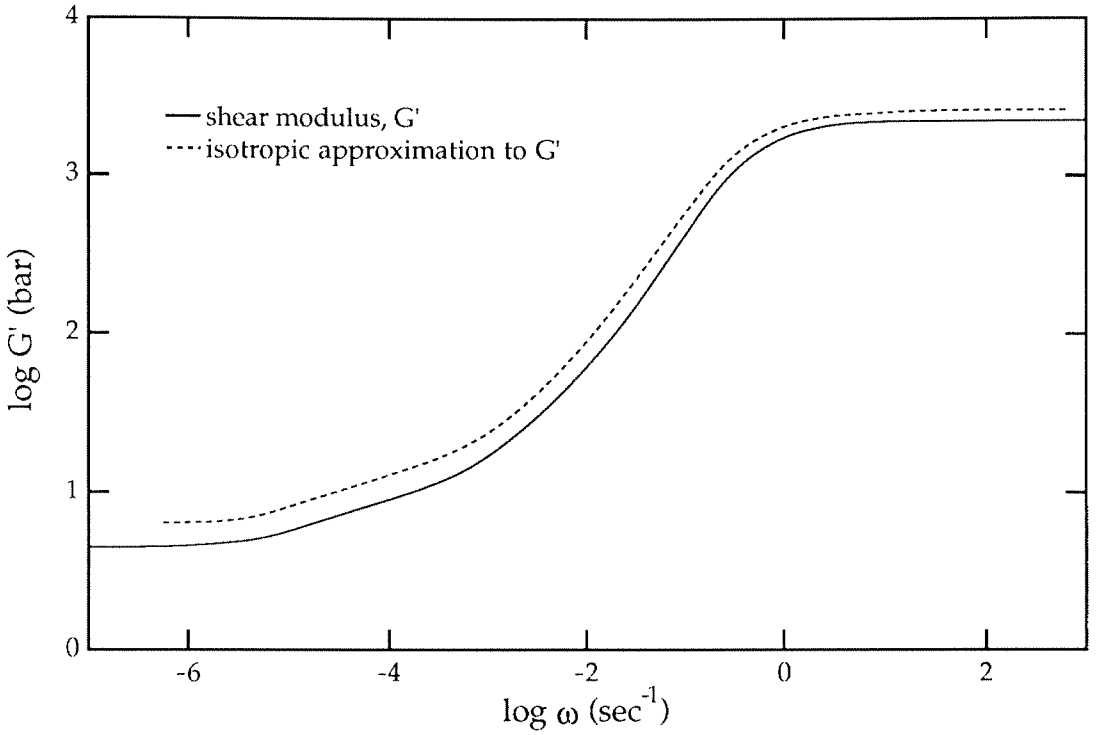

Figure 5.9a: Comparison of shear storage modulus for composite and the isotropic approximation to the shear modulus predicted from Young's modulus and Poisson's Ratio

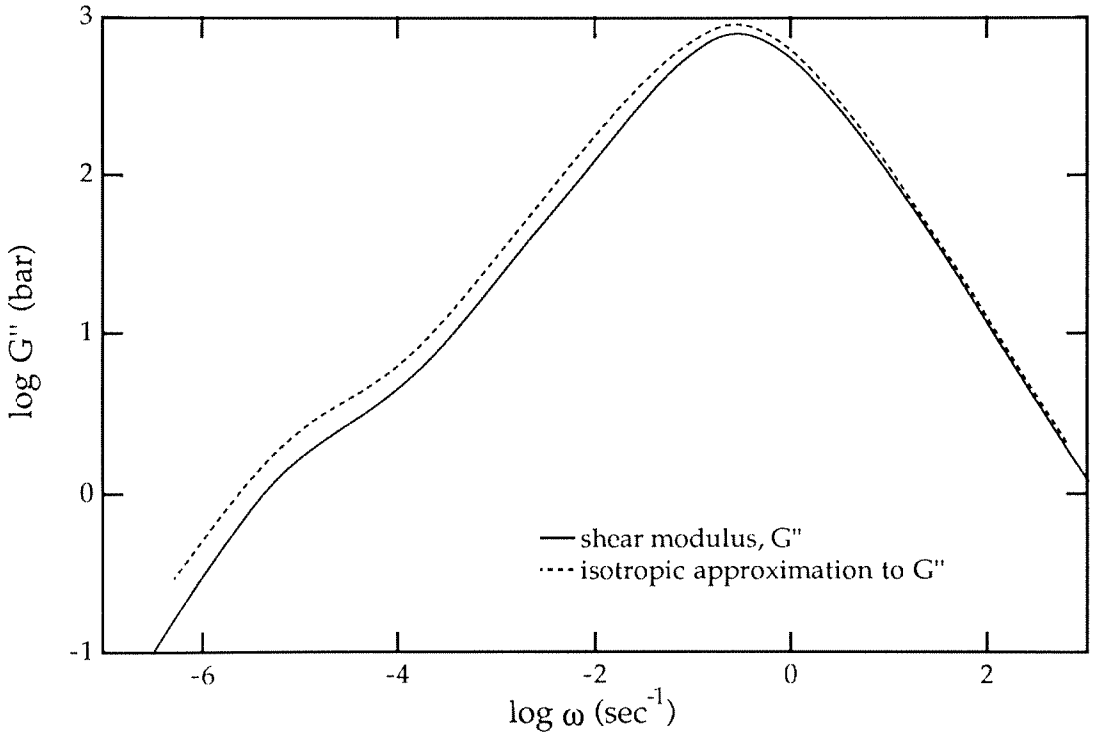

Figure 5.9b: Comparison of shear loss modulus for composite and the isotropic approximation to the shear modulus predicted from Young's modulus and Poisson's Ratio

VI. THERMOMECHANICAL RESULTS

As discussed in the Introduction Section, many homogeneous polymers have been shown to be thermorheologically simple materials that permit time-temperature interchange. The amount of shift of modulus properties at one temperature along the log-time axis necessary to obtain the corresponding properties of the material at a new temperature is called the shift factor, a_T. The empirically determined shift factor can be represented as a continuous function of temperature through the general form of the WLF equation[4]

$$\log a_T = -\frac{c_1^0(T - T_0)}{c_2^0 + T - T_0}, \tag{6.1}$$

where the parameters c_1^0 and c_2^0 are related to the free volume of the polymer and are dependent on the chosen reference temperature T_0. For example, the shift factor for low molecular weight polystyrene shown in Figure 1.3 displays both the empirically determined shift factor, calculated from Figures 1.1 and 1.2, and the resulting WLF equation shift factor, where the free volume constants determined are indicated on Figure 1.3.

Since each phase in the composite studied here is considered to be a thermorheologically simple material, the modulus functions and WLF parameters are known at their reference temperatures and can be used via (6.1) to determine the modulus functions of each phase at any desired temperature. The numerical analysis developed in this work makes use of this procedure in shifting the individual phase data to obtain the average effective complex modulus of the composite at any temperature. The usual relatively small vertical shift for the density and entropic correction ($\frac{T\rho}{T_0\rho_0}$) is also applied to

each phase in the same manner. This vertical shift is applied over the whole frequency range as a multiplicative factor to the value of the modulus itself.

It should be noted that the formulation of the finite element analysis does not address the dilatational effects of thermal expansion for the materials studied. Changing the temperature of the composite will cause a constant pre-stressed state in the material. One is concerned in this study only with perturbations from that state for modulus determination. Also all points in the composite are held to be at the same constant temperature for the calculation of the moduli as functions of frequency. Energy dissipation effects in the form of heat are neglected.

Limit Case: Elastic Inclusion

For clarity in explanation of later results, it is prudent to first examine a limit case of the general problem in which one of the phases is elastic. In this event, only one of the materials in the composite has properties that vary with time and temperature. Therefore the relaxation mechanisms of the viscoelastic phase will also be those of the composite. Using the shift factor concepts, one can plainly show this equivalence by considering the composite material at two different temperatures, T_1 and T_2. Letting P_e denote the properties of the elastic phase and $P_v(t,T)$ denote the properties of the viscoelastic phase as a function of time t and temperature T, one can define the properties of the composite, P_{comp}, at T_1 and T_2 as an unknown function of the individual phase properties

$$\begin{aligned} P_{comp}(t,T_1) &= \mathcal{F}(P_e, P_v(t,T_1), B) \\ P_{comp}(t,T_2) &= \mathcal{F}(P_e, P_v(t,T_2), B), \end{aligned} \tag{6.2}$$

where the parameter B represents all other factors of the geometry and the loading lumped together. But, for the viscoelastic phase with a shift factor $a_T = a_T(T_2,T_1)$, it is known that the properties at T_1 are related to the properties at T_2

$$P_v(t,T_2) = P_v(ta_T,T_1) \tag{6.3}$$

Thus, the properties for the composite at T_2 can also be written

$$P_{comp}(t,T_2) = \mathcal{F}(P_e,P_v(ta_T,T_1),B) \tag{6.4}$$

In fact, comparing (6.4) to (6.2), it is clear that the composite properties at any temperature are related to its properties at any other temperature through the same time shift factor as that for the viscoelastic material:

$$P_{comp}(t,T_2) = P_{comp}(ta_T,T_1) \tag{6.5}$$

Thus the majority of the thermorheological behavior of a viscoelastic composite with only one viscoelastic phase is identical to that of its viscoelastic component. The small density and rubbery entropic contributions to the thermorheological variation in properties, however, cannot be shown to be identical in the composite and its viscoelastic constituent. In fact, because the change in properties due to density and rubbery entropic behavior is manifested as a multiplicative factor to the properties themselves, for any random unknown function of the phase properties as in (6.2), the density and rubbery entropic behavior with temperature will be different in the composite from that in the pure viscoelastic phase. Fortunately, the effects of these vertical corrections are less than 1% of the modulus values for a given temperature change and therefore, for all practical purposes, the time-temperature behavior of a viscoelastic composite with only one viscoelastic phase will be the same as the time-temperature behavior of its viscoelastic phase.

As an example, consider the Young's modulus of the composite of previous sections, represented by the unit cell in Figure 2.2, with the "soft" viscoelastic material in the matrix, but replacing the "stiff" viscoelastic inclusion with an elastic inclusion with a shear modulus of $G=300\ bar$, and bulk modulus of $K=10{,}000\ bar$. The volume fraction of the stiff elastic inclusion is taken to be 25%. Only the example of elastic inclusions in a viscoelastic matrix will be presented here; the corresponding case of an elastic matrix with viscoelastic inclusions is comparable. The density for the "soft" viscoelastic phase is taken to be $\rho_0=1.2\ g/cc.$ at $T_0=300\ K$ and its variation with temperature is taken to follow

$$\rho(T) = \frac{\rho_0}{1+3\alpha(T-T_0)} \tag{6.6}$$

where α is the thermal coefficient of expansion and is taken to be 6.0×10^{-4}. The shift factor for the "soft" matrix phase is represented by the WLF equation (6.1) with constants $c_0=16$ and $c_1=110$. A plot of this shift factor's variation with temperature is shown later in Figure 6.4 along with a shift factor for the "stiff" viscoelastic phase.

Shown in Figures 6.1 and 6.2 are the storage and loss Young's moduli of this composite material at two different temperatures, 0° and 27°C. The complex Young's moduli of the viscoelastic matrix and the constant Young's modulus of the elastic inclusion are also given for comparison. It should be noted that the constant elastic modulus is a degenerate case of complex modulus where the real part is constant with frequency and the imaginary part is zero.

Figure 6.3 contains the storage and loss moduli of the composite where the 0°C curve has been shifted with the free volume shift factor a_T and the rubbery entropic correction $(\frac{T\rho}{T_0\rho_0})$ of the matrix material to 27°C. The result af-

firms the earlier proof that the time-temperature behavior of the composite with only one viscoelastic phase is identical to the time-temperature behavior of its viscoelastic phase alone. The time-temperature shift factor of the matrix material, when applied to the composite modulus at one temperature to attain the modulus at another temperature, provides perfect superposition of the two curves along the log time axis: the curves for 0° shifted to 27° coincides on the log time scale exactly with the calculated 27° curves. Also as predicted, the small vertical rubbery entropic correction for predicting the modulus curve at one temperature from another temperature is not the same for the viscoelastic phase and the composite. The vertical shift factor of the matrix material, when applied to the composite modulus at one temperature to attain the modulus at another temperature does not permit perfect superposition: there is a small vertical mismatch between the 0° storage modulus curve shifted to 27° and the calculated 27° curve. This mismatch is less than 1% of the modulus values, confirming that the effect of temperature on the amplitude of the modulus is relatively small. Therefore when dealing with composites of only one viscoelastic phase it is acceptable, for all practical purposes, to assert that the relaxation mechanisms and the behavior of the material with time and temperature is that of the viscoelastic phase alone. There will be multiple reference to this result later on in this work.

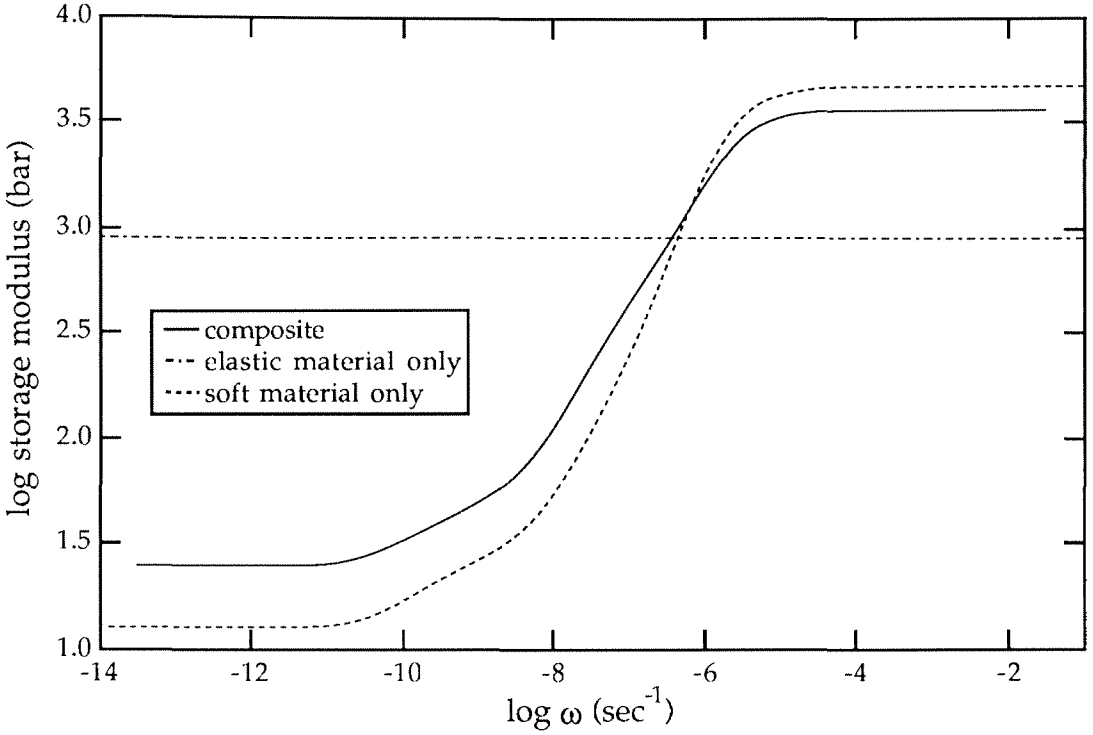

Figure 6.1a: Storage modulus for composite with elastic inclusion at 0°C

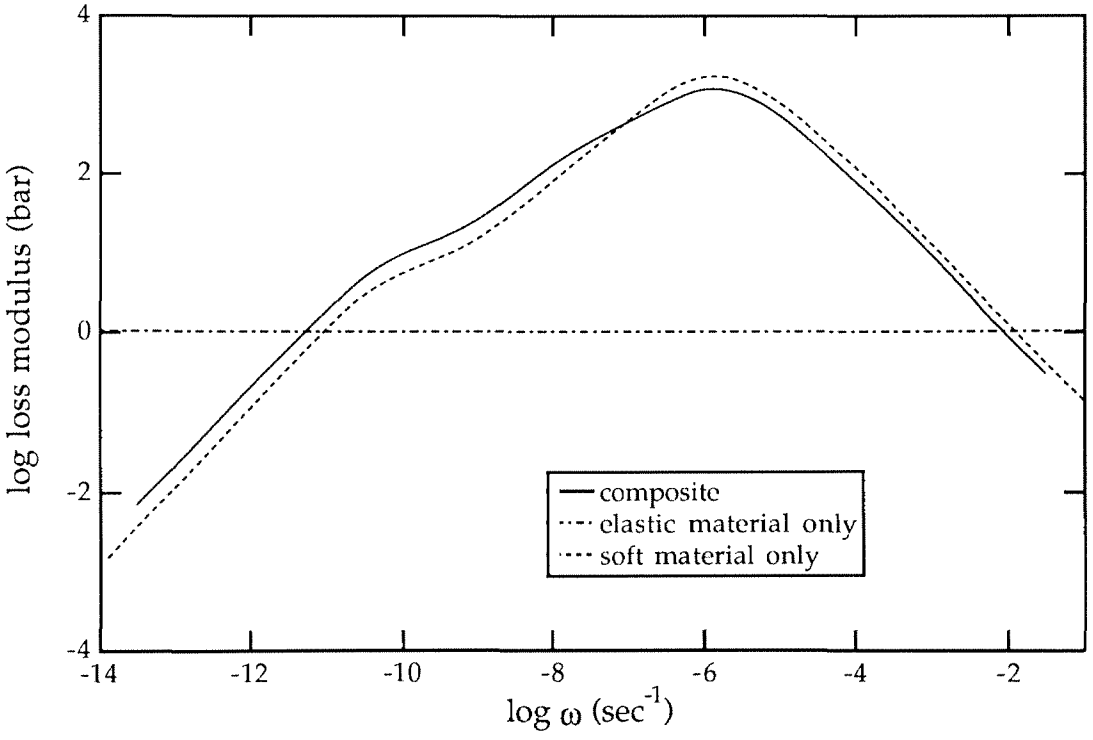

Figure 6.1b: Loss modulus for composite with elastic inclusion at 0°C

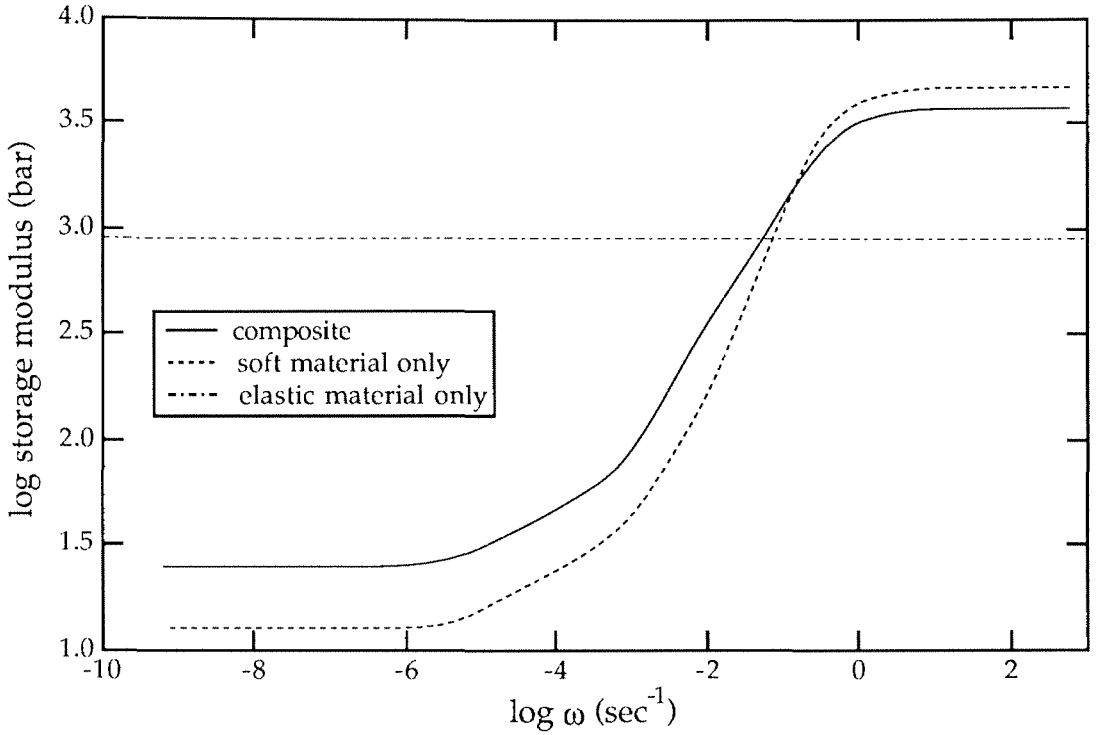

Figure 6.2a: Storage modulus for composite with elastic inclusion at 27°C

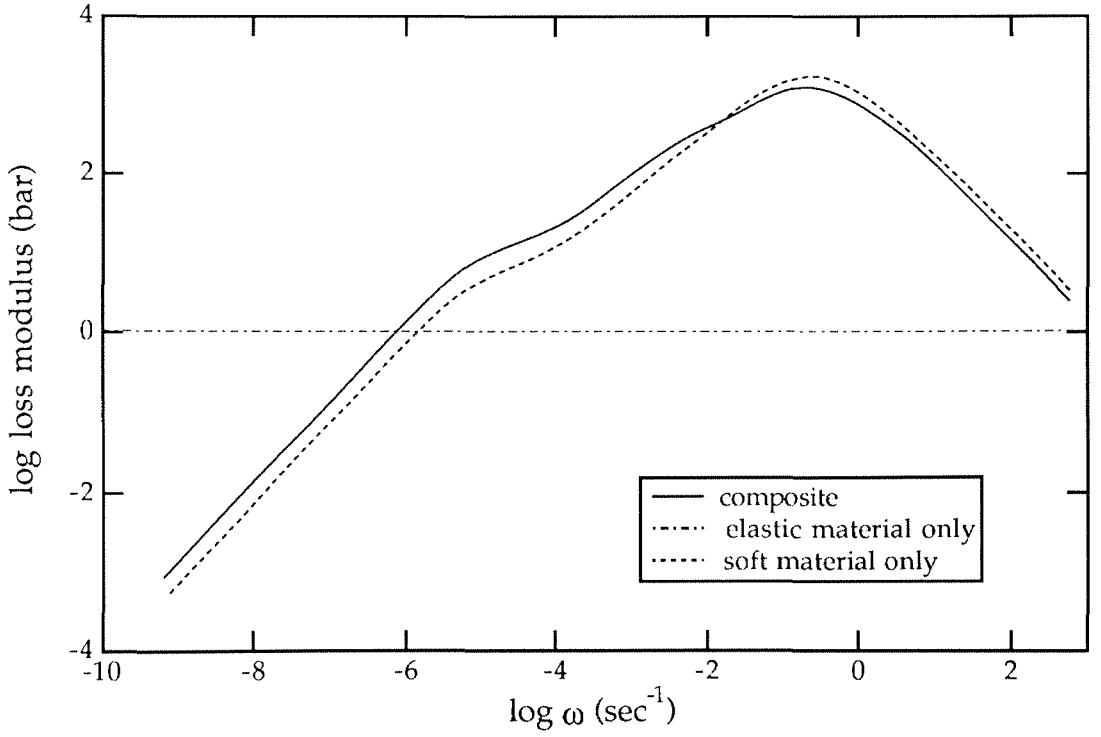

Figure 6.2b: Loss modulus for composite with elastic inclusion at 27°C

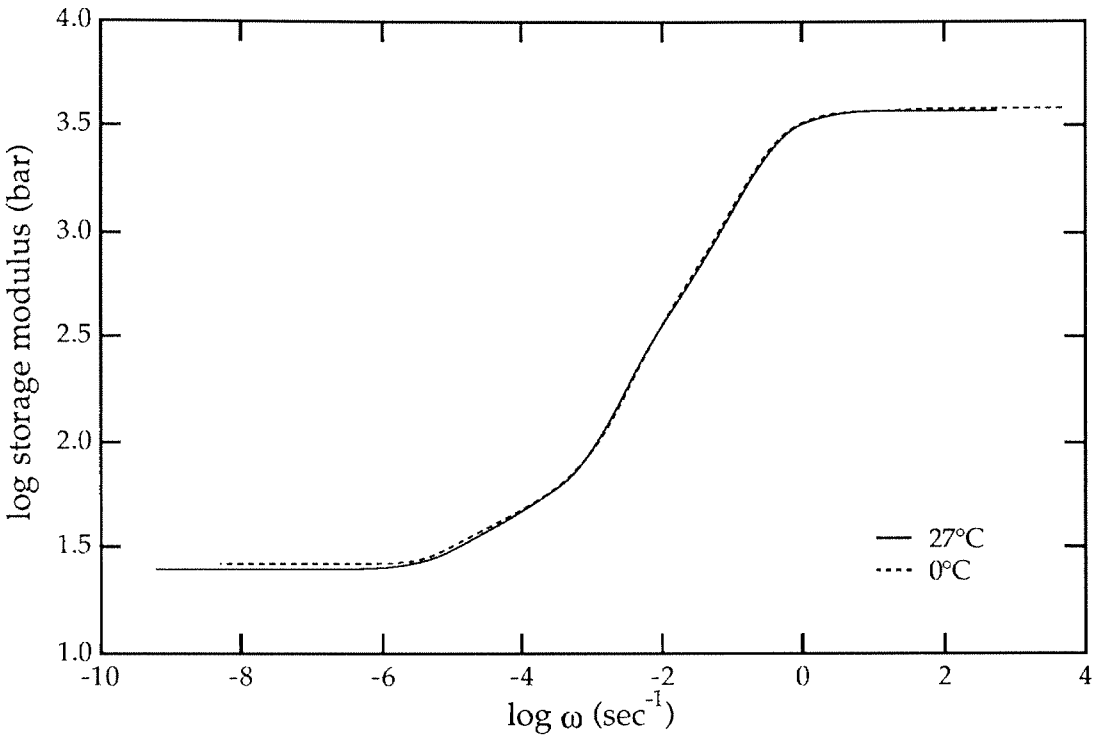

Figure 6.3a: Storage modulus for composite with elastic inclusion. 0° curve shifted to 27°

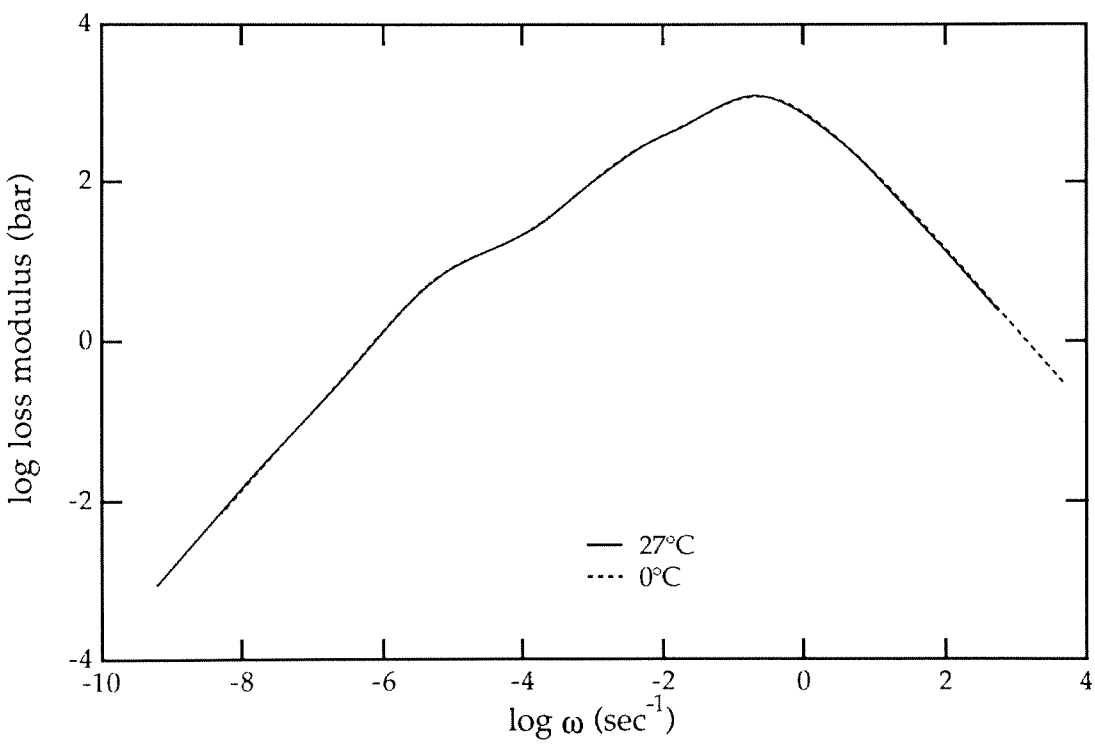

Figure 6.3b: Loss modulus for composite with elastic inclusion. 0° curve shifted to 27°

Two Viscoelastic Phases

For clarity of presentation, some initial thermomechanical results are given here for which the individual phase properties are again the idealized viscoelastic properties: the modulus functions of each phase have distinct long-term and glassy asymptotic values and one phase is "stiffer" at all times than the other, "softer" phase (refer to Figure 4.1). In this set of results, the stiff phase is taken to be that of cylindrical inclusions at 25% volume fraction arranged in a square array within the softer matrix; the interlayer modelling of a transition region between the two phases (see discussion below) is suppressed. Only the results for the loss moduli are presented and discussed since the thermorheological complexity of the material is depicted most clearly in that function. No further information on TRC behavior is gleaned by examining the storage modulus.

The WLF constants for the soft phase were given in the previous sub-section. The free volume shift factor for the stiff phase is represented by WLF constants of $c_0=19.4$ and $c_1=85$ at the reference temperature $T_0=300\ K$. A plot of the variation of the shift factor with temperature is shown in Figure 6.4 along with the shift factor for the soft viscoelastic phase. For both phases in this set of results, the small (vertical shift) factor from density and rubbery entropic corrections has been omitted.

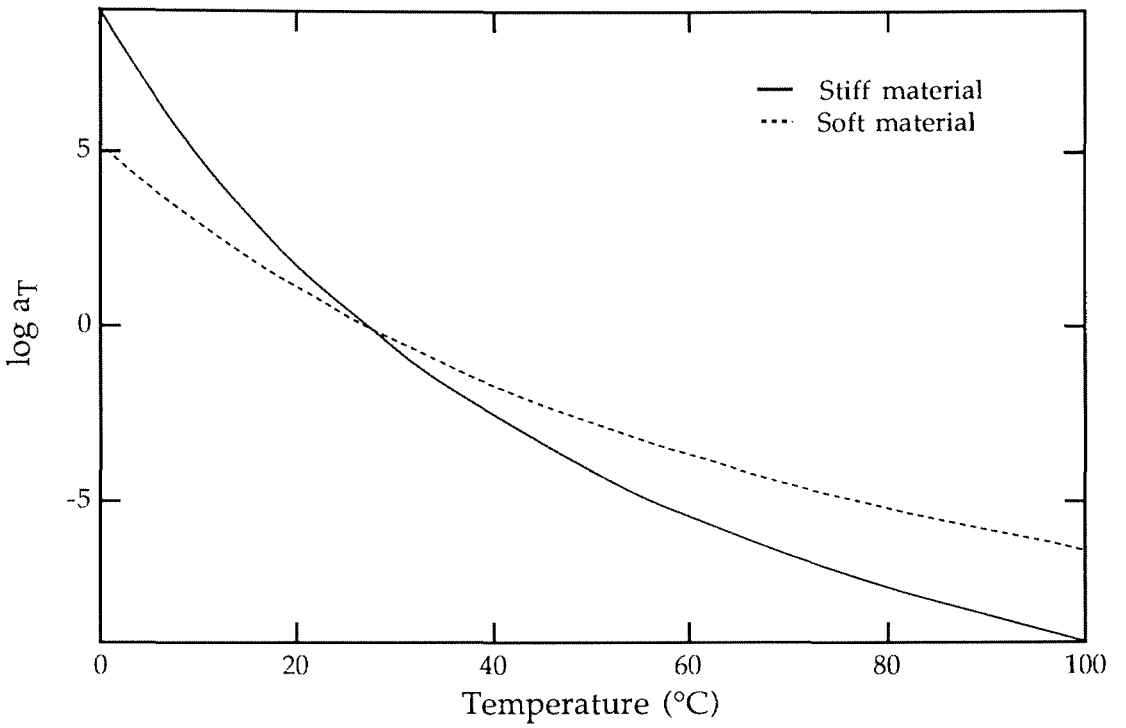

Figure 6.4: Shift factors for soft and stiff materials at T_{ref}=27°C

Figures 6.5a and 6.5b show the loss moduli for the composite obtained from the developed numerical procedure together with the loss moduli of the individual phases on the same axes for two temperatures. The distinct difference in the shape of the composite loss modulus at low frequencies for these two temperatures is clear. This observation is further illuminated by plotting the composite loss moduli at three temperatures together in Figure 6.6, where, for ready comparison, all curves have been shifted such that the high frequency ends coincide.

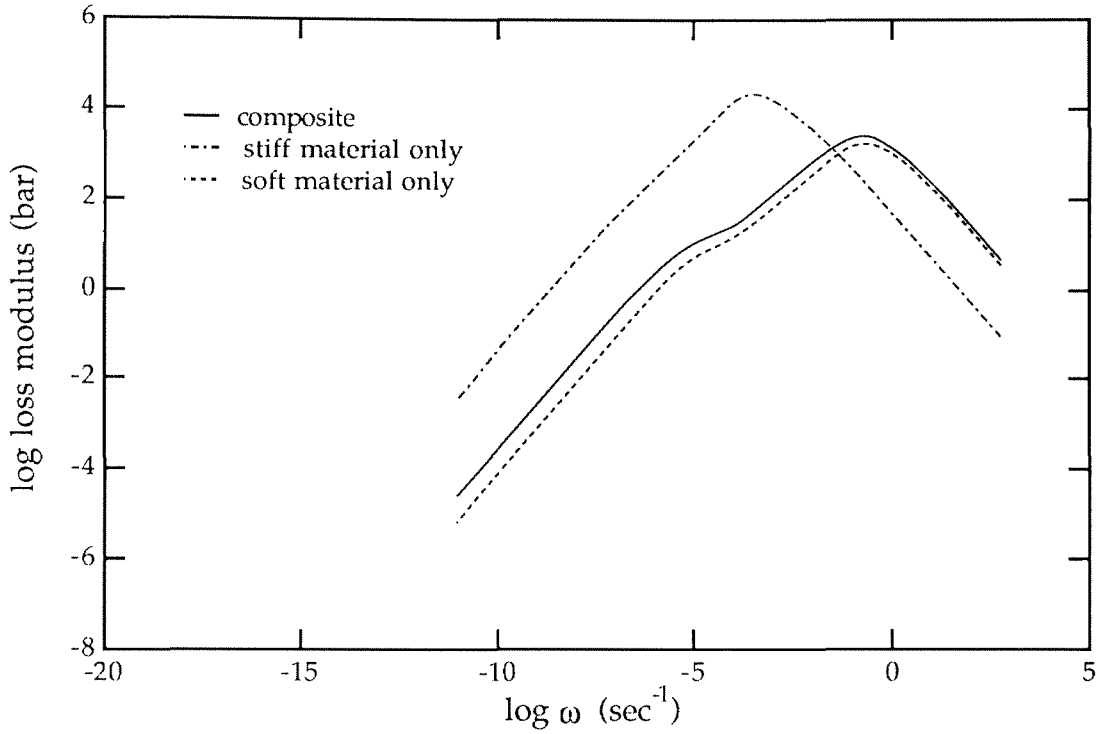

Figure 6.5a: Composite and individual phase properties at 27°C

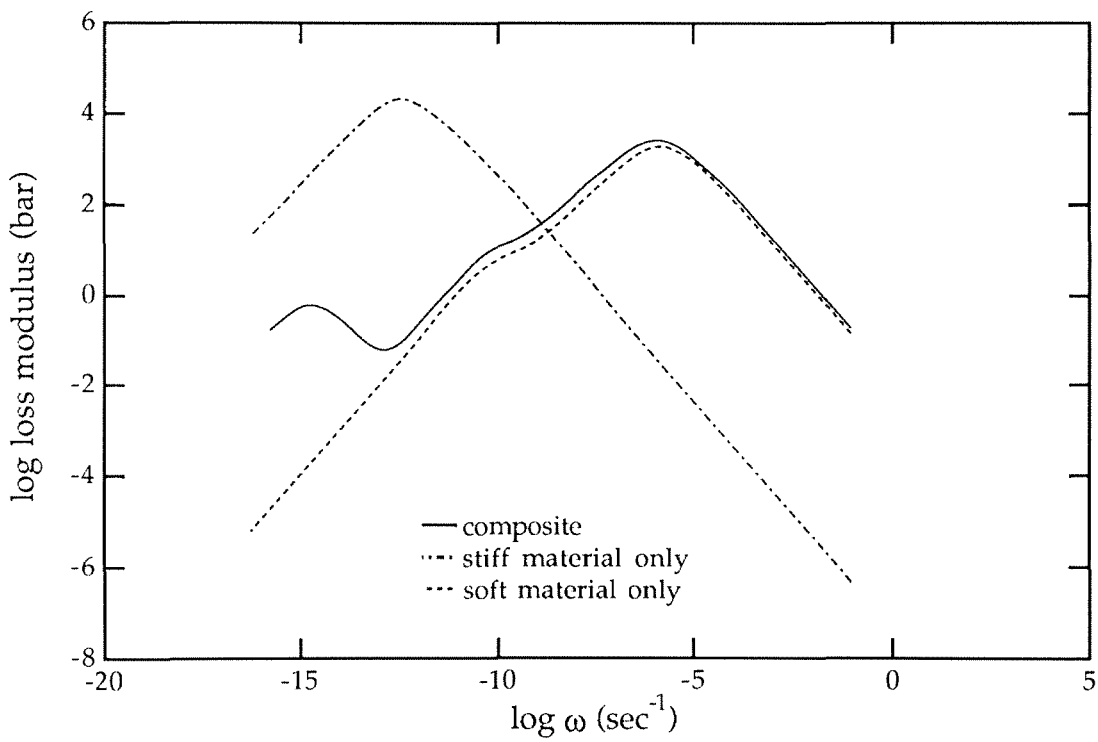

Figure 6.5b: Composite and individual phase properties at 0°C

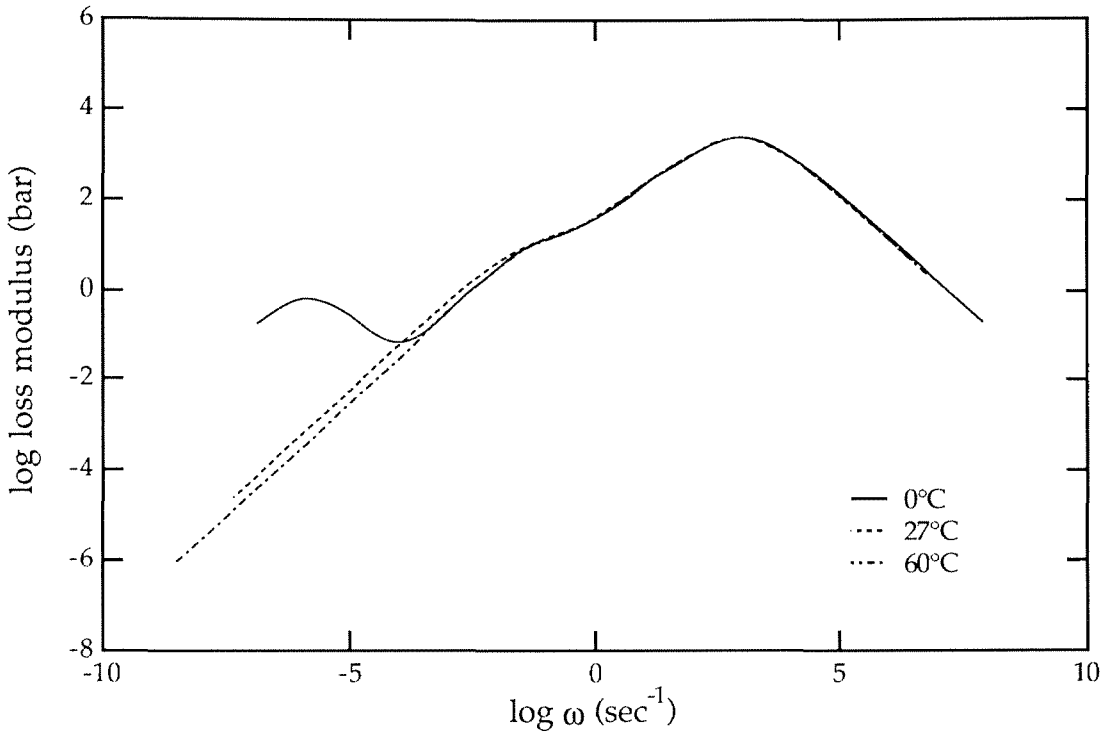

Figure 6.6: Breakdown of thermorheological simplicity, referenced to 60°C

From these results it is clear that the (loss) modulus of the composite tends to be dominated in both magnitude and in the shape of the glass-to-rubber transition region by the modulus of the matrix material. That is, the magnitude, location, slope, time range, and general shape of the modulus curve describing the transition from glassy to rubbery behavior of the composite is controlled primarily by those same features of the matrix material. The significant deviation from this general rule occurs at frequencies at which the glass-to-rubber transition in the inclusion phase occurs. Therefore at temperatures and frequencies where the inclusion is in the glassy portion of its behavior, the viscoelastic properties of the composite are completely governed by the relaxation mechanisms of the matrix material. However at frequencies where the inclusion material begins to proceed through its transition, the

time dependent properties of the composite are no longer dominated entirely by the matrix.

Returning to Figures 6.5a and 6.5b, the glass-to-rubber transitions (g-r transition) for the inclusion and matrix phases (symbolized by the peaks of the loss modulus) occur at different frequencies when the material is at various temperatures. In addition, the difference in thermorheology of the inclusion and matrix material (*i.e.*, different shift factors) causes the location of the g-r transition of the two materials to change relative to one another as the temperatures changes. For example, at 0° C the g-r transitions of the individual phases are separated by approximately 9 decades of time (Figure 6.5b), whereas at 27°C these transitions are separated by only 2 decades (Figure 6.5a). Therefore, at 0°C two quite distinct loss peaks appear in the composite properties, the first one at high frequency due to the soft matrix material and the second one at lower frequency as a contribution from the "stiffer" inclusion. At 27°C the loss peak in the composite arising from the stiffer material has begun to coincide with the loss peak from the soft matrix material, and at 60°C (not pictured here) the loss peaks of the two individual phases are at nearly the same frequency and therefore only one peak is experienced in the composite.

If one tries to shift the response curves obtained at different temperatures through (log-)time to obtain a single master curve (as one would do for a homogeneous material), one obtains the situation shown in Figure 6.6. Here the individual curves have been shifted along the log-time scale such that the high frequency ends coincide. The reasoning behind overlaying the high frequency ends is that because the matrix is a softer material with a lower glass transition temperature (T_g) than the inclusion material, at most temperatures

its g-r transition lies at higher frequency than that of the inclusion material. Therefore at sufficiently low temperatures the composite behaves for nearly all frequencies like the soft material with an elastic filler, the elastic modulus of which is the glassy asymptotic modulus of the stiff material. As the temperature is raised, the onset of the g-r transition of the inclusion approaches the g-r transition of the matrix material from the low frequency end. In this example, at 0°C from $log\ \omega=-12$ (the onset of the g-r transition of the inclusion) to all higher frequencies, the composite properties are entirely governed by the matrix properties. At higher temperature of 27°C, for example, this is true from only $log\ \omega=-4$ and up. As shown in the elastic inclusion subsection, viscoelastic materials filled with elastic solids exhibit the same time-temperature behavior as the viscoelastic material alone, and therefore have the same shift behavior. This TRS-like behavior occurs because in this case only one phase exhibits temperature dependent behavior. In the multi-phase viscoelastic composite then, the high frequency segments of the response of the composite, the range in which the inclusion is glassy-elastic at each temperature, will shift perfectly as a TRS material with the shift factor of the matrix material for all temperatures until the temperature at which the g-r transition of the stiff phase begins to occur at higher frequencies than the g-r transition of the soft phase.

The distinct failure of the curves to superpose in Figure 6.6 demonstrates clearly the thermorheologically complex behavior of multi-phase viscoelastic composites. Time and temperature are no longer equivalent to one another in terms of modulus response in the simple sense as applies to homogeneous polymers. The interaction of the two phases in the composite and the different time temperature behavior of each phase cause the modulus of the com-

posite to have a distinctly different character at different temperatures. The shape of the modulus function at each temperature is quite different than the shape at the other temperatures, in contrast to TRS materials for which the shape of the modulus curve is identical at all temperatures, but merely translated through time along the (log-)time axis.

There is thus clearly no simple way through which time and temperature can be related for composites of multiple viscoelastic phases. Obviously a single shift factor that is a function of temperature is inappropriate, however a shift factor that is a function of time and frequency is also not adequate. This observation is especially clear for non-monotonically increasing or decreasing functions such as the loss modulus, where it is possible for points on a curve at one temperature to have no corresponding value on a modulus curve at another temperature.

TRC Parameter

At this point it is convenient to introduce a measure of the thermorheological complexity of a material: the TRC parameter, κ. This parameter is a measure of the amount of non-shift of two modulus curves at two different temperatures upon shifting to the same temperature such that the high frequency ends coincide. In terms of the example of Figure 6.6, the TRC parameter is a measure of the difference in the modulus of the different curves shown. The TRC parameter is a function of the two temperatures being compared and is defined in terms of the loss modulus, normalized by the glassy asymptotic modulus:

$$\kappa(\omega, T2, T1) = \frac{E''_{T1}(\omega) - E''_{T2}(\omega)}{E'_0}, \tag{6.7}$$

where E''_{Tj} represents the loss modulus of a material at a temperature Tj and E'_0 is the asymptotic value of the storage modulus at large frequencies.

For the example of Figure 6.6, $\kappa(\omega,0,60)$, $\kappa(\omega,27,60)$, and $\kappa(\omega,027)$ can be determined. These are plotted in Figure 6.7. Values of κ for temperature ranges *(0,27)* and *(0,60)* are quite similar over frequency as one would expect from Figure 6.6, but there is quite a noticeable difference between *(27,60)* and the other two. One notes that the value of the TRC parameter is zero at high frequencies for all curves, indicating the manifestation of TRS behavior there. Since the TRC parameters in Figure 6.7 are comparisons of the moduli curves reduced to 60°C, the change in the TRC parameter from zero in each case occurs over the frequency range in which the inclusion material has its loss peak at 60°C. Also, comparing the moduli curves at 27° and 60° where the peaks of the loss moduli of the two phase materials almost coincide, $\kappa(\omega,27,60)$ is close to zero for the entire frequency range implying that there is relatively little difference in TRC behavior for these two temperatures, <u>not</u> that the composite exhibits nearly TRS behavior for the frequency range shown at these temperatures. Another feature of the TRC parameter curve is that there is a region of influence in frequency of the loss modulus of the included phase, which changes the value of κ from zero, after which κ takes on a (non-zero) constant value again.

One can also use the TRC parameter for the same temperature change to compare differing amounts of TRC behavior due to other factors. For example, an interesting application is to compare the amount of TRC behavior of differing volume fractions of inclusions for the same temperature change. That is, does the amount of TRC behavior of a composite change by varying the volume fractions of its phases? In Figure 6.8 the resulting $\kappa(\omega,0,27)$ has

been plotted for the composite of Figures 6.5 and 6.6, but for which the volume fraction of the stiff inclusion has been varied to 25%, 36%, and 64%. The plot of $\kappa(\omega,0,27)$ shows clearly that there is not only a difference in modulus when the volume fractions of the materials change (as shown in Section IV), but there is also a noticeable difference in the TRC behavior of the composite. The greater the volume fraction of the stiff inclusion, the more thermorheologically complex is the composite: there is more pronounced non-shift in modulus curves for the same temperatures in the composite with the higher volume fraction of inclusion compared to the composite with the lower volume fraction of inclusion. The TRC parameter shows this difference much more clearly than looking at plots similar to Figure 6.6 for each case and overlaying them to determine if and in what manner they differ from one another.

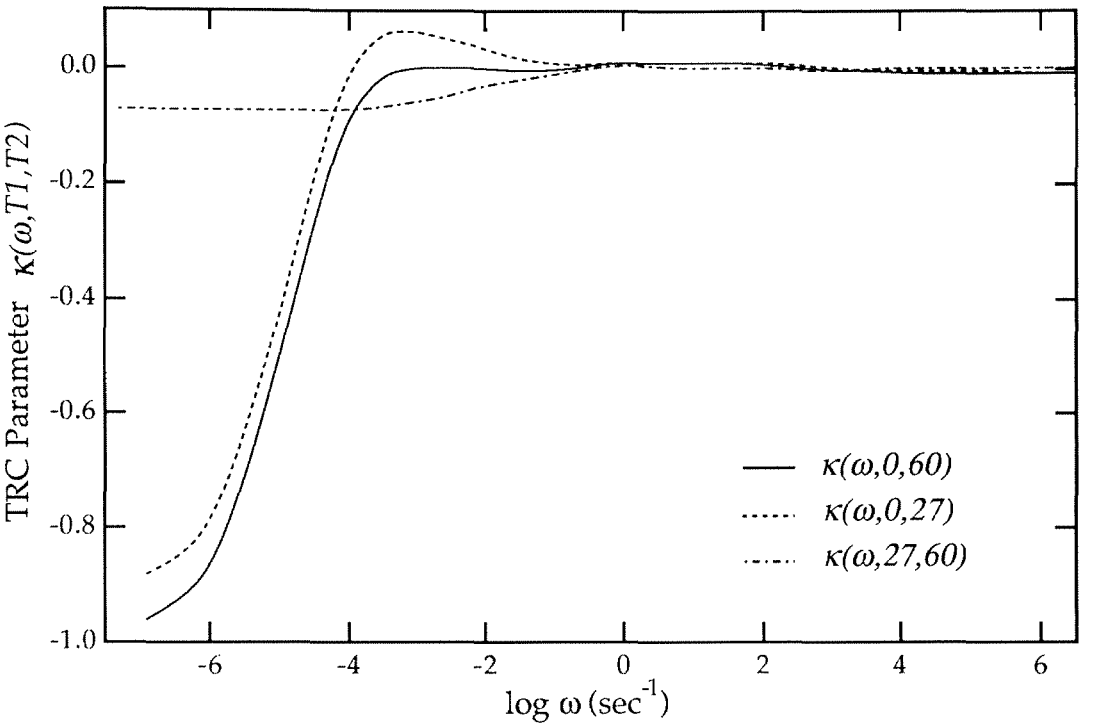

Figure 6.7: TRC parameter comparing three temperatures of Figure 6.6. Frequency values are for each temperature shifted to 60°C.

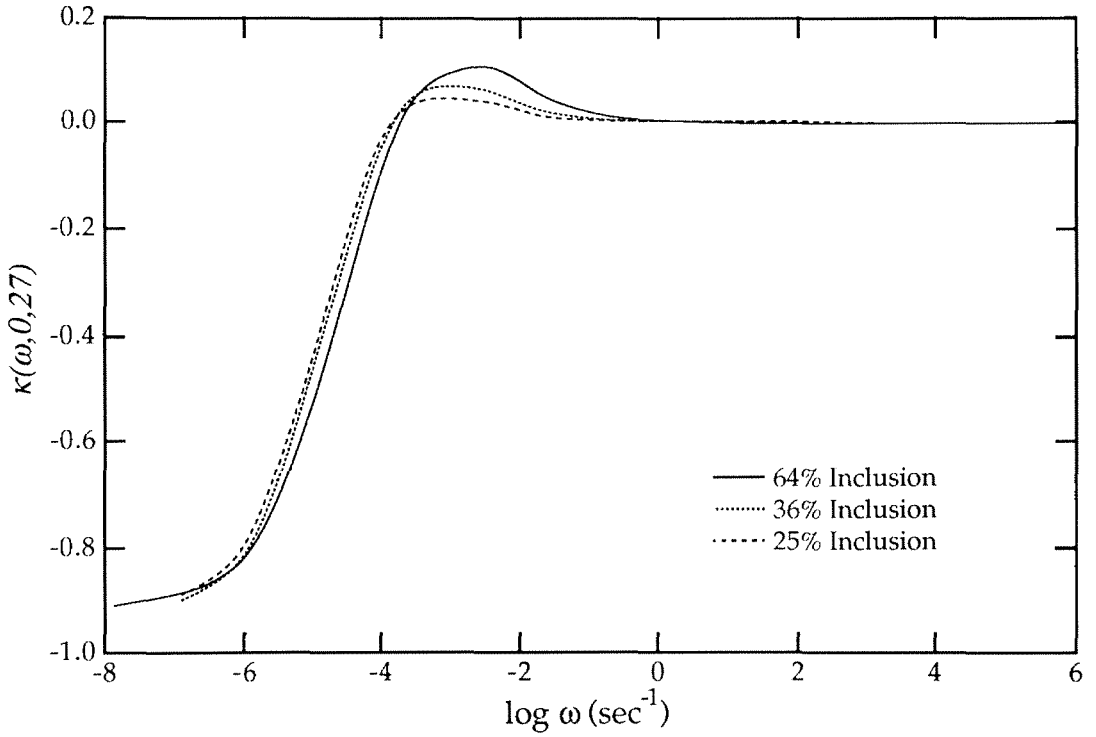

Figure 6.8: TRC parameter comparing three different volume fractions in the unit cell to show their effect on TRC behavior. Frequency values are for each temperature shifted to 60°C.

VII. EXAMINATION OF AN SBS BLOCK COPOLYMER

Introduction to Block Copolymers and SBS

In order to examine the ability of the analytical tool developed to adequately predict moduli of multi-phase composites based on individual phase data, it is necessary to apply it to experimental data of a material system. To do so requires data with a sufficiently wide range of time or frequency and temperature. In addition, it is prudent to effect such a comparison with a material with a minimal difference in geometric detail at the microscopic size scale. The initial model is based on a composite with a very regular microstructure, where two phases exist as a dispersion of one phase of cylindrical inclusions in a matrix of the second phase. Furthermore, the inclusions are regular both in size and in spacing. While it will certainly be possible in the future to create more complex models for the computational procedure, which will eliminate some of these restrictions (see Conclusion Section), it is best at this initial stage of analysis to maintain simplicity in the model for clearer and easier understanding of results.

Block copolymers are multi-phase viscoelastic materials that consist of two distinct phases arranged in a regular microstructure. The smaller volume fraction phase usually exists as spheres or rods within a matrix of the larger volume fraction, or if the volume fractions are nearly equal, the two phases exist as lamellae. In addition, the inclusions (or lamellae) are generally quite regular in size and in spacing. The solvent used in synthesis, rate of evaporation of solvent, and annealing all affect the type of domain structure and its regularity.[31] In block copolymers the two phases are not miscible, creating the microstructure of distinct phases. However, at the interface between the two

phases, chain ends from each polymer are intermixed, resulting in intermolecular non-covalent bonding. This molecular bonding at the boundary of the phases gives the inclusion-matrix connection strength—the boundary of the two phases is not necessarily a weak domain in which slippage occurs.[39]

These factors make block copolymers a type of multi-phase viscoelastic material that readily fits within the microstructural geometry of the current physical model. Some experimental data does exist in the literature for the time and temperature dependence of the properties of certain of these materials. A very common block copolymer is Styrene-Butadiene-Styrene (SBS). SBS usually consists of either spherical or cylindrical inclusions of polystyrene (T_g=93°C) embedded in a hexagonal array within a polybutadiene matrix. For the copolymers with cylindrical polystyrene domains, the approximate, median dimensions of the cylinders are 200Å diameter and 10μm length, which allow the approximation of the cross-section as a two-dimensional problem, which can be formulated in the context of plane-strain.

Due to the extremely regular microstructure of SBS and the fact that time-temperature experimental data is available, this particular copolymer was chosen as an example for comparison with results from the model presented earlier. An SBS was therefore modelled for which the matrix contains 1,2-polybutadiene (T_g=-7°C) instead of the more common 1,4-polybutadiene (T_g=-88°C) so that the glass transition temperatures of the two phases would be closer together (than in the 1,4-SBS case) and so that the thermorheologically complex behavior would be more evident in experimental time and temperature ranges. Existing experimental modulus data that contain time-temperature information show significantly more prominent TRC behavior for 1,2-SBS than for 1,4-SBS. A very thorough and careful study of the varia-

tion of the mechanical properties of 1,2-SBS with time and temperature has been presented by Cohen and Tschoegl.[18] Their data is presented in this section and it is the basis for comparison with the numerical results.

Experimental Results

Shown in Figure 7.1 is the experimental data determined by Cohen and Tschoegl.[18] Short term modulus tests were performed over frequency at thirteen different temperatures for the Loss and Storage Compliance of SBS. They then shifted the results along the log-frequency axis such that the high frequency ends coincided with a shift factor, the parameters of which are nearly identical to those of a homopolybutadiene of similar structure. This equivalence of the SBS shift factor obtained from superposition of the high frequency ends of isothermal modulus curves with the polybutadiene shift factor is expected on the basis of the argument presented in Section VI: at high frequencies only the relaxation mechanisms of the softer matrix material are operative in the composite when the stiffer inclusion is glassy-elastic. In Figure 7.1 the curve segments at low temperatures (from 1°-58°C) all shift uniformly onto a smooth "master curve" demonstrating a temperature dependence of mechanical properties at low temperatures governed purely by the polybutadiene relaxation mechanisms. Modulus curve segments above 65°C however, no longer map onto a single curve when shifted. Instead, these curves deviate more markedly from the low temperature "master curve" as temperature is increased. This clear illustration of the thermorheological complexity of the SBS material is especially noticeable in the loss compliance.

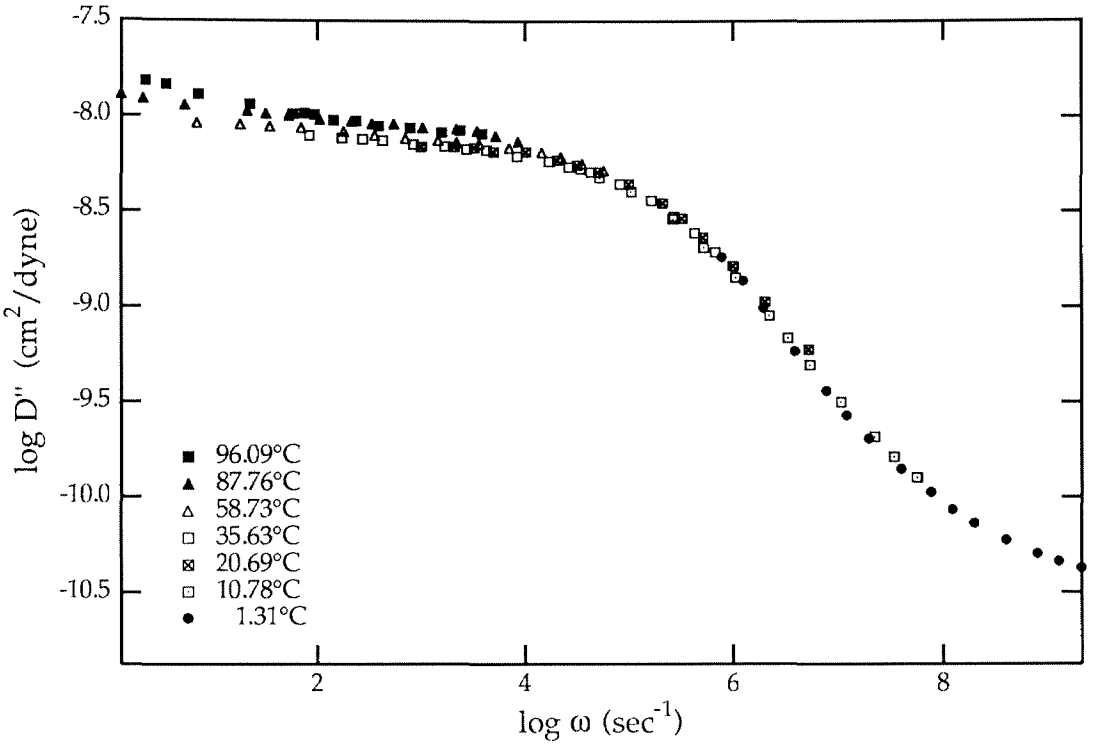

Figure 7.1a: Storage compliance of SBS shifted to 85°C (Cohen & Tschoegl)

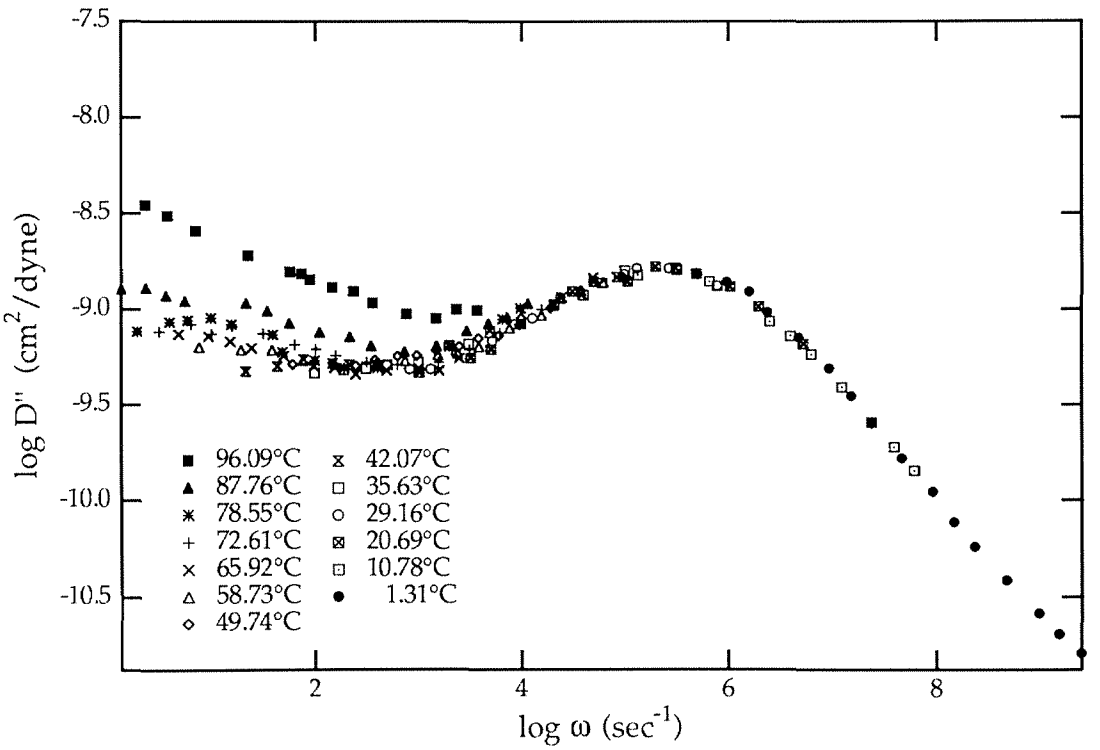

Figure 7.1b: Loss compliance of SBS shifted to 85°C (Cohen & Tschoegl)

Properties for Numerical Study

The SBS composite investigated by Cohen and Tschoegl consists of 106,000 molecular weight polybutadiene centerblocks containing 90% vinyl 1,2- addition with 7% cis 1,4- addition and 3% trans 1,4- addition, as well as 16,000 molecular weight polystyrene endblocks. This composition yields a 23% volume fraction of polystyrene for the copolymer. The microstructure of Cohen and Tschoegl's SBS was modeled for the numerical analysis as a polybutadiene matrix with rod-type polystyrene inclusions. Although no electron micrograph is available for Cohen and Tschoegl's composite, many electron micrographs recorded on various kinds of SBS composites of similar volume fractions all show a regular arrangement of rod shaped inclusions. Figure 7.3 is an example of an electron micrograph from Dlugosz for an SBS material of the same volume fraction;[40] all micrographs with which the author is familiar for rod-shaped structures of SBS show this same arrangement. Note the extreme regularity of the polystyrene domains, appearing white inside of the black stained polybutadiene matrix. In addition, following the theory of Helfand on the thermodynamics of polymeric mixtures, Figure 7.2 can be constructed[41] which shows a phase diagram for polymeric mixtures of immiscible phases based on the total molecular weight of the composite and the volume fraction of the phases. Designating polystyrene to be phase I and polybutadiene to be phase II, the situation for Cohen and Tschoegl's 1,2-SBS falls into the middle of the rod category (cylinders of I in II) with an overall molecular weight of 138,000 and 23% volume fraction of Polystyrene.§

§ It was determined after this work was completed, through personal communication with N. W. Tschoegl, that the assumption of regular cylindrical inclusions in the SBS composite of Cohen and Tschoegl is not correct. Tschoegl stated that although the molecular weights and volume fractions of the individual constituents indicate a cylindrical domain structure, these parameters alone are not conclusive for determining the microstructure. Although an electron

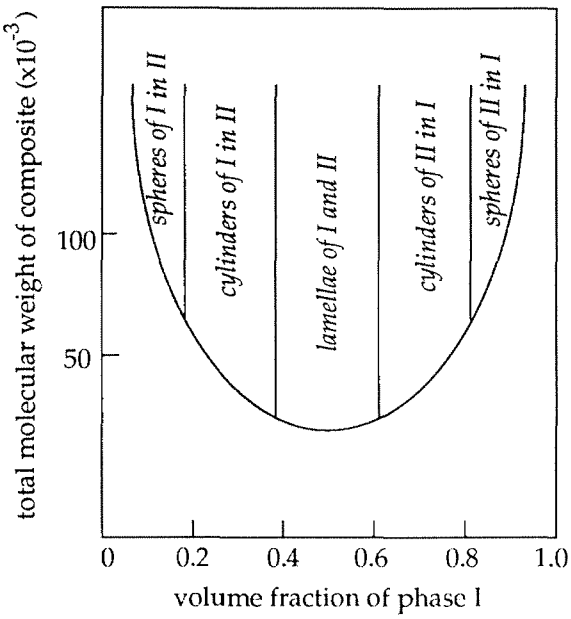

Figure 7.2: Phase diagram showing microstructure of a mixture of two immiscible polymers (I and II)[41]

micrograph was not taken of the SBS material, Tschoegl stated that they had chosen the many physical parameters of the copolymer components in hopes of attaining a spherical domain structure. In this sense then, the analysis here is an approximation of a three dimensional spherical domain structure by two dimensional circular domains. After consultation, Tschoegl concurred that the results obtained from the two-dimensional study of circular domains would differ from a full three-dimensional analysis of spheres primarily in the magnitude of the modulus; the time-temperature information, which is the main thrust of the present analysis, should not be significantly affected.[Tschoegl, 1990 #60]

Another consequential factor regarding the material geometry is that even if cylindrical domains are present, in a macroscopic specimen the cylinders would not be uniformly arranged throughout the entire body. Rather, the cylinders would exist as regular arrays in smaller, separate domains interconnected somewhat like grains in metals. Again, in view of the anisotropy study performed in Section VIII, the moduli of a body composed of grains of regularly arranged cylinders and the moduli of the idealized body studied here of a single uniform cylindrical array (Figure 2.1) would differ primarily in the magnitude of modulus; the time-temperature behavior of the composite should not be greatly altered.[Tschoegl, 1990 #60]

Thus, in the study presented here, the proper coupling between the phases of the composite is accounted for.[Tschoegl, 1990 #60]

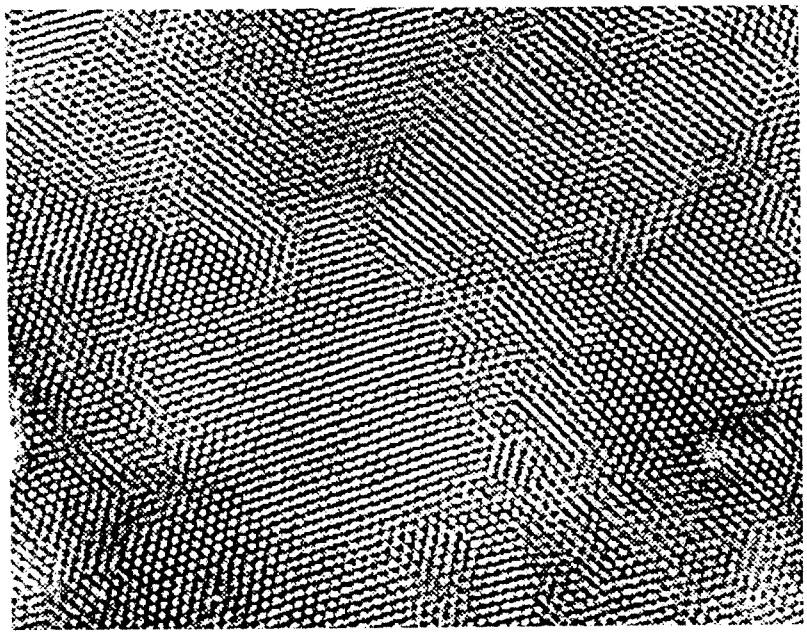

Figure 7.3a Ultramicrotome section cut perpendicular to the extrusion direction of an SBS plug. The dark regions correspond to the Osmium stained butadiene matrix. Magnification 50,000X.

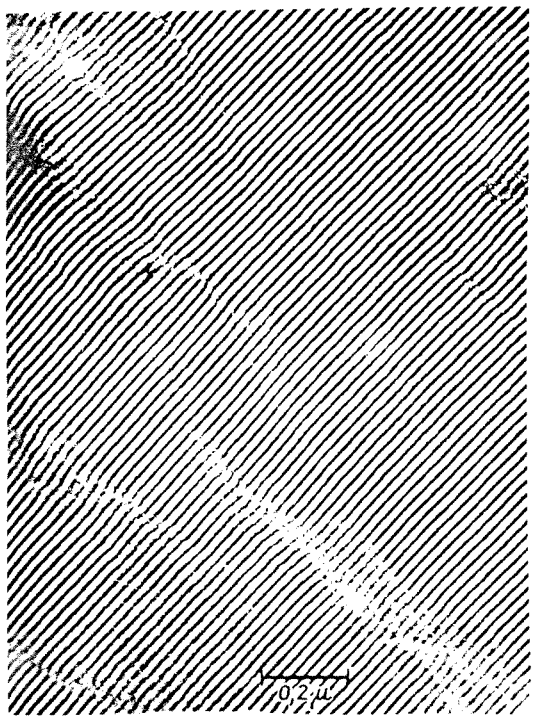

Figure 7.3b Parallel section in optimum contrast position showing a large area of striated structure with some faulted regions.

Figure 7.3: Electron micrograph from Dlugosz *et al.*[40] for a Styrene-Butadiene-Styrene block copolymer showing cylindrical polystyrene inclusions in a polybutadiene matrix.

The phase properties used in the numerical model for Cohen and Tschoegl's composite were mostly obtained data available in the open literature. Although care was taken to find properties for polymers of similar structures to the constituents of SBS, it should be stated here that the accuracy of the individual phase properties as applicable to the Cohen SBS system may be questioned: variability of polymeric properties according to different synthesis procedures and the probability that the phase polymers in microdomains on the order of 200Å will exhibit different behavior than that demonstrated by the bulk homopolymer data, leave doubt as to the accuracy of the phase property data for this application. The shear modulus and shift factor for polystyrene were taken from data by Plazeck for a polystyrene of (low) molecular weight 16,400.[6] The shift factor below the glass transition temperature for polystyrene was taken from analysis by Rusch.[42] The polybutadiene shift factor was taken from data by Sanders and Ferry for a polybutadiene of 99,000MW containing 91.5% vinyl 1,2-, 7% cis 1,4-, and 1.5% trans 1,4-.[43]

The characterization of the polybutadiene matrix was taken, however, from the low temperature SBS composite transition and plateau regions with the magnitude adjusted to agree with the comparable data on 1,2-polybutadiene from Sanders and Ferry. This choice was made for the following reason: since the composite behavior is largely dominated by the matrix behavior at low temperatures (see Section V and VI), earlier numerical results stressed the importance of having accurate properties for the shape of the transition region of the matrix material modulus. At temperatures below 30°C the composite acts like polybutadiene filled with an elastic medium (the glass transition temperature of the polystyrene is 93°C), and consequently the shape of the plateau and transition regions will be those of polybutadiene.

Therefore, data from 1.31° to 29.16°C from Cohen and Tschoegl's SBS composite were used to obtain the character of the transition behavior for the 1,2-polybutadiene phase. This method accounts for the filler effect and effective crosslink density for polybutadiene as it exists in the matrix of the composite, factors that are not well defined, and that would have to be added into any homopolybutadiene properties used.[17] The magnitudes of the modulus functions for polybutadiene taken from the composite curve are, however, too large because of the extra stiffness added by the (elastic) inclusions and therefore were adjusted downwards to represent polybutadiene data. This procedure for procuring reasonable matrix material properties was used by Fesko and Tschoegl in their paper modelling 1,4-SBS behavior analytically.[17]

Time or frequency dependent bulk moduli for the individual phase materials could not be found in the literature and as a result constant bulk moduli were assumed for both phases. This assumption is at least approximately valid because for a typical viscoelastic material the bulk modulus function through the transition region decreases in magnitude by a factor of only two or three, as compared to the shear modulus function, which changes by multiple powers of ten.[4] Consequently, the transition region of Young's modulus function, which is the result obtained in this study, is completely dominated by the character of the shear modulus transition. Results substantiating this claim are given in Figure 7.9 later in this Section. In that example, reasonable time-dependent bulk moduli are assumed for each constituent phase of the composite, then the composite moduli are determined and compared to results for which the bulk moduli of the individual phases were assumed constant. There is less than a 0.1% difference in the values of the Young's Modulus functions of the composite for the two cases and no difference in the ther-

morheological behavior. Thus, the assumption of constant bulk moduli for the component phases of SBS is justified. The values for the bulk moduli for polystyrene and polybutadiene used in the numerical analysis were taken from a paper by Arridge examining SBS elastically, which consequently employed constant values for moduli.[44]

As mentioned in Section II, the results of the study of SBS composite will suggest consideration of an intermediate phase, called an interlayer, between the two main constituent phases of SBS. The existence of an interlayer consisting of a molecular mixture of polystyrene and polybutadiene as a transition region between the two phases has been postulated extensively in the literature,[24, 26, 27, 45, 46, 47] but there are no properties available for this additional phase. In fact the interlayer probably does not really exist as a single separate phase of distinct homogeneous properties, although some researchers have spoken about a "glass transition temperature of the interphase."[18, 24] Here, a single phase interlayer will be used to model a possibly complex transition region and best estimates were made based on the information available regarding appropriate properties of an interlayer. It has been suggested that the transition region is rich in polystyrene[48] and therefore the shape of the interlayer properties chosen is based primarily on the polystyrene properties. The glass transition temperature is also suggested to be lower than that of polystyrene[18, 24, 26] and 75°C was chosen for that property of the interlayer. The numerical procedure was then applied to partially solve the "inverse problem" in a short iterative process that refined the properties of the interlayer in order to match the complete sense of the experimental data as closely as was possible and could be reasonably expected. This "fine-tuning" is discussed in greater detail later in this section as well as in Section IX on sensitivity.

The size of the domains in the SBS composite are chosen based on the stated 23% volume fraction of polystyrene. The present procedure is insensitive to the size scale of the unit cell; therefore the actual size of the domains does not come into account and knowledge of the volume fraction is sufficient. For a unit cell without an interlayer, polystyrene is chosen to occupy 23% of the volume and polybutadiene 77%.

For considerations involving an interlayer, the literature contains estimates for sizes of an interphase that deviate widely from one another depending on the theories used, the exact phase materials considered, the molecular weights of the materials, measurement methods, etc.[24, 26, 27] In addition, the solvent used, rate of evaporation of the solvent, and the annealing processes will all also affect the size of the interphase domain and the influence of these parameters on interlayer size has not been systematically studied. Therefore in the present work a median size for the interlayer was assumed. To accommodate the suggestion that polystyrene is represented in the interlayer more than polybutadiene, a greater percentage of polystyrene than of polybutadiene is subtracted from their volume fractions in the unit cell devoid of an interlayer to compose the volume fraction of the interlayer. A moderate 16% of the volume fraction of the unit cell is assumed for the interlayer, with a domain size of pure polystyrene at 13% and the pure polybutadiene matrix at 71%. Compared to the average sizes for SBS microstructures mentioned in the beginning of this section, these percentages yield a 150Å diameter inclusion, a 37Å thick annular interlayer and a 370Å square lattice parameter (2L).

Another factor of importance concerns the plane-strain aspect of the analysis, an assumption necessary for the two-dimensional formulation of the numer-

ical problem. The specimen size for Cohen and Tschoegl's work was 0.38 cm in thickness and 0.14 cm^2 in crossectional area; the strain was applied perpendicular to the plane of the crossection. The experiments to attain the modulus of the material were performed in compression, but because of the exceedingly small strain values, ≈0.01%, there is believed to be no significant effect from bulging of the specimens.[49] Due to this fact and the experimental set-up, described in detail by Cohen and Tschoegl,[18] in which the specimen is constrained "in the thickness direction" throughout the test, the experimental test is not a true "uniaxial tension test", nor is it a true "plane-strain test". It is believed, however, that the plane-strain modulus determined from the numerical analysis is a reasonable approximation to the modulus derived from the experimental results.

Results

The model studied initially did not allow for an interphase. The global effective Young's modulus functions for this model were determined numerically at a variety of temperatures. The Young's modulus curves obtained were then shifted along the log-frequency axis with the polybutadiene shift factor such that the high frequency ends coincided. The modulus curves were also "inverted" to attain compliance curves to facilitate direct comparison with the experimental results of Cohen and Tschoegl shown in Figures 7.1.

In the absence of an interlayer, the non-superposability of the isothermal modulus curves indicative of thermorheologically complex behavior did not occur at the same temperatures as the experiments showed. In fact, the numerical modulus curve generated for the 96°C temperature, which shows extreme non-shiftability with the lower temperature data in Cohen and

Tschoegl's measurements, shifts well to coincide precisely with the lower temperature numerical data in the frequency range of interest. At higher temperatures however, for example at 120°C, the numerical results do begin to show TRC behavior in the experimental frequency range. These results are shown in Figure 7.4 for the loss compliance.

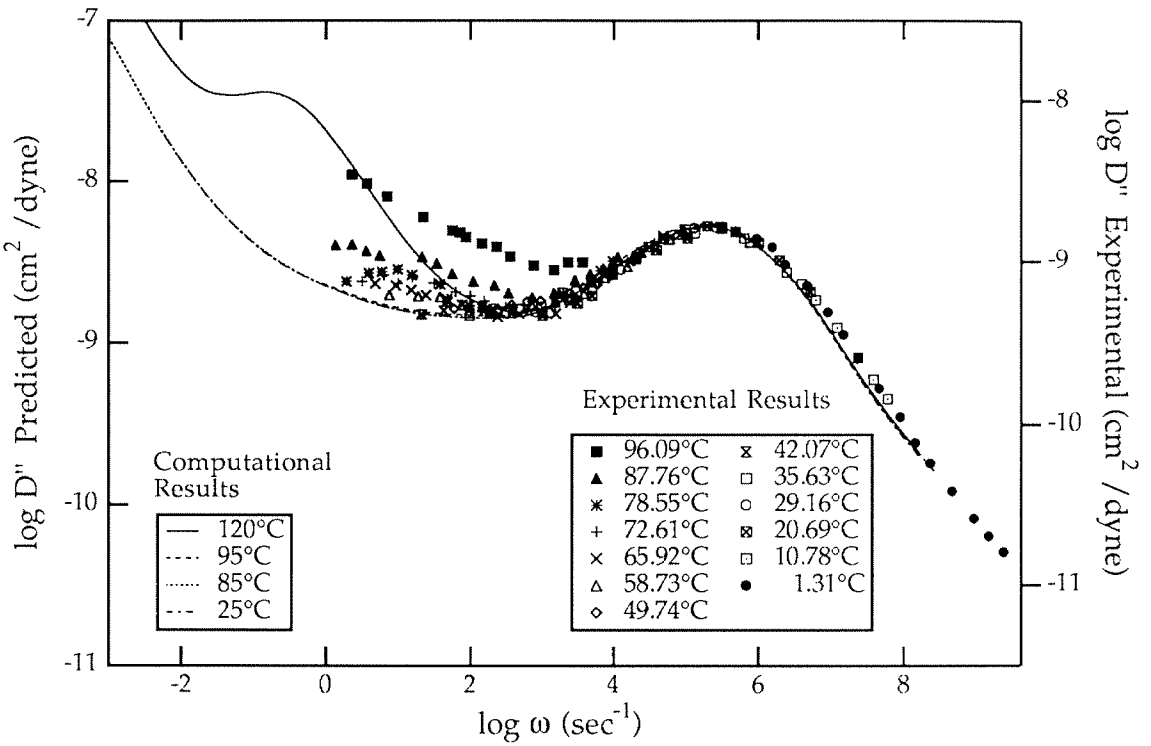

Figure 7.4: Loss compliance of 1,2-SBS without an interlayer

Thus, in the absence of an interlayer, the TRC behavior at any given temperature does not occur until the transition of the polystyrene domains has been reached; this result is consistent with the earlier ones on the idealized material in Section VI. At 96°C, the polystyrene transition occurs around *log ω=-10* and cannot, therefore, affect the shifting of the composite near *log ω=0.*[*] At

[*] The numerical results would show non-shifting at 96°C at lower frequencies, but we cannot attain those results numerically because the polybutadiene moduli become very small relative to the polystyrene values. This excessive modulus ratio results eventually (at log ω=-5) in producing a (nearly) singular stiffness matrix.

120°C however, the polystyrene transition has shifted to $log\ \omega=2$ and therefore has begun to affect the shifting of the composite in the frequency range of the experiments. The relative locations of the glass-to-rubber transitions of each phase and the composite are illustrated in Figures 7.5 and 7.6 at 85°C and 120°C.

The experimental data, on the other hand, show non-shiftable behavior from temperatures as low as 60°C. Considering this discrepancy, one notes that the numerical code solves the mechanics of the problem accurately, subject only to the restrictions of finite elements and the accuracy of the model of the material represented; furthermore, it is not reasonable that the relaxation times of the modulus data used for polystyrene would be incorrect by 6 decades of time. One concludes, thus, from these observations of misfit in the location of the onset of TRC behavior that an additional physical phenomenon must be operative in this SBS material, which is not being accounted for in the numerical model, and that produces TRC behavior at temperatures well below the glass transition temperature of polystyrene at high frequencies.

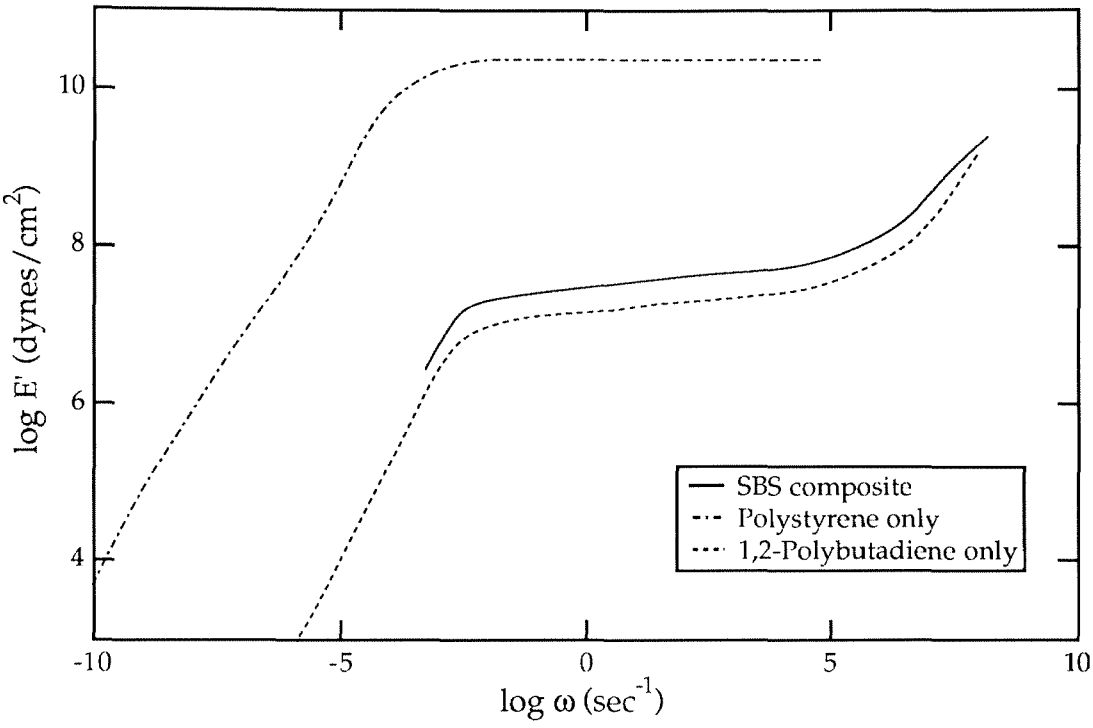

Figure 7.5a: 1,2-SBS composite and constituent storage moduli at T=85°C, no interlayer

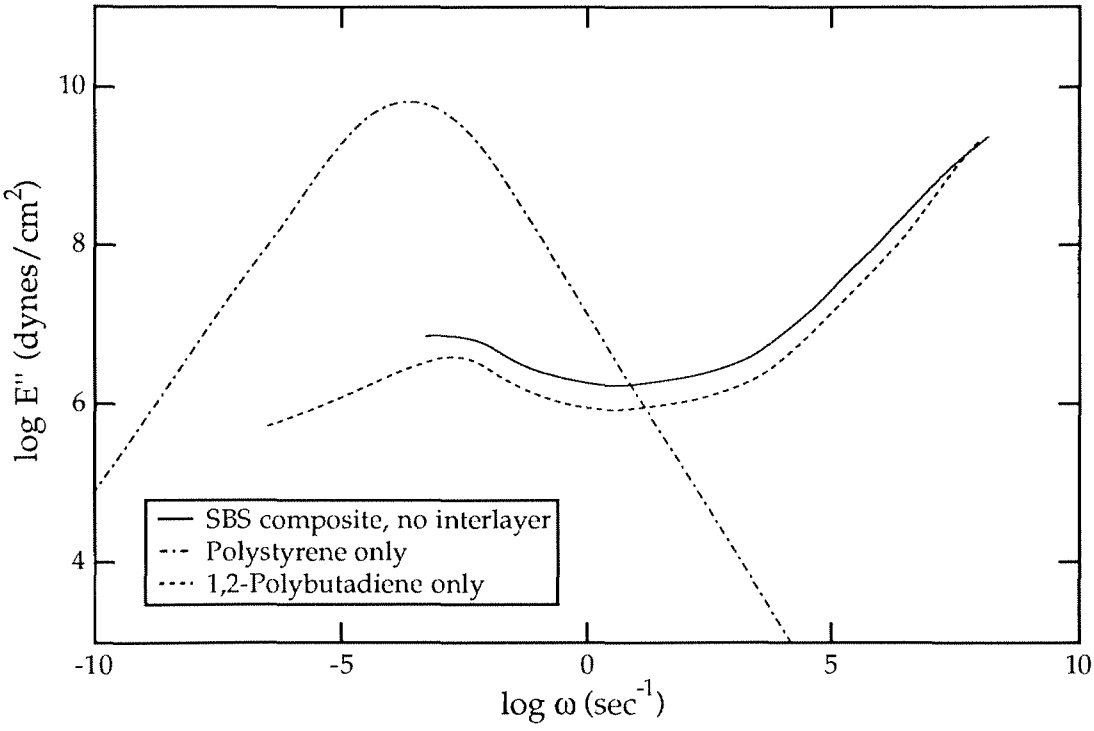

Figure 7.5b: 1,2-SBS composite and constituent loss moduli at T=85°C, no interlayer

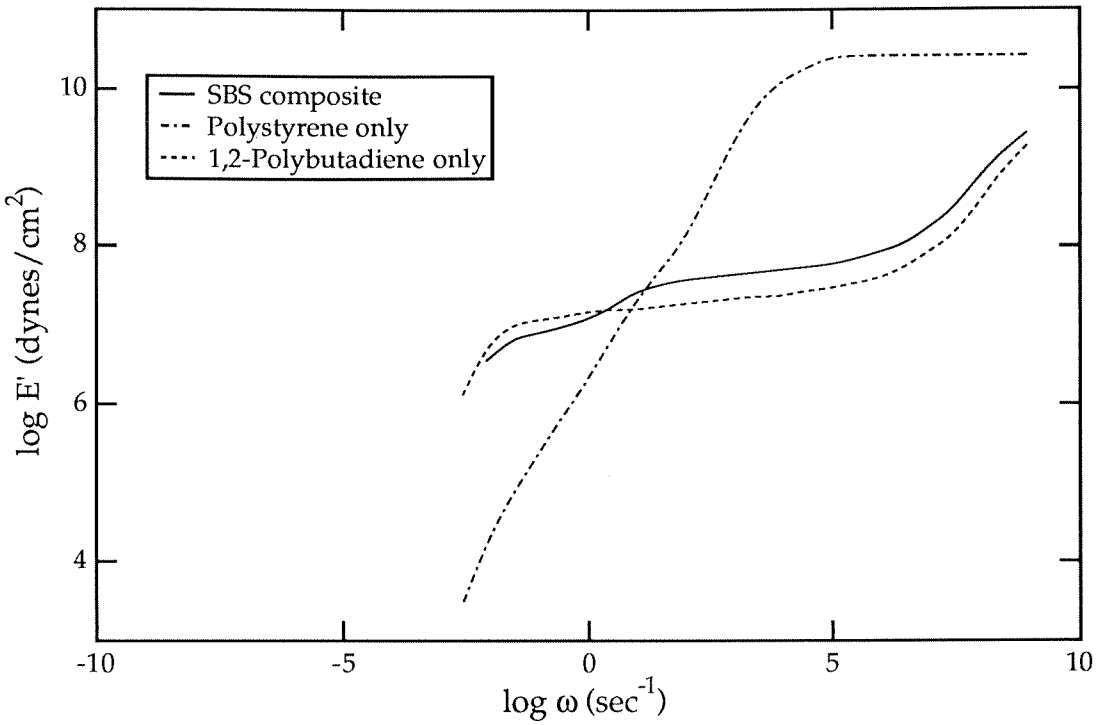

Figure 7.6a: 1,2-SBS composite and constituent storage moduli at T=120°C, no interlayer

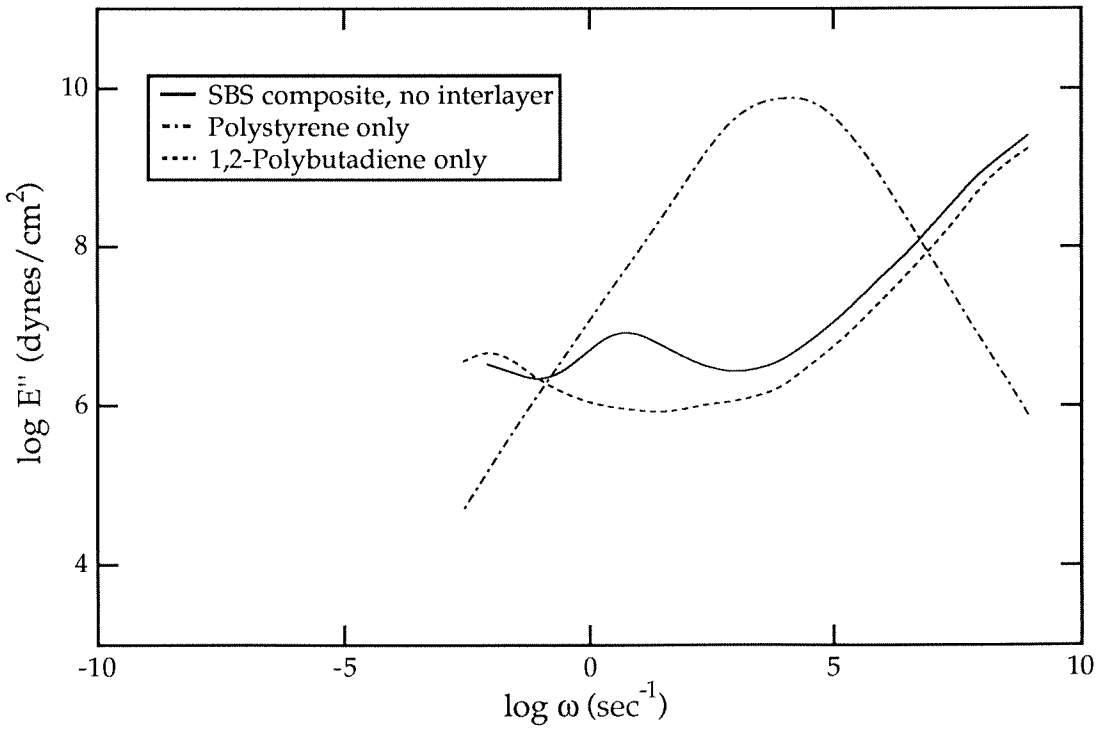

Figure 7.6b: 1,2-SBS composite and constituent loss moduli at T=120°C, no interlayer

It is this significant misfit in the time response of the viscoelastic composite that demands consideration of a transition phase with properties that are "intermediate" to those of the two primary phases. In much of the literature there is experimental and theoretical support for the existence of this third phase between the two main phases in both multi-phase polymers in general and in SBS in particular.[24, 26, 27, 45, 46, 47]

This transition region is a domain of molecular mixing of the two phases and exhibits properties that are different from those of either phase alone. The existence of an interphase is not incompatible with the fact that polystyrene and polybutadiene are immiscible in one another. At the boundary, polymer chains and, in particular, ends of polymer chains of the two phases bond together. One can consider polymer ends at the boundary to be like monomers (or short segments) of the polymers anchored at one end; in fact the monomers of styrene and butadiene are partially soluble in one another. Thus, it is conceivable that at the boundary the two phases mix to form an interphase with properties different from either phase alone. As far as the size scale of the interphase is concerned, a polystyrene monomer measures about 7Å and therefore an interlayer of 37Å is not unreasonable.

An interlayer was thus incorporated into the model as discussed earlier to emulate the actual physical transition region present in the composite material. It is expected that the addition of such an interlayer possessing properties intermediate to those of polystyrene and polybutadiene would explain the experimentally shown TRC behavior of SBS in regions where the polystyrene g-r transition region is not even close to being encountered. When attempting to create an analytical shift factor as a function of both temperature and

time for a 1,4-SBS material, Fesko and Tschoegl[17] were also forced to incorporate an interlayer into their model to be able to emulate experimental results.

The final set of modulus properties chosen for the interlayer are shown in Figures 7.10 along with the polystyrene and polybutadiene data, and results for the composite. The shift factors for all three materials are shown in Figure 7.7. The numerical results for several temperatures, all shifted to 85°C with the shift factor for polybutadiene such that the high frequency ends coincide, are shown in Figures 7.8 along with the experimental data. Note again that compliance curves, instead of modulus curves, are plotted in Figures 7.8 for ready comparison with the experimental data.

Figure 7.8 shows that one can indeed account for the experimental results showing TRC behavior in SBS at 60°C at relatively high frequencies by incorporating an interlayer into the physical model of the material. The properties chosen for the interlayer appear reasonable in magnitudes and shapes in comparison to the individual phase properties. It must be reiterated that the existence of an interlayer of homogeneous material properties is somewhat artificial; in this form the interlayer is a modelling tool to include the effect of a transition region between the two phases without much knowledge about the physical characteristics of the region. In the Conclusion Section some plausible ways in which this initial approximation of the real transition region may be expanded are mentioned.

The results shown in Figure 7.9 are the assessment of the effect of time-dependent bulk modulus data on the composite properties. They confirm that assuming constant bulk moduli for each phase of the composite as mentioned in the Properties subsection is reasonable. Figure 7.9 shows the calcu-

lated storage and loss moduli of the composite for the cases of constant and time varying bulk moduli for each phase. For the case of time varying bulk moduli, the change in bulk modulus from glassy to rubbery behavior was assumed to be approximately a factor of two for each phase and the relaxation behavior was represented by the model of a standard linear solid,[32] where the rubbery modulus was equivalent to the bulk modulus used in the case of constant bulk modulus. The difference in the resulting moduli for these two cases is less than 0.1% and the curves for the two cases cannot be distinguished within plotting accuracy; therefore the constant bulk modulus assumption is believed to be acceptable.

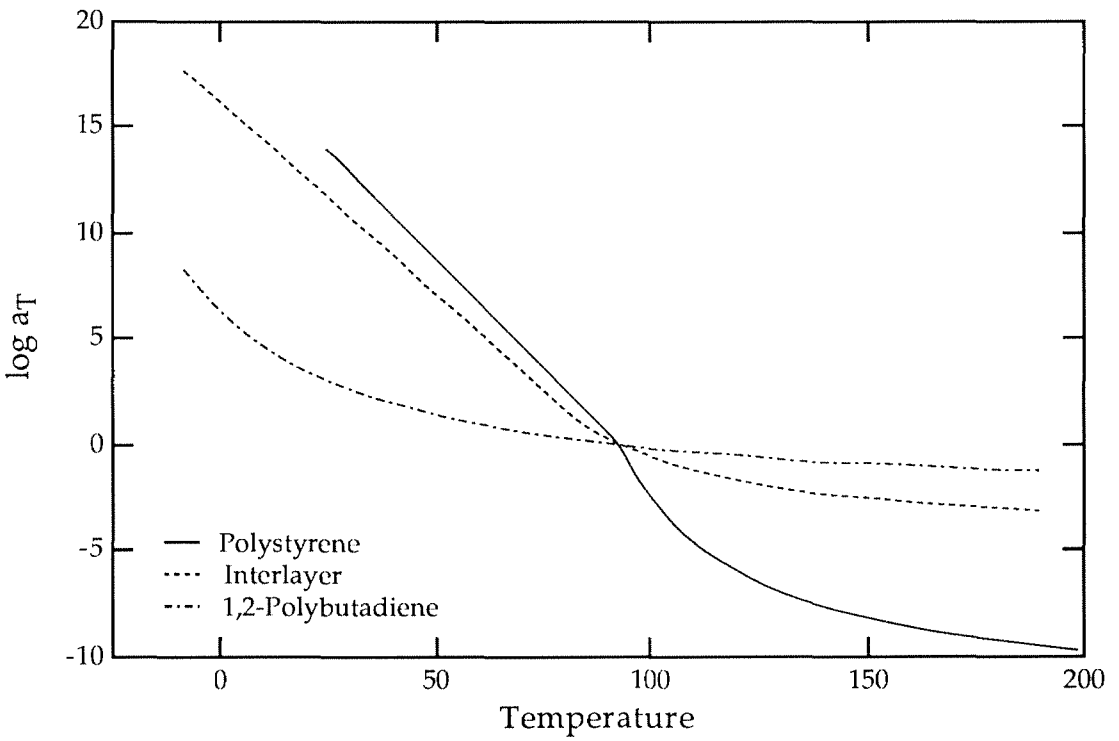

Figure 7.7: Shift factors for individual phases of composite at T_{ref}=93°C

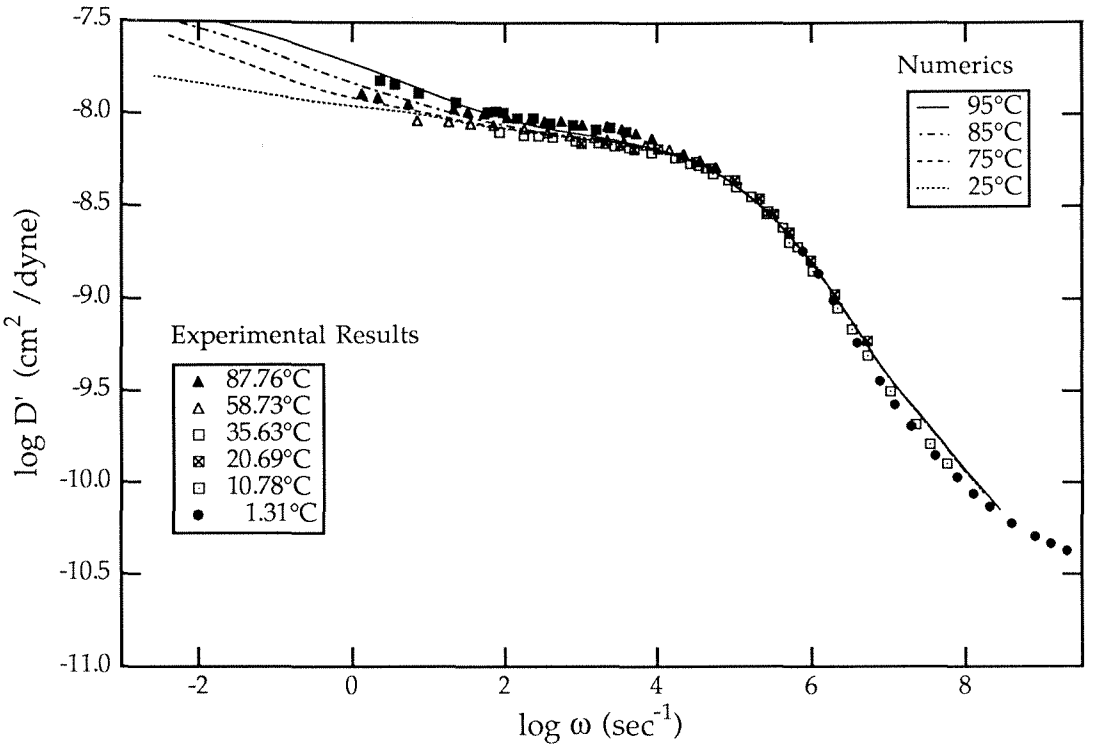

Figure 7.8a: Numerical results for storage compliance of SBS with interlayer and experimental data all "shifted" to 85°C

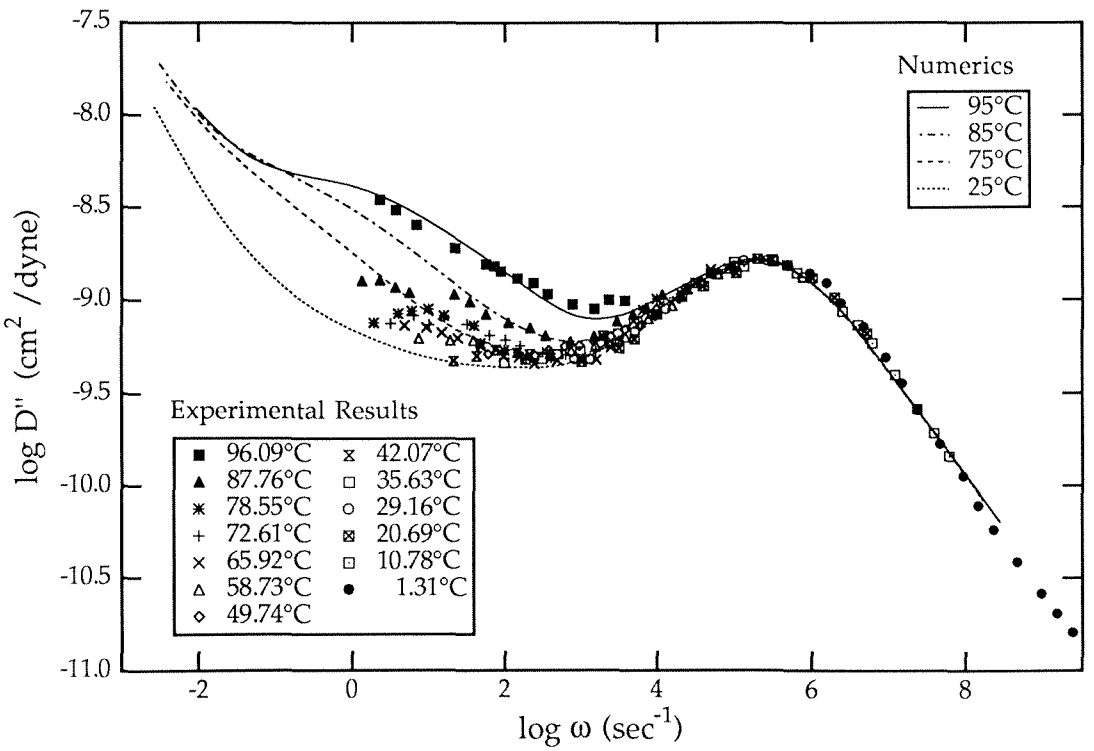

Figure 7.8b: Numerical results for loss compliance of SBS with interlayer and experimental data all "shifted" to 85°C

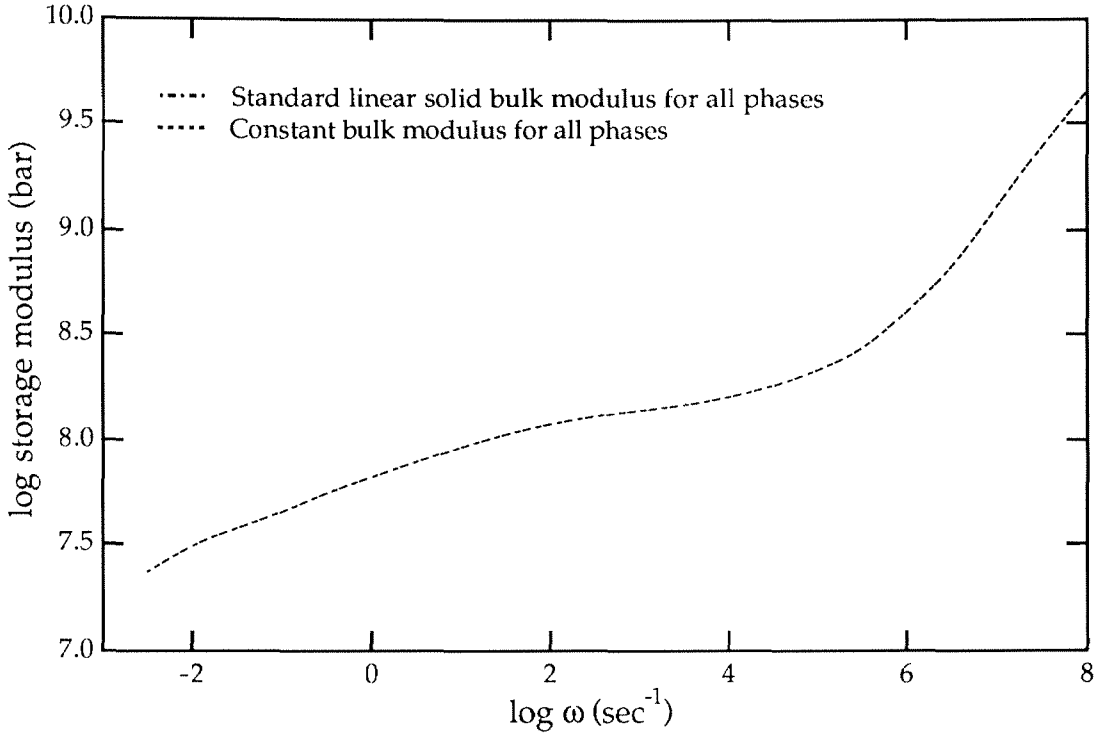

Figure 7.9a: Comparison of SBS composite storage modulus results with constant and standard linear solid bulk moduli for all phases: results identical within plotting accuracy

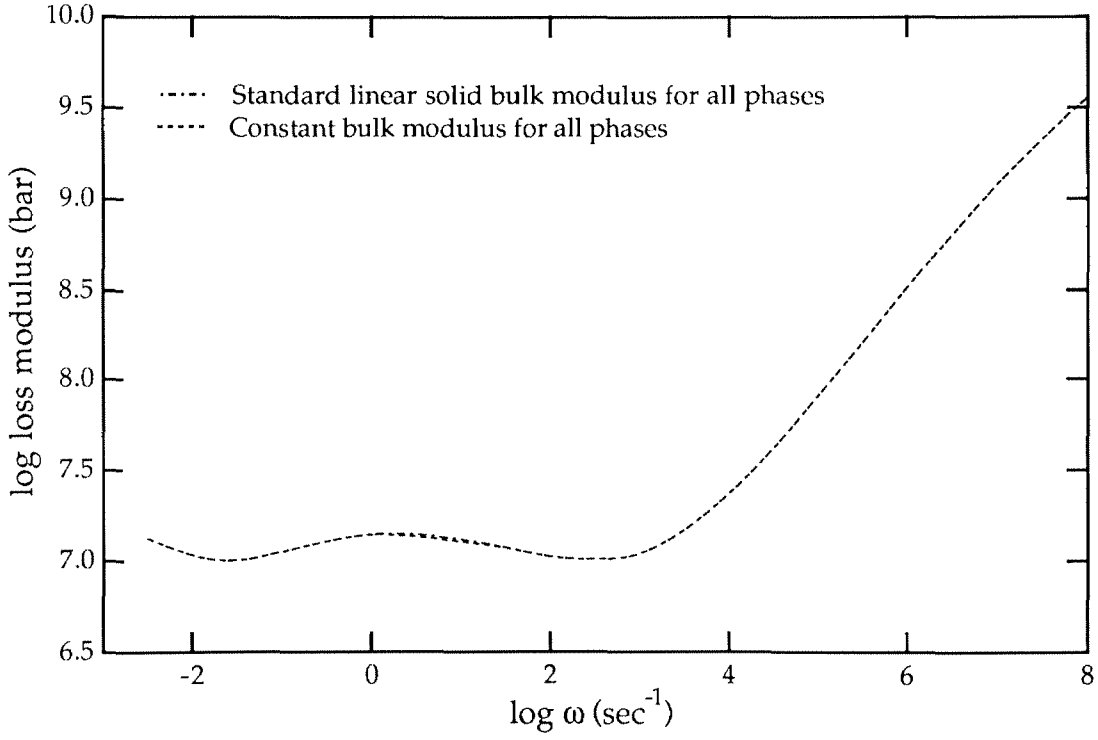

Figure 7.9b: Comparison of SBS composite loss modulus results with constant and standard linear solid bulk moduli for all phases: results identical within plotting accuracy

Discussion

With a complete and accurate set of data for the material properties of the individual phases of a multi-phase polymer the analysis tool presented allows the determination of the global effective viscoelastic properties of the composite. In the results of the previous sub-section the computational procedure was applied to a real material and the results were compared to experimental data. The numerical results confirm the existence of an interphase region in SBS, which has been postulated by other researchers. An interphase between the polystyrene and polybutadiene domains with "intermediate" properties is necessary in order to effect thermorheologically complex behavior in the numerical results at the same frequency and temperature as in the experiments.

Because of the lack of precise information on the interphase properties, the analysis of the SBS copolymer at present amounts to a data-fitting procedure for the determination of a reasonable set of properties for the interlayer based on the experimental data; with this caveat and the numerically determined interlayer properties, the computational scheme can be applied to compute moduli at all frequencies and temperatures. There is little doubt that the properties determined here for the interlayer are not necessarily unique, because by varying the size and properties of the interlayer more than one set of data could yield nearly the same desired results. However, it is not asked that the properties determined for the interlayer from the numerical analysis be unique at this stage; rather, the thrust of the present explanation is that if one had knowledge *a priori* of the physical properties of the transition region (size, gradients of properties...), then it would be possible to model them in

this numerical method to obtain the modulus functions of the composite at all temperatures and frequencies. Furthermore, it is believed that if determination of the interlayer properties was the desired objective, this analysis tool could accurately solve the inverse problem and provide a reasonable single set of properties for the interlayer, provided that there was available a sufficiently large range of detailed experimental data on the properties of the composite.† In particular, low frequency data at many temperatures would be required.

Figures 7.10 show the individual phase moduli of the interlayer, inclusion, and matrix materials along with the resulting composite moduli from the numerical analysis to aid in discussion of the TRC behavior of the composite. Similar to the idealized property case in Section VI, the composite behaves as a TRS material at temperatures and frequencies where the interlayer and the inclusion are behaving as glassy materials with constant glassy viscoelastic moduli. So, considering two temperatures of composite modulus data at frequencies above which the interlayer and the inclusion have not yet undergone their glass-to-rubber transition, in both cases the composite will have the same relaxation behavior and therefore the moduli curves will have the same shape (that of the matrix material) and be shiftable. This TRS-like shifting of high frequency data is because the relaxation mechanisms active in the composite will be only those of the matrix material at frequencies above the g-r transitions of the included phases. The composite moduli curves for 25°C and 85°C for example, have identical shapes for frequencies above the interlayer transition.

---

† See subsequent subsection, "Discussion of Interlayer Properties," to see how certain aspects of the interlayer properties are determined by the experimental data.

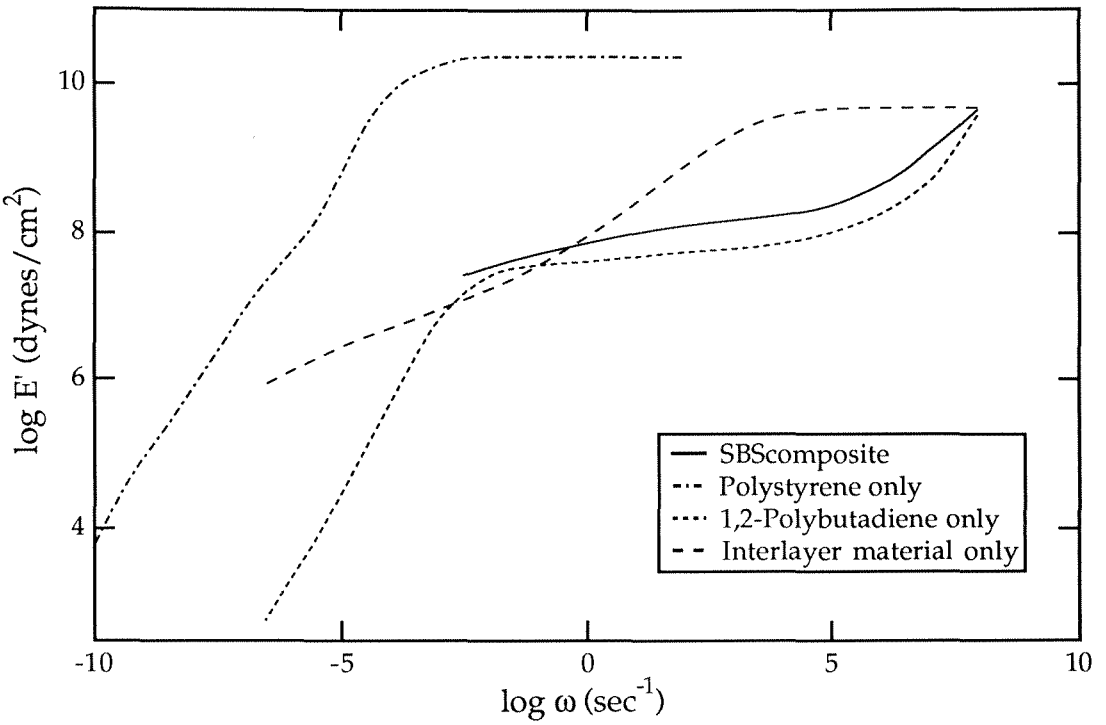

Figure 7.10a: 1,2-SBS composite and constituent storage moduli at 85°C

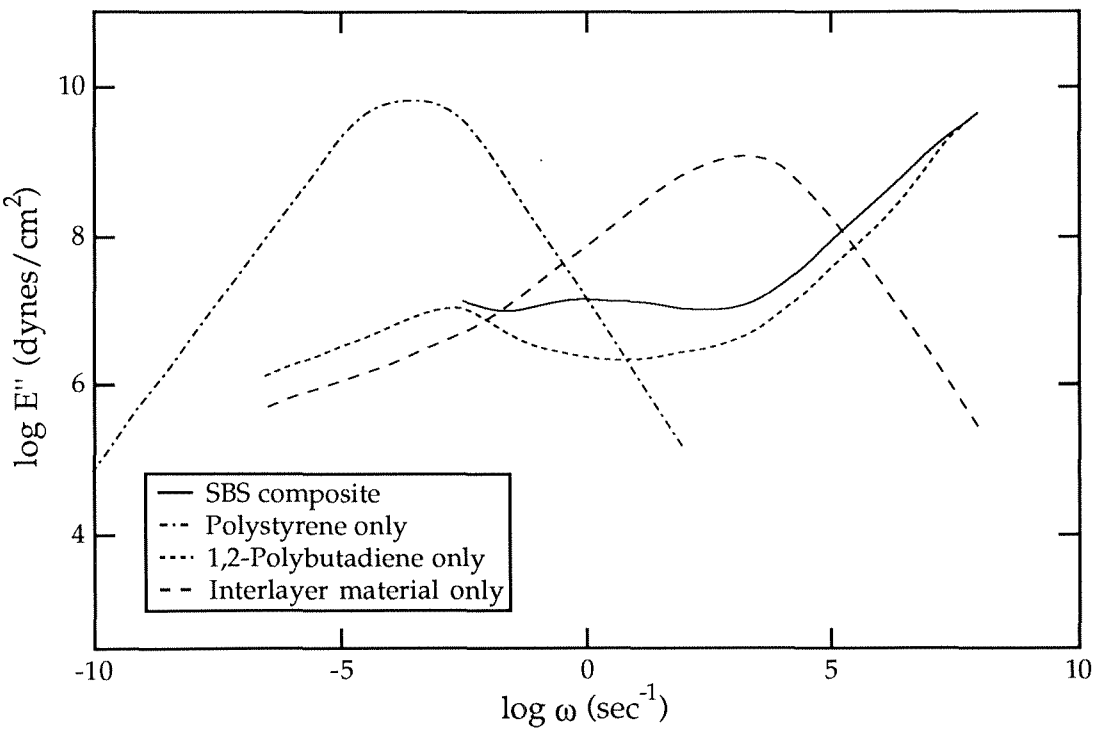

Figure 7.10b: 1,2-SBS composite and constituent loss moduli at 85°C

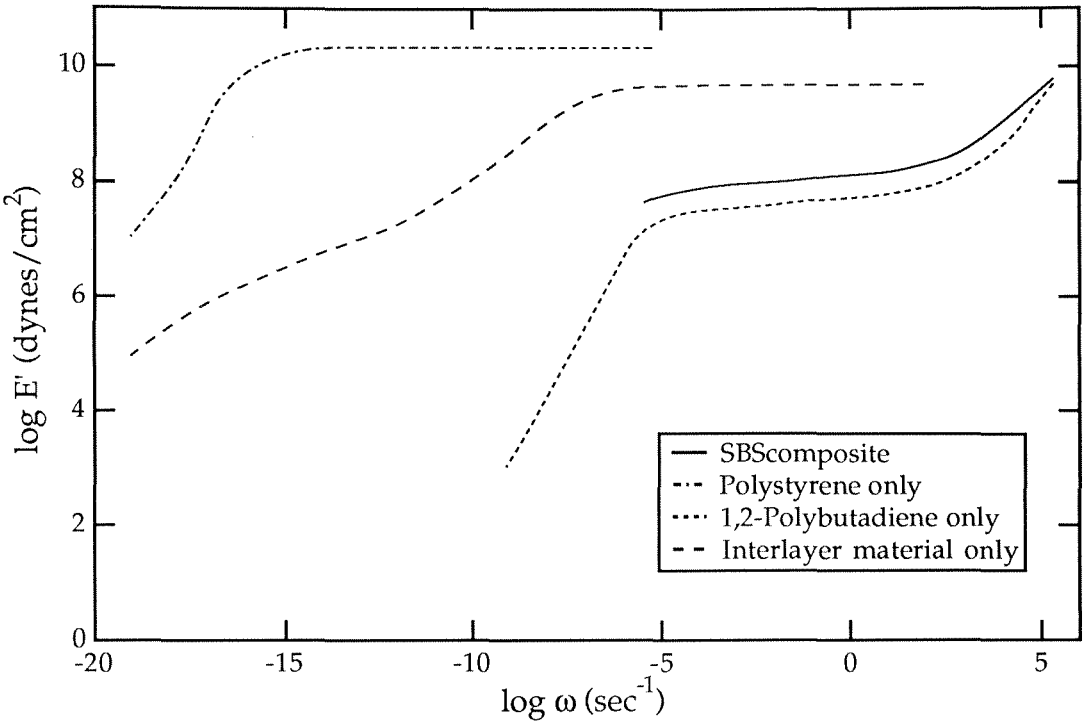

Figure 7.10c: 1,2-SBS composite and constituent storage moduli at 25°C

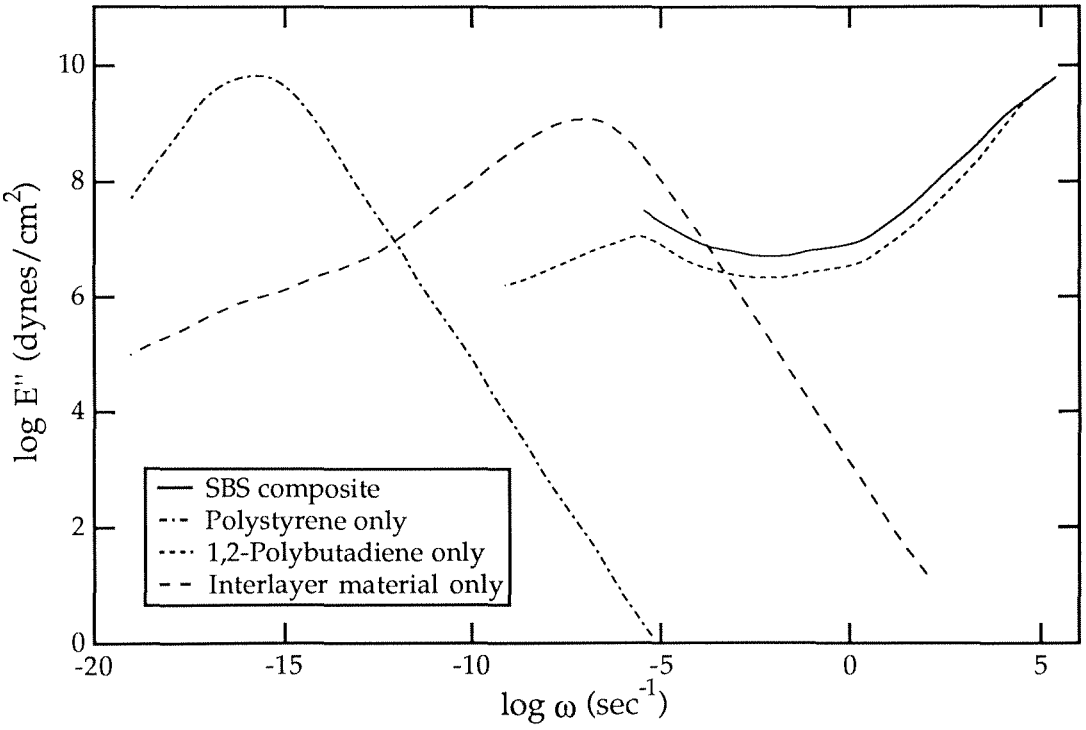

Figure 7.10d: 1,2-SBS composite and constituent loss moduli at 25°C

The relative rate of change of the properties of the individual phases for a given temperature change is important to the results for the composite. Differences in the rate of change of properties with temperature of two materials are most notable near the glass transition temperature of each phase, where the properties of a material are extremely temperature sensitive. Thus, the shift factor possesses a high slope near the T_g, which quickly abates with increasing temperature. For example, for the shift factor of polystyrene in Figure 7.7, near the T_g a change in temperature of only 10°C produces a time shift in properties of 3-4 decades, whereas 40°C above the T_g the same 10°C change in temperature produces a shift of only 1/2 a decade in time.

Because of this phenomena of rapid change in properties of each phase near the glass transition temperature and because of the large difference in the glass transition temperatures of the phases in SBS, the relative amounts of shift of the two phases become quite noticeable in the results: As temperature increases, the g-r transitions of the interlayer and the inclusion shift more through time than the g-r transition of the matrix causing the TRC behavior of the composite, which is manifested near the transition of the interlayer, to appear at higher frequencies. For the entire temperature range of the experiments, the polybutadiene matrix is in its rubbery phase and therefore the properties shift very little on the time axis with changing temperature (only 3 decades in time for a change in temperature of 60 °C, from 25° to 85°. See Figures 7.10 and 7.11). Thus, when the temperature of the composite approaches the 75°C glass transition temperature of the interlayer or the 93°C glass transition temperature of polystyrene, these two phase properties, which are 5-10 decades lower in frequency than the transition of the polybutadiene properties at 25°C, rapidly come into the time and frequency range that is

experimentally measurable, and in fact the g-r transitions of the matrix and included phases begin to coincide. At the frequency where the g-r transition region of the interlayer or inclusion is encountered, the behavior of the composite changes from that of an elastically filled polybutadiene to a composite with truly complex properties.

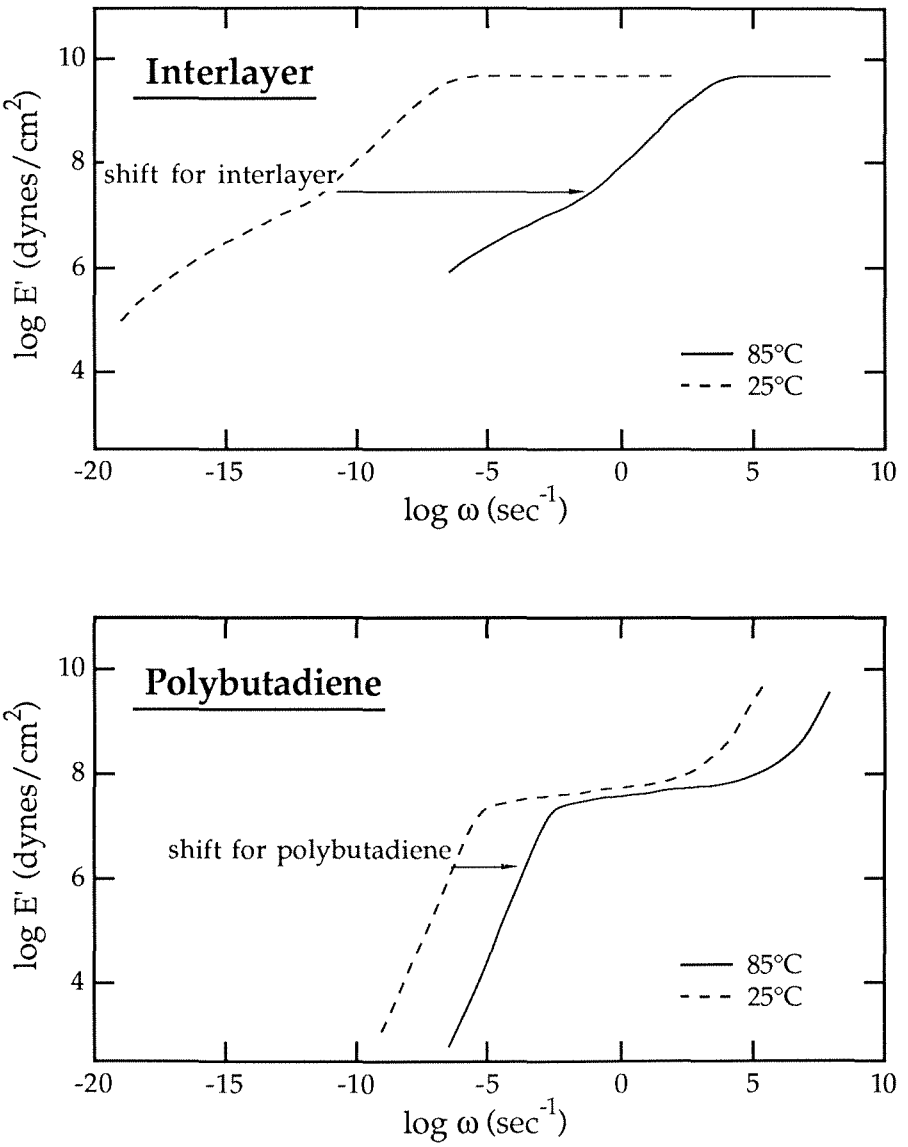

Figure 7.11: Difference in shifting of matrix and interlayer materials for the same temperature difference, near T_g of interlayer

In Figure 7.8 one notices that not every aspect of modulus curves at each temperature is matched exactly by the numerical results. In particular, the experimental curves at 75°C and 85°C appear to possess a second decrease in the loss compliance at *log* ω*=1* that does not occur in the numerical results. With the current single interlayer model it does not seem reasonably possible to match this secondary dip at 85°C and preserve the proper characterization for the 95°C curve. If a multiple phase interlayer was employed, however, it might be possible to adjust the individual properties to account for this secondary dip in the loss compliance at 85°C (and to a lesser extent at 75°C) while still maintaining full representation at 95°C. As stated earlier we do not feel comfortable, however, incorporating a multiple phase interlayer at this time because of lack of information on the actual transition region in the real material, but it is believed that the numerical procedure is able to capture the major features of the experimental data with the single interlayer model with commensurate precision.

There is a special feature of the numerical results for both the idealized composite of Section VI and the SBS composite that is worth considering. For both composites in the case of stiff inclusions (and interlayers) in a softer matrix material there is an apparent frequency lag between the glass-to-rubber transition of the included phases and the appearance of the secondary loss peak in the composite moduli. One notes from Figure 7.10 that the interlayer in SBS has the loss peak at *log* ω*=3* at 85°C; the composite, however, shows the secondary loss peak due to the interlayer at *log* ω*=0*. Also, in the idealized composite in Figure 6.5b, the stiff material alone has the loss peak at *log* ω*=-12* at 0°C while the composite shows its secondary loss peak due to the stiff material at *log* ω*=-15*. It appears thus that in these cases the composite *begins* its

secondary loss peak at the maximum of the loss peak in the included phase material. Further elucidation for this phenomenon arises from the study of the sensitivity of the composite to interlayer properties in Section IX. It will be shown in that section that the location in frequency of the secondary peak in the composite loss modulus due to the interlayer (or inclusion) transition can be moved by changing the relative magnitude of the modulus of the interlayer (or inclusion) to the magnitude of the matrix material modulus. This interplay between the amplitude of the modulus of the included phase and the frequency at which its relaxation mechanisms affect the composite properties possibly emerges from the rate sensitivity of these viscoelastic materials. Further explanation of this effect is postponed to Section IX.

Discussion of the Properties for the Interlayer

A portion of this overall study in Section IX examines the sensitivity of the composite results to the interlayer properties. Such a study is necessary in the effort to solve the inverse problem: determination of the properties of the interlayer given the composite properties. In the SBS example, there is not quite enough experimental data on the composite properties at many temperatures and low frequencies to allow for determination of definitive, unique interlayer properties. However, by means of the investigation in Section IX and from other observations on the thermorheological behavior of the composite, a reasonable set of properties for the interlayer was determined. This sub-section explains how some of the properties of the interlayer were confined to lie within specific ranges by the experimental data.

From the investigations and observations surrounding the glass transition temperature of a phase, the associated g-r transition region, and their effect on

composite properties, one concludes that the location of the g-r transition region of the viscoelastic properties for the interlayer and the glass transition temperature of the interlayer are quite important. To match the experimental data for the SBS composite, the g-r transition of the interlayer, considered as a homogeneous phase, must be in the vicinity of $log\ \omega=3$ at T=85°C, because the SBS composite begins to exhibit TRC behavior at that frequency and temperature. The location of the transition is not pinpointed exactly, however, because different shapes of the g-r transition region of the interlayer properties can accommodate moderately differing transition locations (±1 decade) to give the same overall effect.

The glass transition temperature (T_g) of the interlayer is also important to the manifestation of TRC behavior in the composite on account of the temperature sensitivity of the shift factor near that transition temperature. Near the T_g of the included phase, small changes in temperature cause large changes in the viscoelastic properties of the included phase, resulting in modulus curves for the composite that are markedly different in shape. For the SBS composite, the TRC behavior changes drastically between 75-95°C, indicating that the T_g of the interlayer should be in that range. Both the location of the g-r transition for the interlayer and the T_g of the interlayer are fixed to within approximately two decades and 20°C respectively by the amount of non-shifting of the experimental data and the temperatures at which it occurs. A T_g of 75°C for the interlayer is a little higher than might be initially anticipated, much closer to the T_g for polystyrene than that for polybutadiene; however it is consistent with the suggestion that the interlayer is rich in polystyrene and with assumptions by Cohen and Tschoegl, namely that the T_g of the interlayer lies within the temperature range in which the TRC behavior is observed in the

composite.[18] After the T_g is determined and the modulus properties are chosen, the shift factor for the interlayer itself is fixed by the location in frequency of the secondary loss peaks in the composite in experimental results at different temperatures. The difference in the 75°, 85°, and 95° curves was used to determine the necessary shift factor for the interlayer in the SBS material after the T_g and modulus properties of the interlayer were chosen.

Other aspects of the interlayer properties are not, however, fixed as clearly by the current set of experimental data. For example one finds from Section IX that the magnitude of the interlayer moduli and size of the interlayer can be "traded off" for a similar overall effect. In the SBS example a median size is chosen for the interlayer, which then fixed the magnitude of the moduli. However, the size of the interlayer is really not known and therefore the magnitude of the interlayer properties is subject to question. In addition, the location of the secondary loss peaks in the composite at a given temperature is also shown in Section IX to depend upon the amplitude of the moduli for the interlayer. Thus, the shift factor is highly dependent on the magnitude of the interlayer moduli. From this, one perceives the interdependence of individual aspects of the interlayer properties on one another in terms of their influence on the composite behavior and one begins to realize the difficulty of fully or uniquely determining the interlayer properties in this example.

An interesting result of the trial and error iteration to obtain the interlayer properties was the shape of moduli that was required. In order to mirror the slow and gradual departure of the experimental modulus curves as temperature increased (in Figure 7.8 and Figure 7.1) from the "master curve" shape at low temperatures (essentially the matrix modulus shape), it was necessary to postulate interlayer properties that varied very slowly over a long frequency

span in the g-r transition. The final interlayer properties used to obtain the results in Figures 7.8 and 7.10 possess a g-r transition region that spans many decades with a slope on the log-log plot less than half that of the polystyrene properties. When one allows for the properties of the interlayer to have a steeper slope in the transition region than that shown in Figure 7.10, the resulting composite modulus curves depart too sharply from the low temperature behavior as the interlayer transition is encountered. The frequency of departure can be made to be correct for each temperature, but the shape of the composite modulus curve will not agree with the experimental data using interlayer properties with sharp g-r transitions. See the example of an interlayer with a "rapid" glass-to-rubber transition (g-r transition occurs over a relatively short frequency range) in Section IX, Figures 9.4a-9.4d.

This result is quite interesting because for the interlayer considered as a homogeneous phase, gradually varying properties in its g-r transition are perhaps indicative of what is likely to be occurring in the real material. The transition region between the two phases is probably a volume in which the properties change gradually from those of the inclusion to those of the matrix. If one were to model this gradual change discretely by several concentric cylinders of interlayers, each of slightly different properties having relatively steep slopes in the g-r transition (as indicated in Figure 7.12), one would experience a situation that would be equivalent in an average *(smeared)* sense to an interlayer of one material with slowly varying properties over time. There is a potential problem with the discretization of the interphase into thin rings. One would have to take care to compare the model size scale with the size scale of the physical materials. For example, if the interlayer is 40Å across, but the length of a monomer of one of the constituent polymers is

10Å, then allowing five rings in the interlayer section, each of different homogeneous material properties, would most likely be inaccurate. In that case, one has departed from traditional continuum analysis.

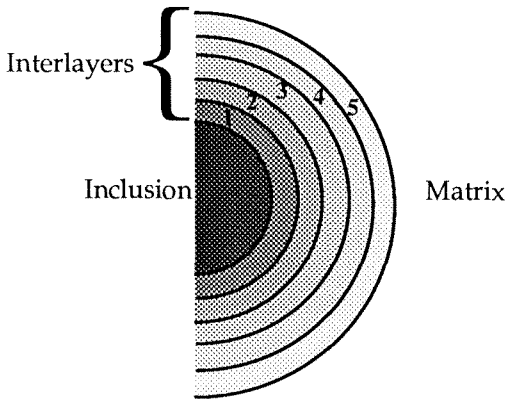

Figure 7.12a Concentric rings of interlayers of varying properties

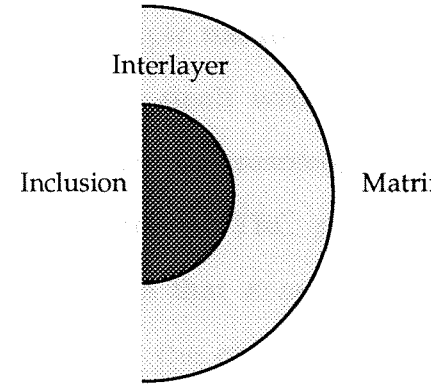

Figure 7.12b Single interlayer with gradual g-r transition

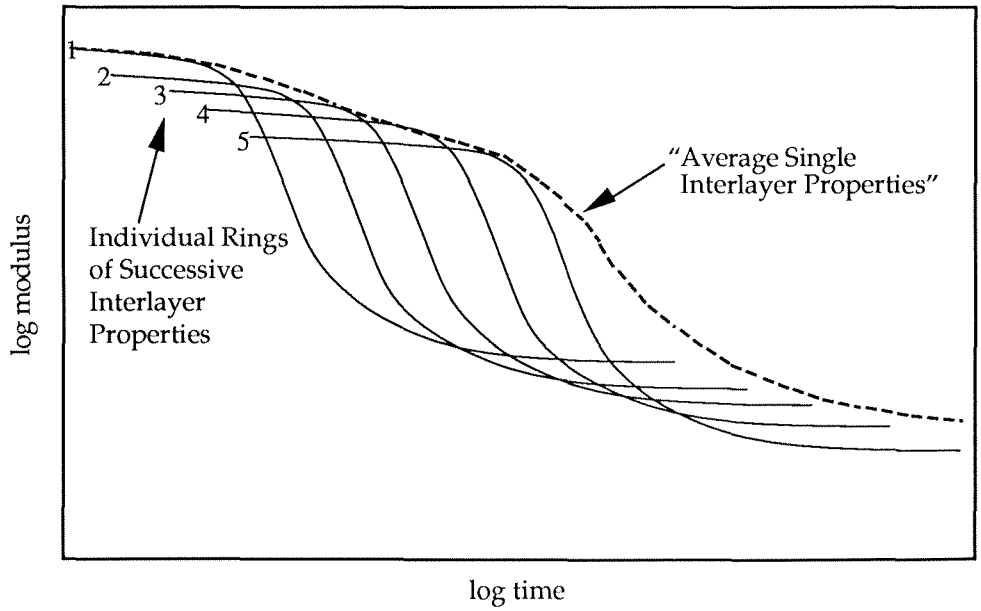

Figure 7.12c: Example of suggested moduli for each of the multiple phases in Figure 7.12a and 7.12b

VIII. ANISOTROPIC EFFECTS

In this section results are presented on the effect of anisotropy on the thermorheologically complex behavior of the SBS composite from the previous section. Referring to Figure 2.1, which shows the global material, it is clear that this material is anisotropic, though of a special anisotropic nature. One measure of anisotropy was discussed in Section V, which dealt with the shear modulus, while here in Section VIII a different measure of anisotropy based on the composite modulus in different directions and the TRC parameter, $\kappa(\omega,T1,T2)$, is discussed. From Section VI, one recalls that $\kappa(\omega,T1,T2)$ is a measure of the TRC behavior of a composite. Because the computations are attempting to capture the TRC behavior of the experimental results, the difference in $\kappa(\omega,T1,T2)$ for the SBS composite in various orientations is of importance. In this section the TRC parameter of the SBS composite in two orientations is discussed.

The viscoelastic moduli of the composite are considered in two different directions here: the first is the y-direction shown in Figure 2.1 (this orientation is used throughout this paper) and the other is the direction at a 45° angle to these x-y axes (as in the x'-y' direction in Figure 5.3). The first case yields a square array of unit cells as is developed earlier. The second case yields a hexagonal array of unit cells. (*n.b.* The second case is not a regular hexagonal array where the centers of the inclusions can be connected to form a hexagon with equal length sides.)

Figures 8.1a and 8.1b show the results for the loss moduli of the SBS composite considered in these two different material reference frames. There is a slight difference in the magnitudes of the moduli of approximately 0.2 dynes/cm^2, but the overall behavior of the moduli over frequency is essentially the same. Also, the effect of the anisotropy on the thermorheological

behavior is slight. This observation is illustrated clearly by the TRC parameter, which relates the magnitudes of the shifted loss moduli at two temperatures to each other as a function of frequency. The TRC parameter, $\kappa(\omega,T1,T2)$, was defined in Section VI, equation (6.7).

The curves for $\kappa(\omega,25,95)$ of the loss compliance for the two different directions of the SBS material considered here are shown in Figure 8.2. Note that at high frequencies for both cases this parameter is equal to zero, indicating thermorheologically simple behavior at high frequencies. At lower frequencies, the values of the parameter for each case differ slightly from one another, indicating minor differences in the non-shifting of isothermal moduli curves; however, the character of $\kappa(\omega,25,95)$ over frequency is identical indicating that TRC behavior occurs at the same temperatures and frequencies in both cases. The magnitude of the difference between $\kappa(\omega,25,95)$ for the square and hexagonal arrays is one tenth of the difference in the TRC parameter between different inclusion sizes from Figure 6.8. This example shows, therefore, that the effect of anisotropy on the TRC behavior of the type of multiphase composite examined in this work is relatively small and indicates that the study of the SBS composite in the x-y orientation (square array) as opposed to the x'-y' orientation (hexagonal array) throughout this work is acceptable.

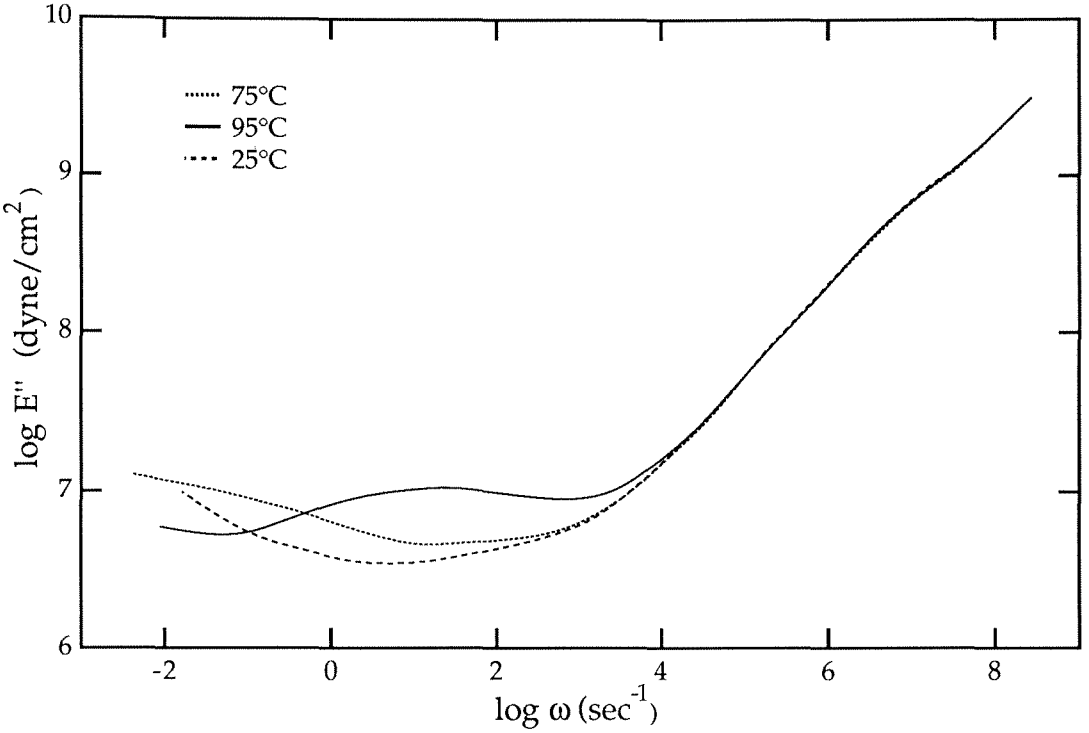

Figure 8.1a: Loss moduli of composite with unit cell orientation for square array. All temperatures shifted to T=85°C.

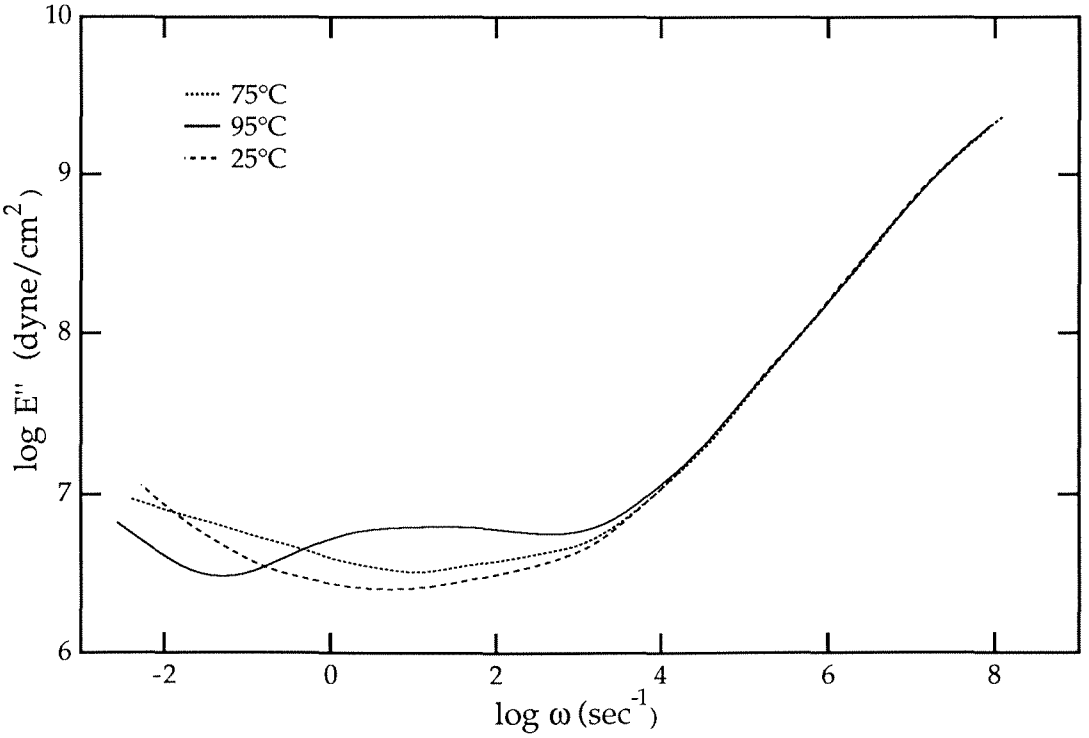

Figure 8.1b: Loss moduli of composite with unit cell orientation for hexagonal array. All temperatures shifted to T=85°C.

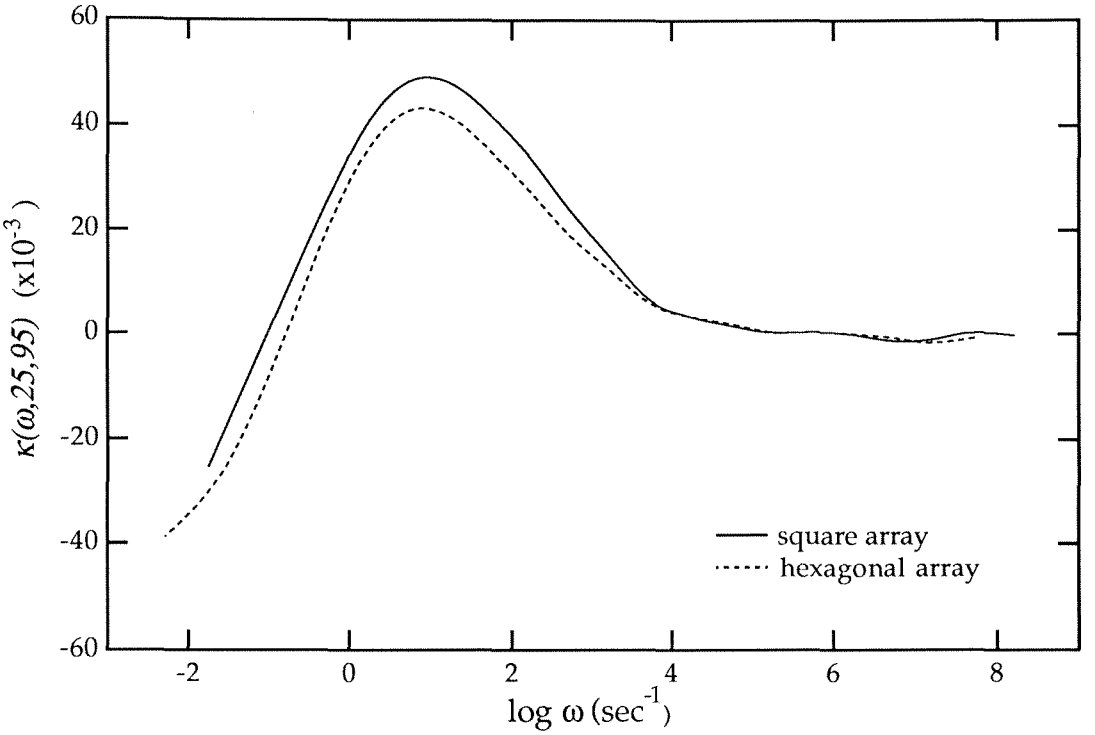

Figure 8.2: TRC parameter $\kappa(\omega,25,95)$ for different orientations of the unit cell to show anisotropy effect. Frequency values are for each temperature shifted to 85°C.

IX. Sensitivity of Composite Moduli to Interlayer Properties

In this section, results will be presented for a systematic study in which some of the material property parameters of the interlayer in the composite are varied individually. Comparisons will be made relative to the "base case" of SBS with the interlayer characterized to obtain the numerical results in Section VII. The difference in the resulting effective moduli of the composite and the difference in thermorheological complexity will be shown for each new interlayer case compared to the base case. A study such as this one is crucial to the iterative procedure used with the numerical analysis developed in this work to solve the "inverse problem," in which one extracts properties of an unknown (or partially unknown) phase in the composite from knowledge of the composite properties. This study demonstrates that the many factors contributing to the composite behavior are inextricably intertwined and further explains the deficiencies of some of the analytical models reviewed in the Introduction Section in terms of predicting composite properties based on relatively simple schemes that do not allow for coupling between factors.

The effect of the following interlayer parameters will be presented: size (volume fraction of unit cell), magnitude of the modulus, location of the glass-to-rubber transition, relaxation behavior, and the shift factor. The effect of each of these parameters on the composite behavior is studied as a separate case. The defining characteristics of each case are listed in Table 9.1. Hereafter, each case will be referred to by its case number.

Case number	Interlayer parameter, which is varied from base case SBS	Description of the parameter change relative to the base case SBS
Case 1	volume fraction	The interlayer occupies 8% of the volume fraction, exactly half that of the base case
Case 2	location of transition	Glass-to-rubber transition of the interlayer is 2 decades higher in frequency than the base case
Case 3	shape of transition	Glass-to-rubber transition of the interlayer is much "sharper" than base case transition: the modulus decreases in magnitude twice as much over same frequency range as that for the base case. See Figure 9.3e.
Case 4	shift factor	Shift factor of the interlayer is less sensitive to temperature change than the base case shift factor. $a_{T=85}(Case\ 4) = a_{T=85}(base\ case)$ $a_{T=95}(Case\ 4) < a_{T=95}(base\ case)$
Case 5	magnitude of modulus	Magnitude of the modulus of the interlayer is lower uniformly by one decade of dyne/cm^2 than base case modulus

Table 9.1: List of cases compared to base case SBS. Each new case varies one parameter of the interlayer properties of the SBS of Section VII.

From the discussion of the interlayer properties at the end of Section VII, it is suggested that the numerical fitting procedure to determine the interlayer properties produces non-unique results. This systematic study of the effects of the individual interlayer properties on the composite properties was performed to attempt to better define the degree to which interlayer parameters could be changed and yet still achieve the same desired results for the composite. Unfortunately, the results from this study are not that easily interpreted. Change in an interlayer parameter affects the composite properties in a highly non-linear fashion; furthermore, change in one interlayer parameter causes change in more than just that same parameter in the composite. This

study does reveal, however, a few important phenomena in terms of the composite response to the properties of included phases.

Figures 9.1a through 9.5d show the response curves for the composite moduli (for each of the individual cases of Table 9.1) that best illustrate the parameter effects. For most cases: the storage and loss moduli of the composite at 85°C are given compared to the base case; the loss moduli at 25° and 85° (shifted such that the high frequency ends coincide) are shown and can be compared to the base case situation in Figure 9.1c; the TRC parameter $\kappa(\omega,25,85)$ for each new case and the base case are compared. Discussion for each of these cases individually is omitted for brevity and because of the qualitative nature of such discussions. Instead, direct comparisons of the figures with one another point out the different effects of each parameter rather clearly. A few particularly salient points on the multiple effects of changing a single parameter are mentioned here.

In Case 2 for which the frequency of the interlayer properties was shifted uniformly two decades toward higher frequencies, the noticeable difference from the base case regards the location of the onset of TRC behavior in the composite. From Figure 9.2b or comparing 9.2c to 9.1c, one sees immediately that, as expected, the TRC behavior arises at higher frequencies in Case 2 than in the base case at the same temperature. However, from examination of Figure 9.2d, one discovers that the character of the TRC behavior is qualitatively different in these two cases. For example, the peak of the TRC parameter is somewhat higher in Case 2 than in the base case. Also, the location of the peak of the TRC parameter in frequency for Case 2 is less than exactly two decades higher than that of the base case; it is approximately 1.8 decades higher. That the composite should evidence different TRC behavior for the

same temperature range is not completely surprising since the transition of the interlayer is at a different location relative to the matrix material modulus for each case: the magnitude of the matrix moduli at the transition of the interlayer differ in Case 2 and the base case.

In another example, Case 5 with a uniformly lower modulus than the base case demonstrates what one would initially expect in Figure 9.5a: the magnitude of the composite storage modulus is subsequently lowered in Case 5 compared to the base case. However, Figure 9.5b showing the loss moduli of each case at 85°C demonstrates a striking difference between the two cases other than magnitude of modulus: the location of the second peak in the composite modulus due to the presence of the interlayer transition has shifted toward higher frequencies in Case 5. Previously in Section VII it was pointed out that the appearance of the second loss peak in the composite due to the presence of the included phase transition does not coincide in frequency with the loss peak of the included phase itself: the second loss peak in the composite is delayed toward lower frequencies by several decades from the actual loss peak of the included phase (interlayer or inclusion). Here, with the modulus of the interlayer decreased uniformly, the position of the second loss peak in the composite has moved toward higher frequencies (log ω =2) and is closer to the loss peak of the interlayer phase itself (which is at log ω =3 at 85°C). From the TRC parameter for these two cases in Figure 9.4d, it is clear that the TRC behavior of the composite with a lower magnitude modulus occurs at higher frequencies then for the base case. In addition the magnitude of the TRC behavior is higher in Case 5 than in the base case. This result has been checked with the idealized composite studied in Section VI. If the magnitude of the stiffer inclusion phase is lowered uniformly by one decade

(in bar), the secondary loss peak in the composite modulus shifts towards higher frequencies and the TRC behavior is larger than for the case shown in Section VI.

These examples express that although the effect of the relaxation mechanisms of the phases appearing at different frequencies at different temperatures is the most easily understood reason for the TRC behavior and non-shifting, it is not the only factor involved. More complicated causes involving the internal stress states of the materials, which vary with additional factors such as the ones examined in this section, are important to manifestation of TRC behavior as well. Indeed, one can certainly conclude from this section that the relative magnitudes of the moduli of the two phases is extremely important to the influence that included phase properties have on the composite properties.

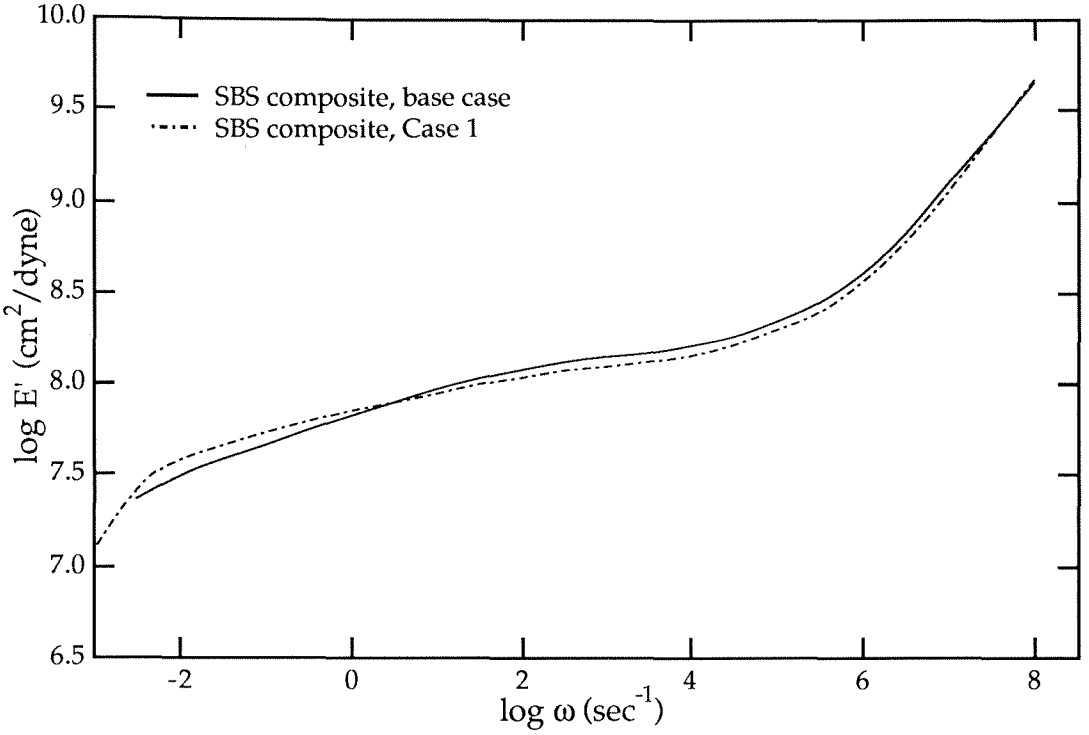

Figure 9.1a: Comparison of storage moduli for SBS with 16% and 8% volume fraction interlayer at 85°C

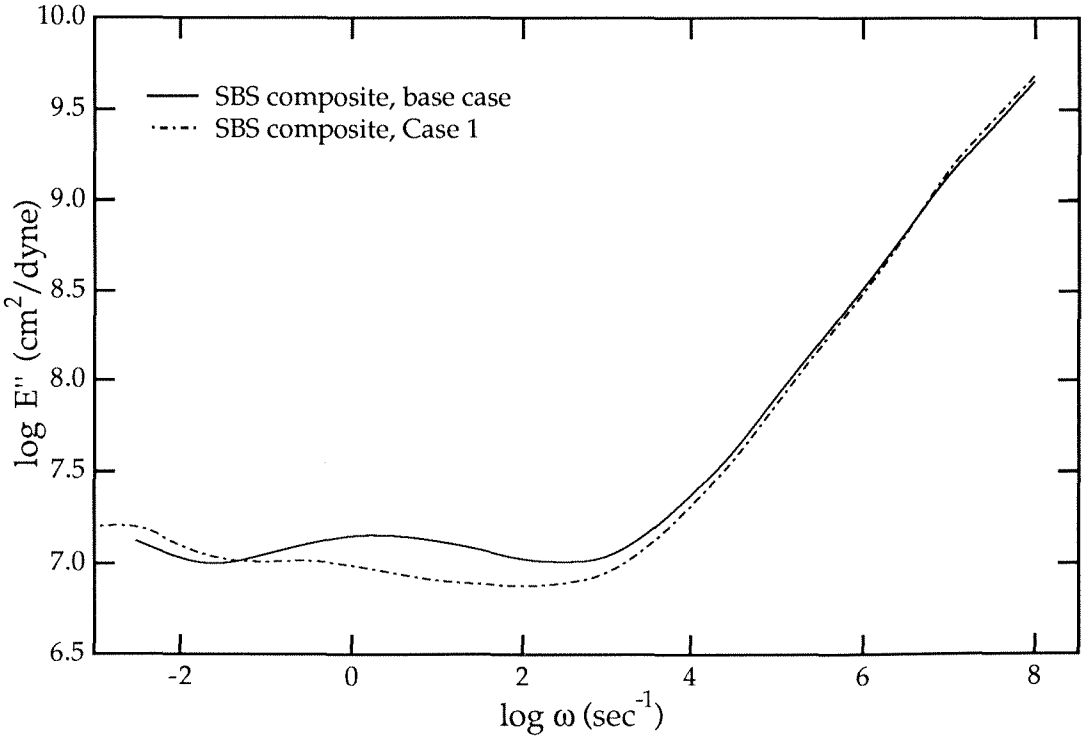

Figure 9.1b: Comparison of loss moduli for SBS with 16% and 8% volume fraction interlayer at 85°C

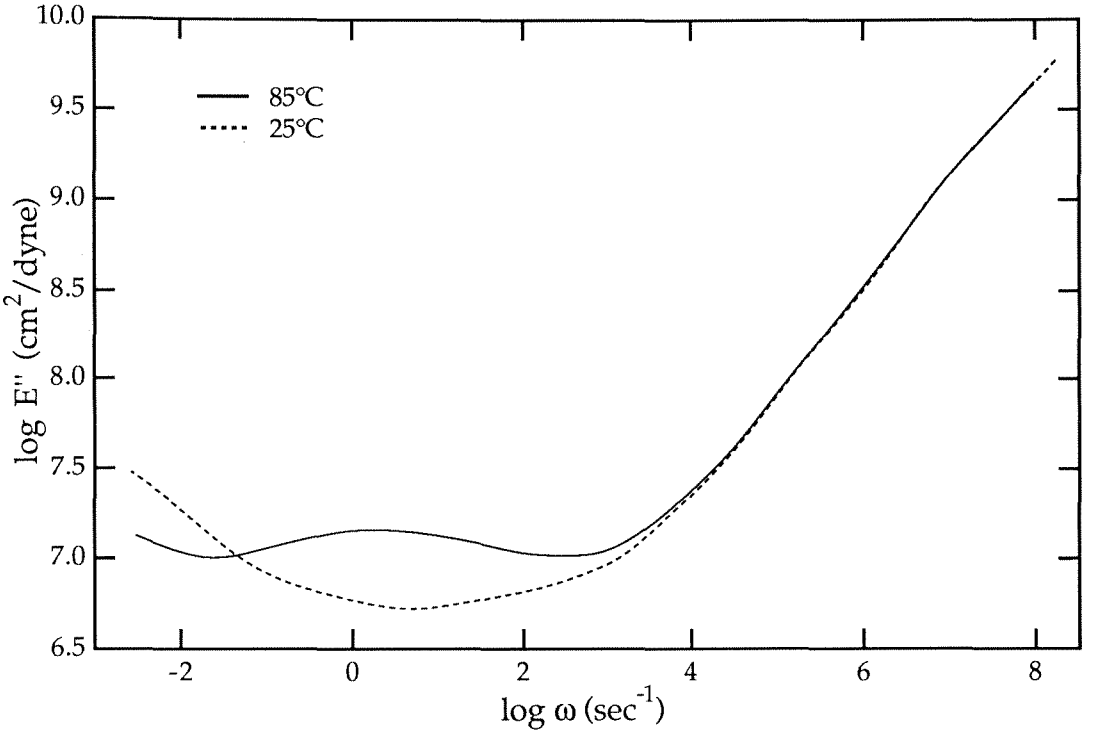

Figure 9.1c: Loss moduli of SBS composite with original interlayer, 25°C curve shifted to 85°C curve

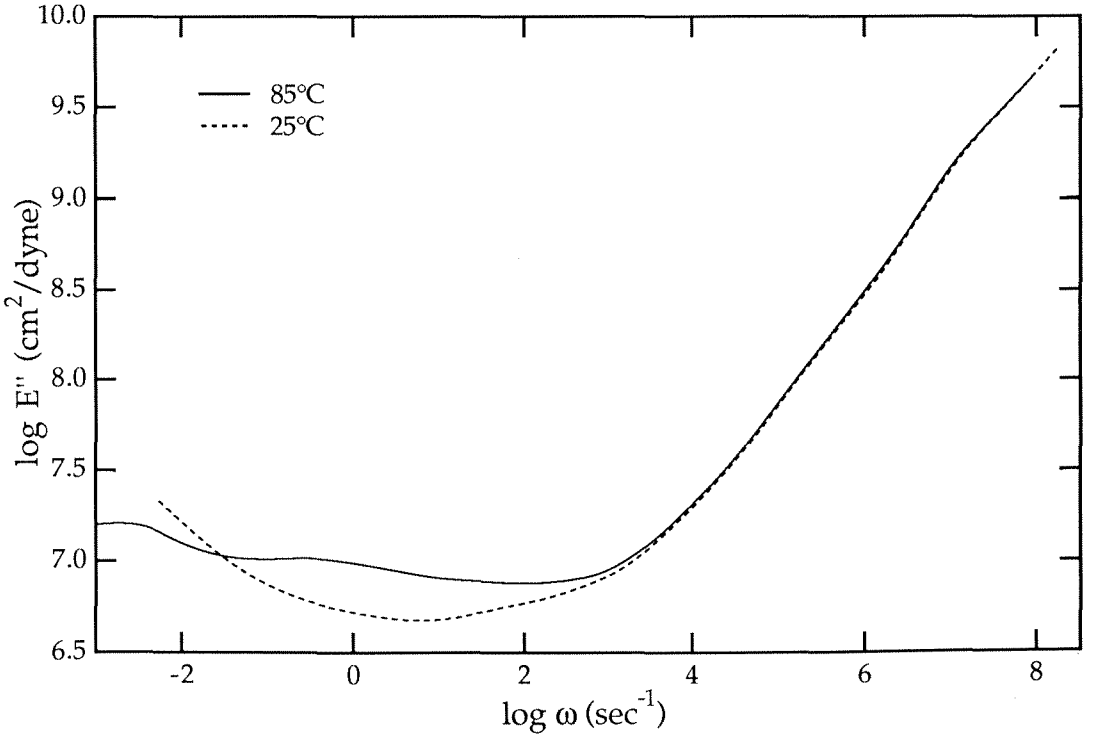

Figure 9.1d: Loss moduli of SBS composite with 8% interlayer, 25°C curve shifted to 85°C curve

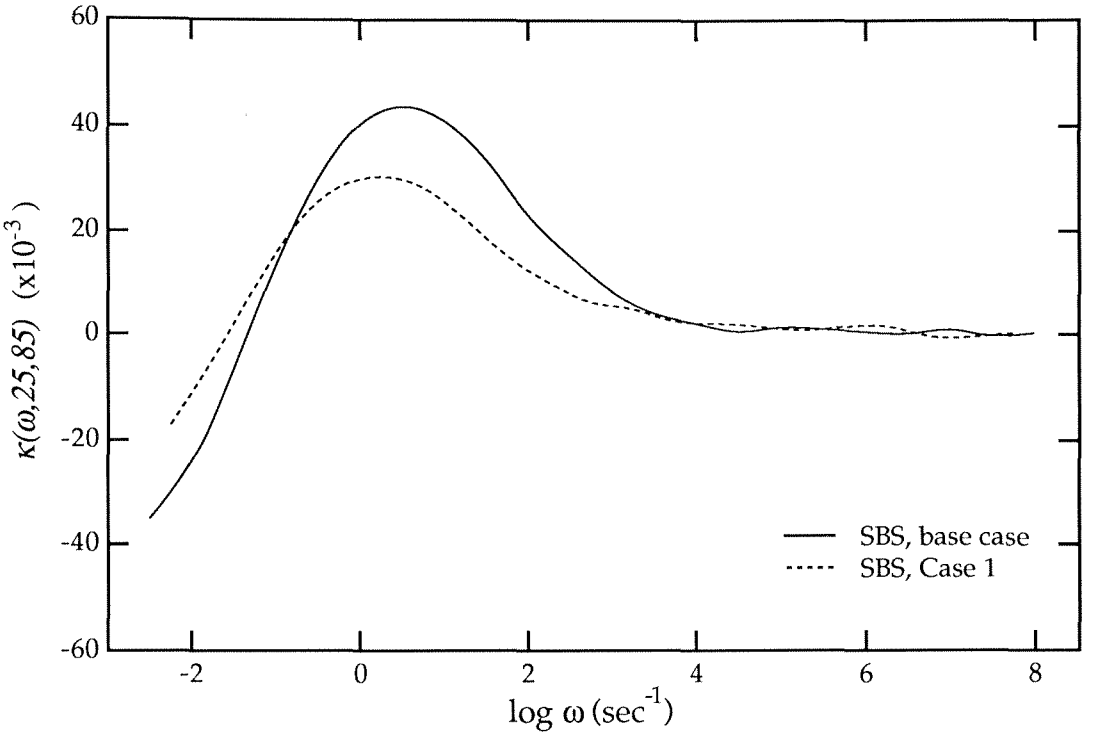

Figure 9.1e: TRC parameter, $\kappa(\omega,25,85)$, for SBS with 16% and 8% interlayer. Frequency values are for each temperature shifted to 85°C

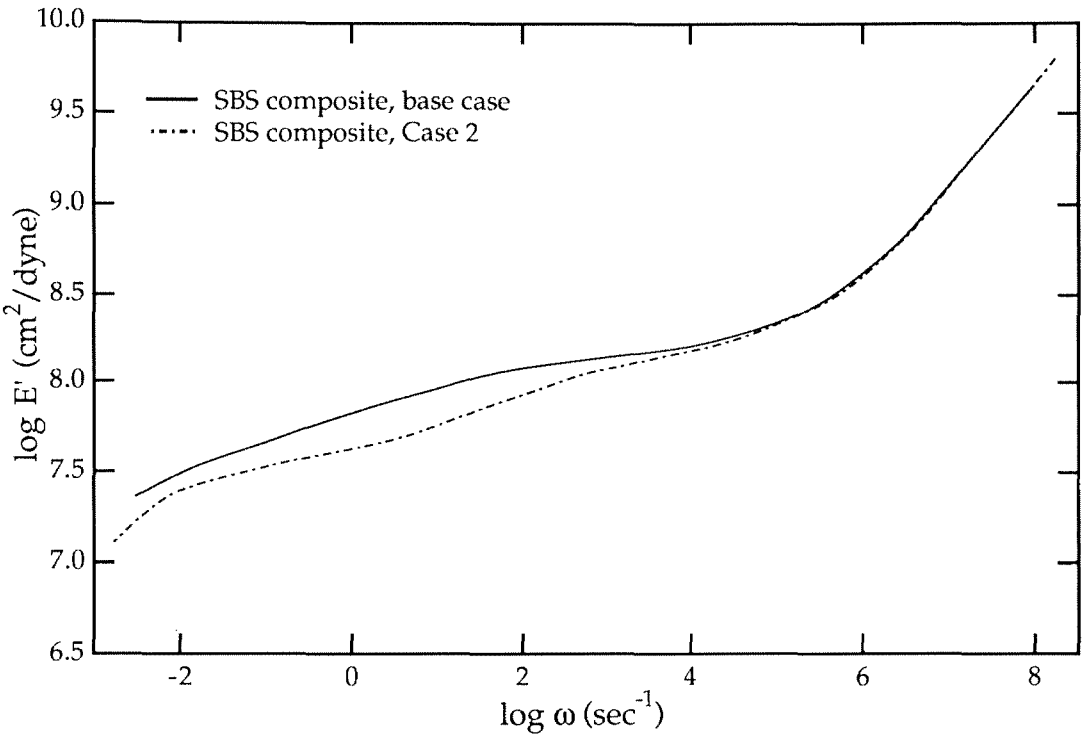

Figure 9.2a: Comparison of storage moduli for SBS with original interlayer and interlayer with transition shifted two decades higher in frequency at 85°C

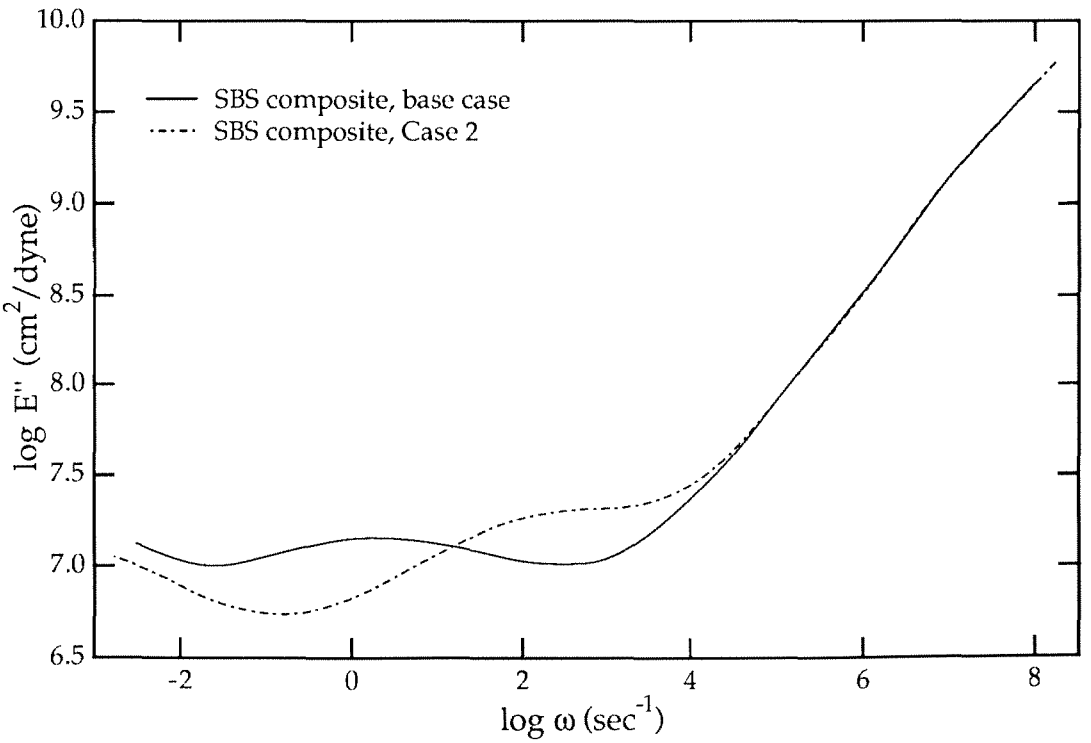

Figure 9.2b: Comparison of loss moduli for SBS with original interlayer and interlayer with transition shifted two decades higher in frequency at 85°C

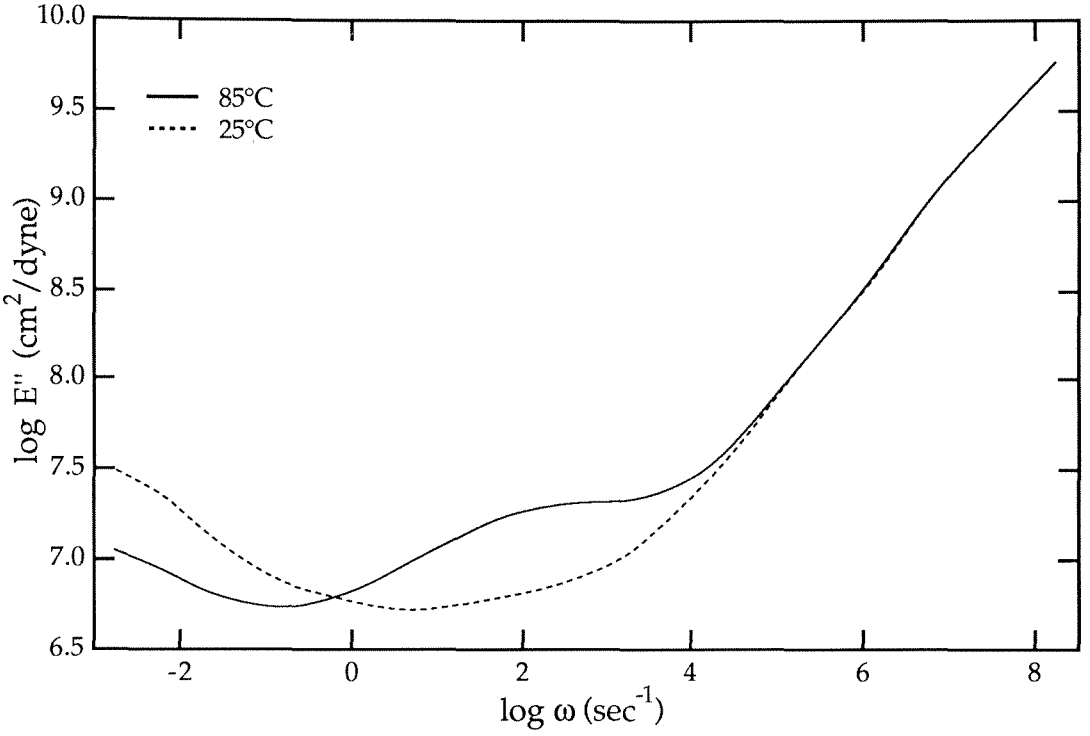

Figure 9.2c: Loss moduli of SBS composite with interlayer transition shifted two decades higher in frequency, 25°C curve shifted to 85°C curve

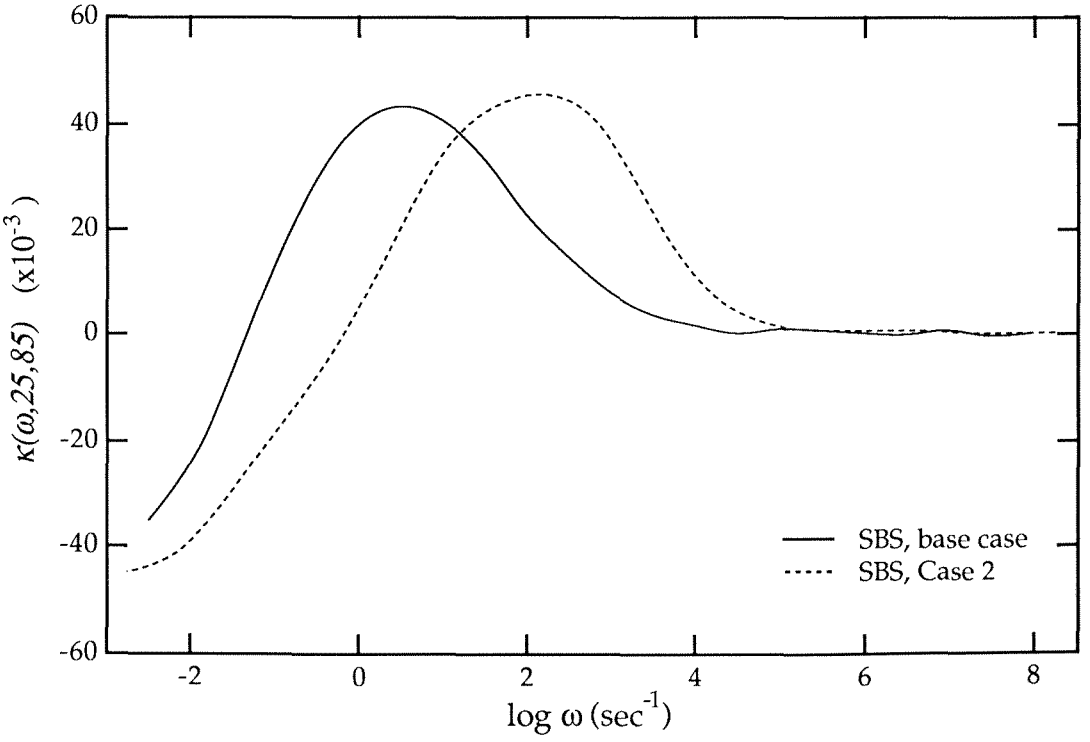

Figure 9.2d: TRC parameter, $\kappa(\omega,25,85)$, for SBS with original interlayer and interlayer with transition shifted two decades higher in frequency. Frequency values are for each temperature shifted to 85°C

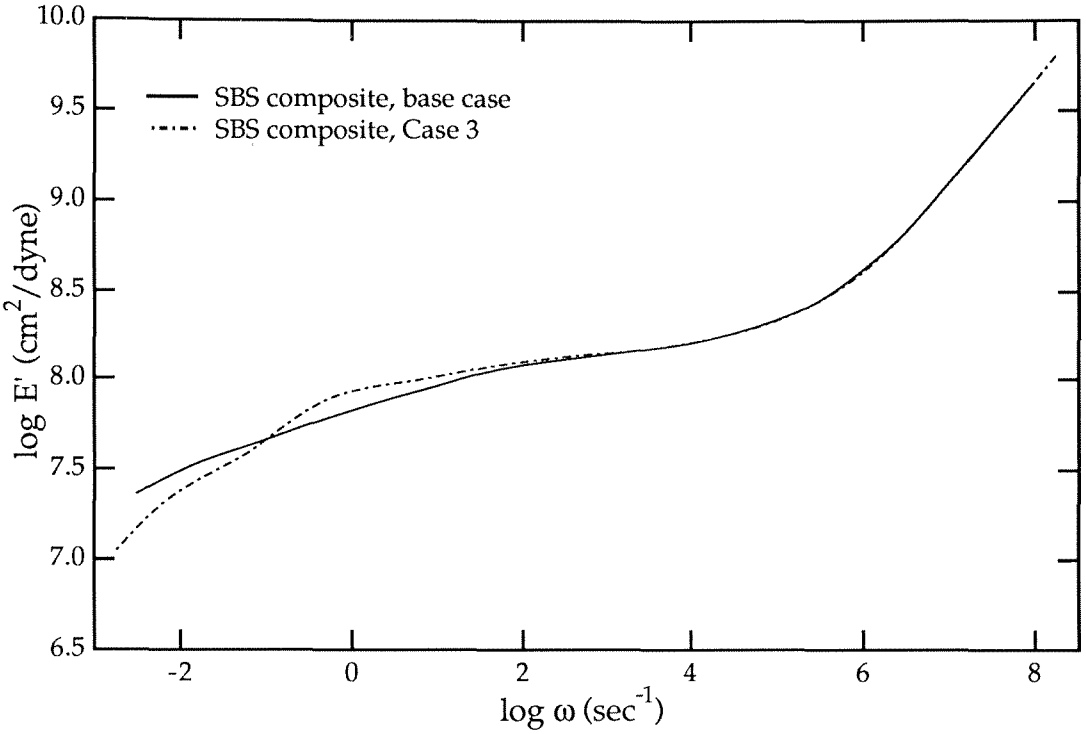

Figure 9.3a: Comparison of storage moduli for SBS with original interlayer and interlayer with sharper transition at 85°C

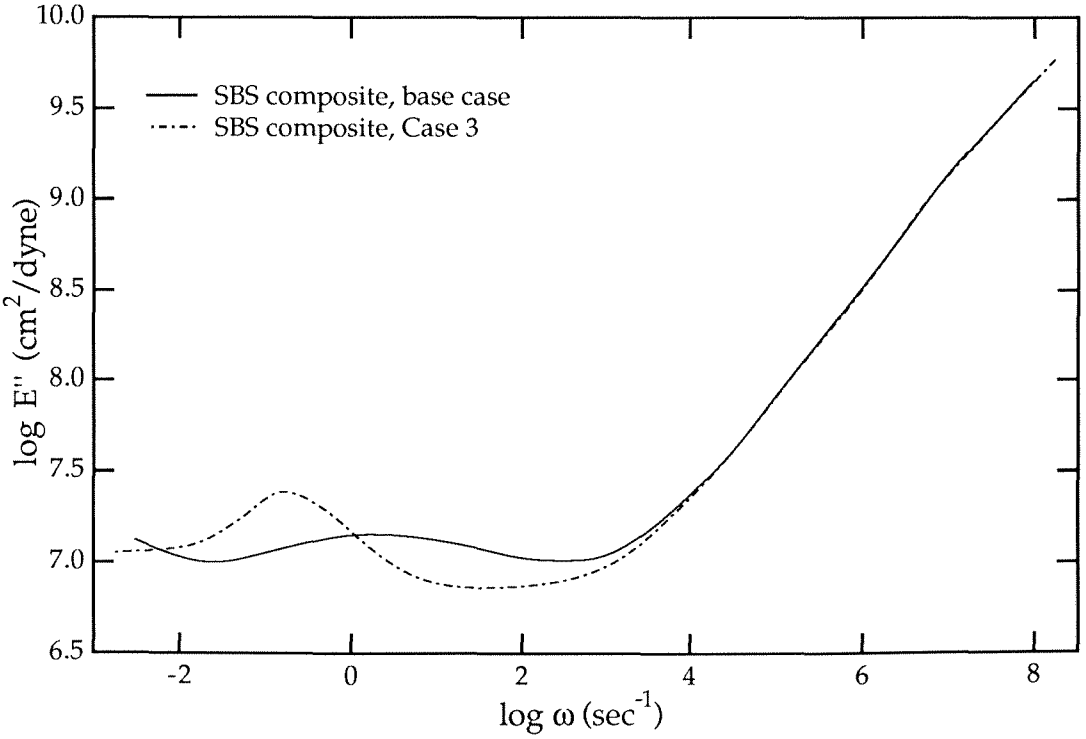

Figure 9.3b: Comparison of loss moduli for SBS with original interlayer and interlayer with sharper transition at 85°C

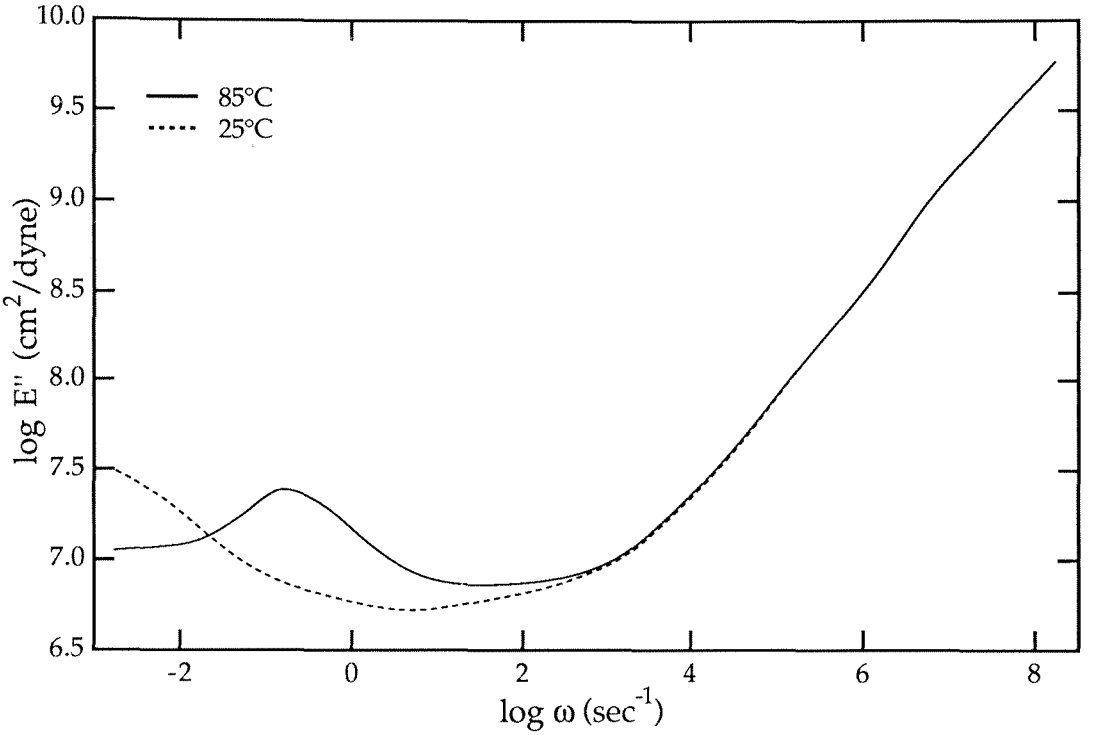

Figure 9.3c: Loss moduli of SBS composite with sharper transition interlayer, 25°C curve shifted to 85°C curve

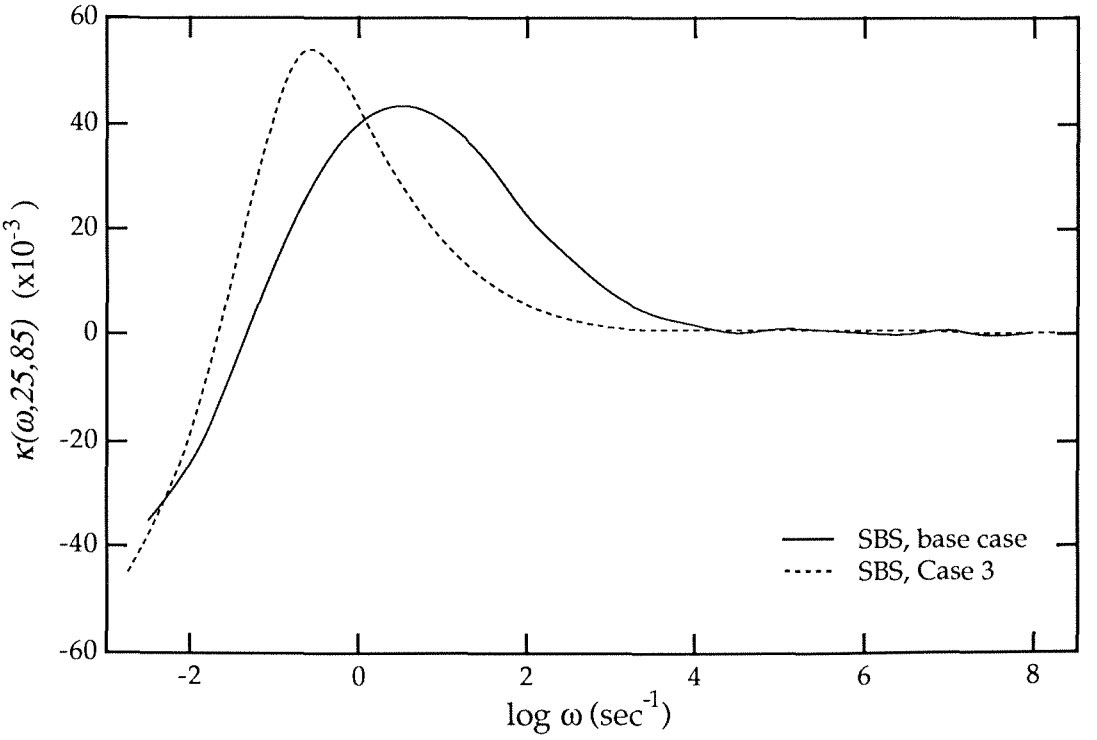

Figure 9.3d: TRC parameter, $\kappa(\omega,25,85)$, for SBS with original interlayer and interlayer with sharper transition. Frequency values are for each temperature shifted to 85°C

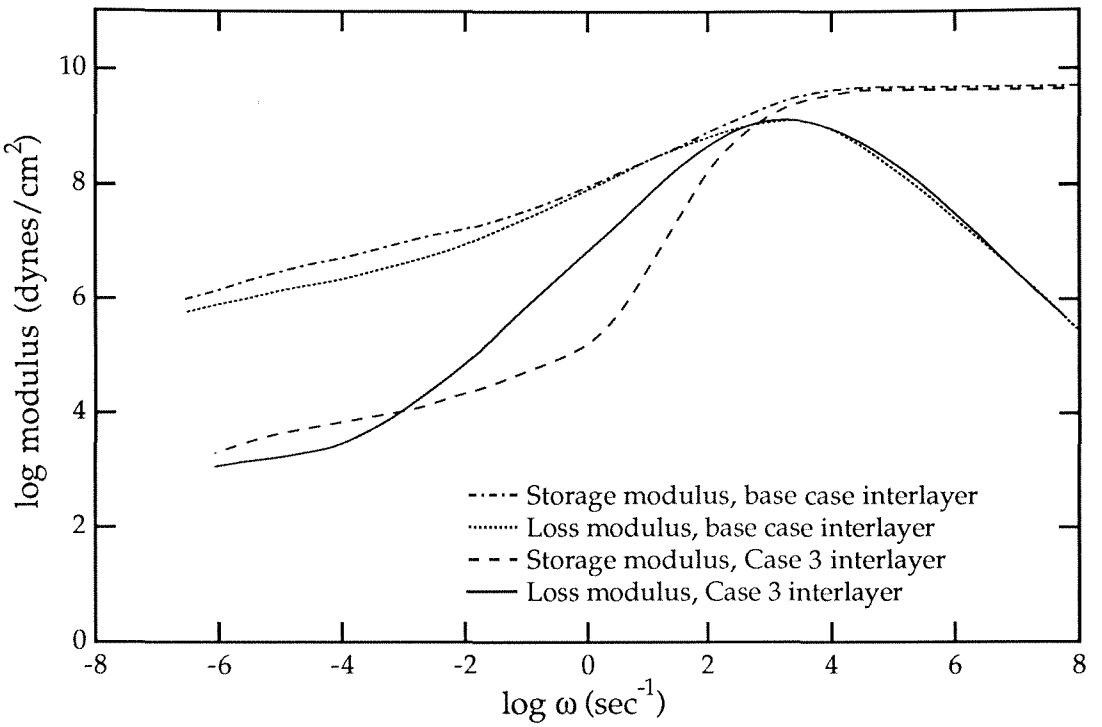

Figure 9.3e: Storage and Loss moduli of interlayer properties for the base case and for the sharper transition case (new case) at 85°C

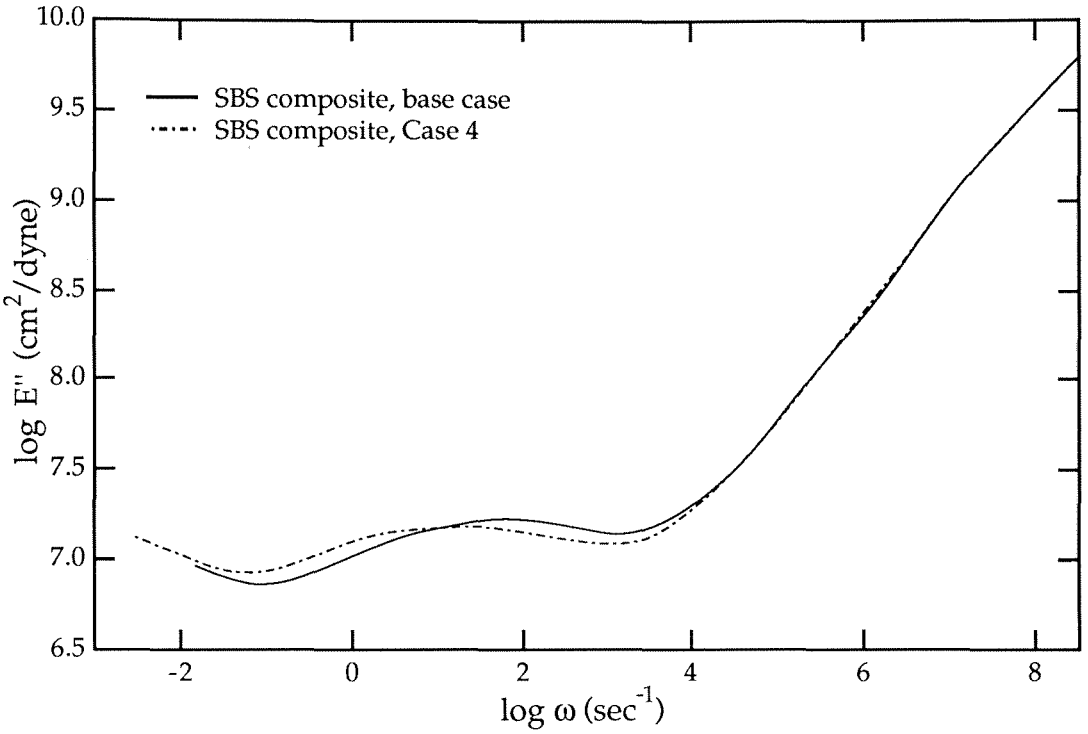

Figure 9.4a: Comparison of loss moduli for SBS with original interlayer and interlayer with changed shift factor at 85°C

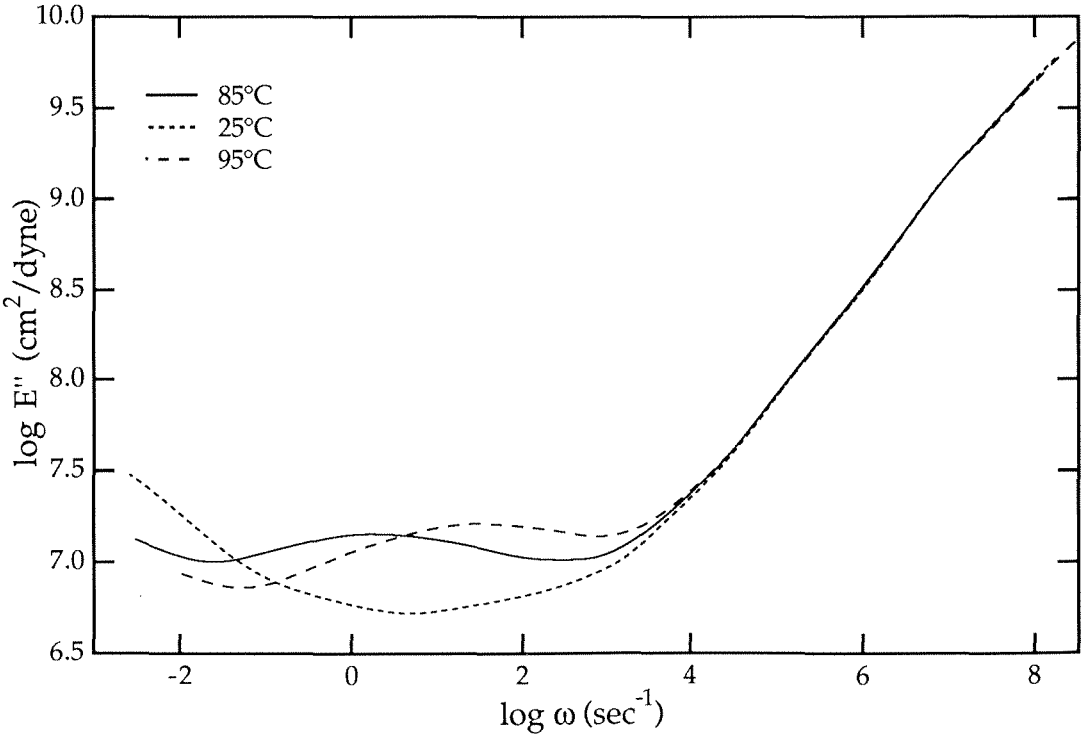

Figure 9.4b: Loss moduli of SBS composite with original interlayer, 25°C and 95°C curves shifted to 85°C

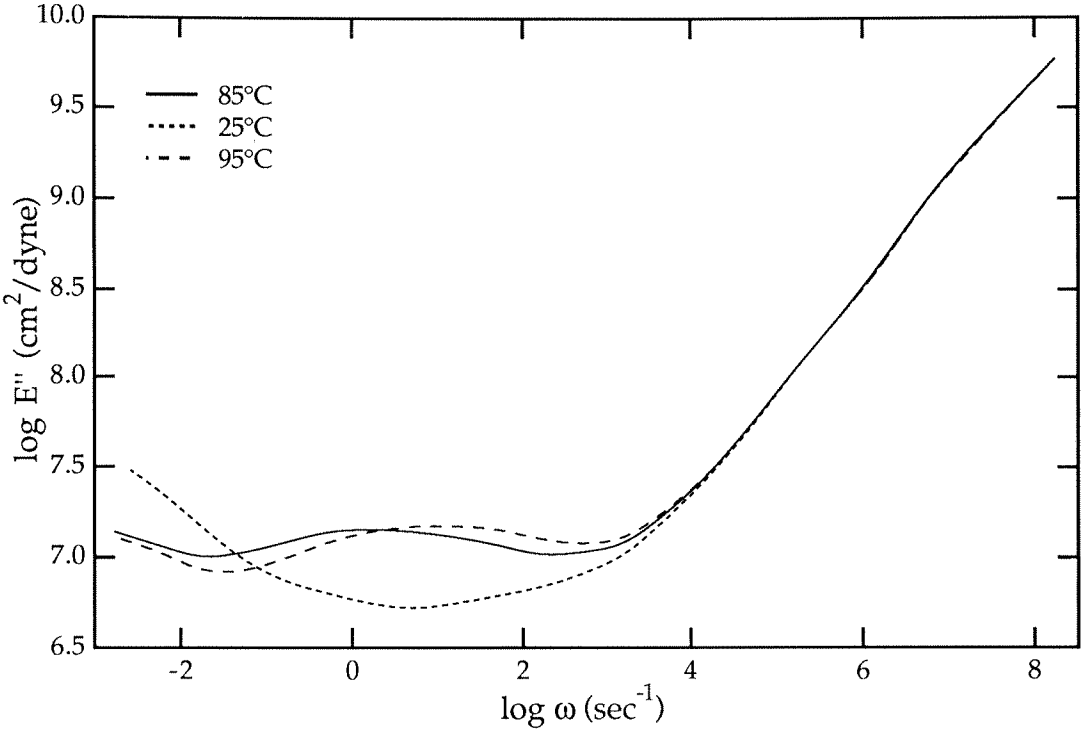

Figure 9.4c: Loss moduli of SBS composite with interlayer with changed shift factor, 25°C curve shifted to 85°C curve

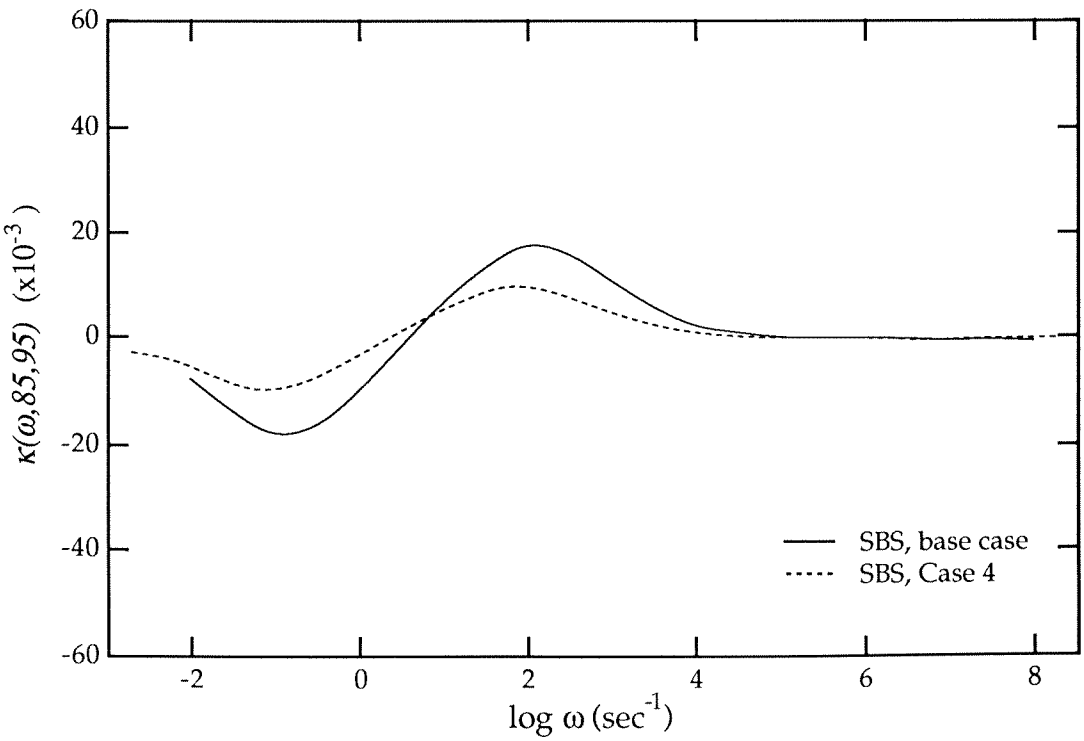

Figure 9.4d: TRC parameter, $\kappa(\omega,85,95)$, for SBS with original interlayer and interlayer with changed shift factor. Frequency values are for each temperature shifted to 85°C

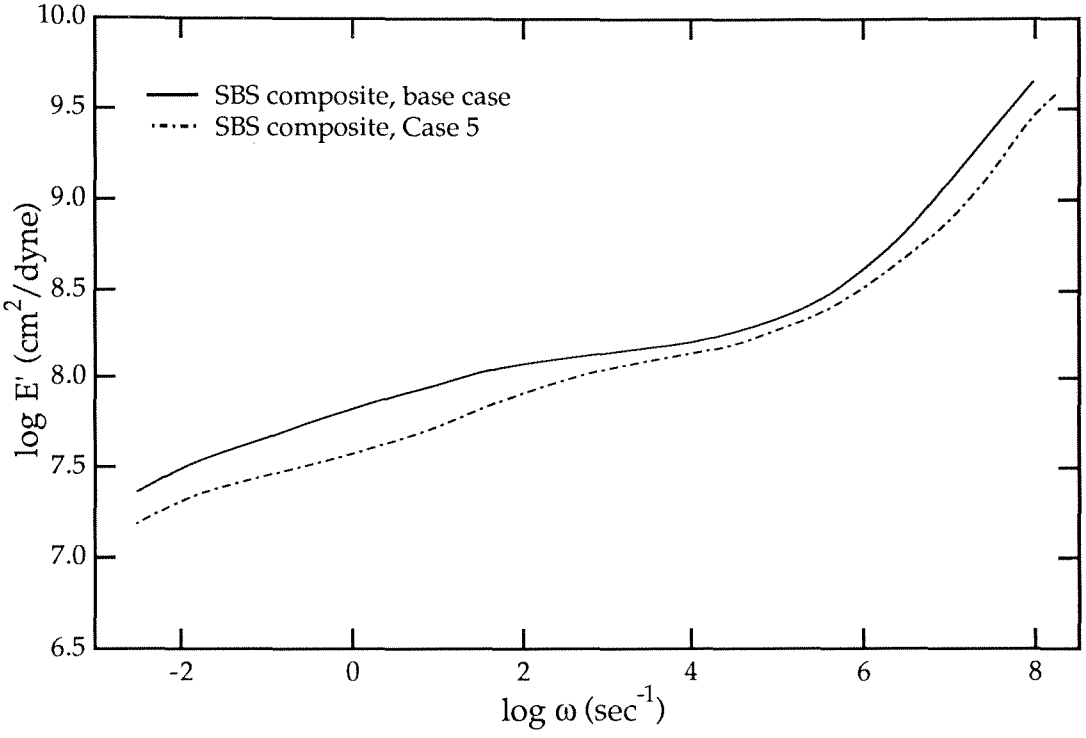

Figure 9.5a: Comparison of storage moduli for SBS with original interlayer and interlayer with lower modulus at 85°C

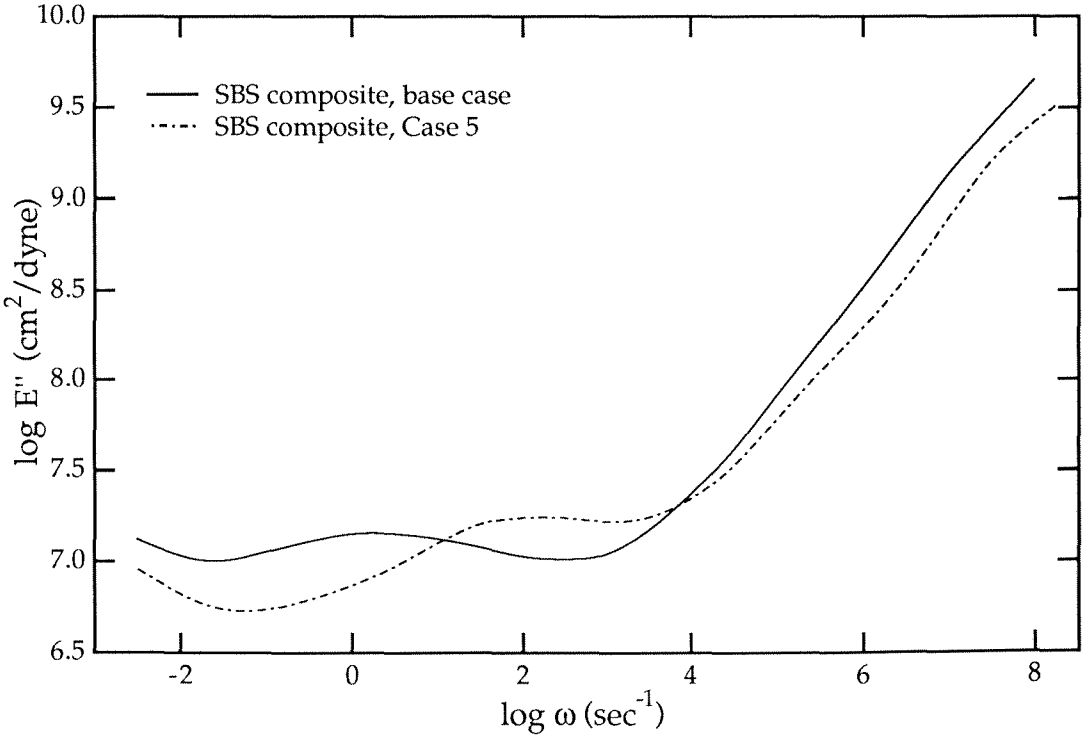

Figure 9.5b: Comparison of loss moduli for SBS with original interlayer and interlayer with lower modulus at 85°C

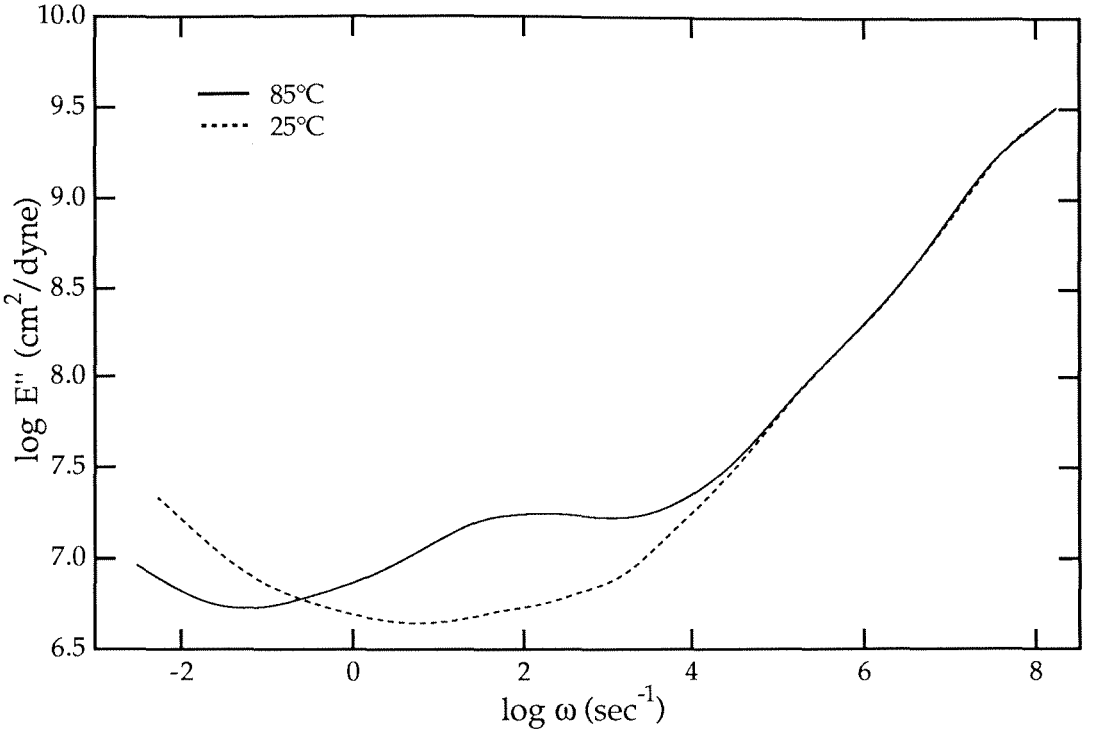

Figure 9.5c: Loss moduli of SBS composite with lower modulus interlayer, 25°C curve shifted to 85°C curve

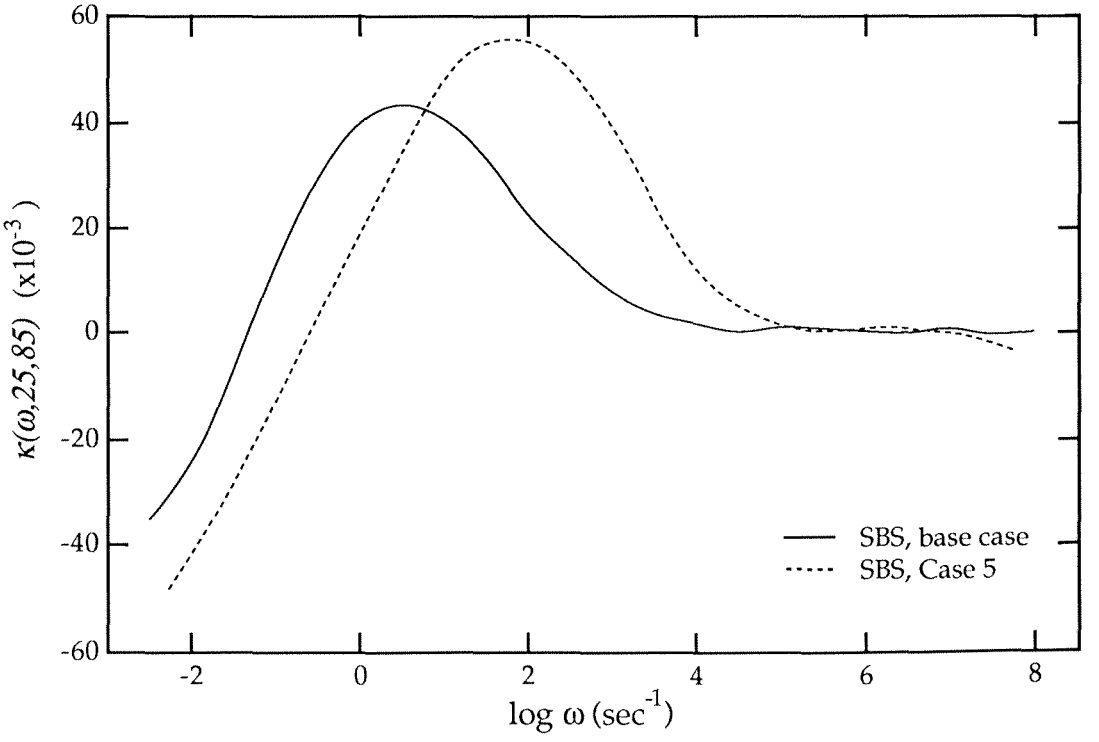

Figure 9.5d: TRC parameter, $\kappa(\omega,25,85)$, for SBS with original interlayer and interlayer with lower modulus. Frequency values are for each temperature shifted to 85°C

X. CONCLUSION

A theoretical and numerical model for examining the properties of multi-phase viscoelastic composites has been developed utilizing the correspondence principle of viscoelasticity to create an elasticity-like finite element analysis with complex variables. From the computational scheme developed, one can obtain the modulus properties of certain classes of multi-phase materials at all times and temperatures from precise knowledge of their microstructure and individual phase properties. This work has confirmed evidence of the existence, and importance to overall material properties, of a transition region between the phases for some multi-phase polymers, specifically for an SBS block copolymer. Unfortunately little is known at this time about the structure and properties of such a transition region and therefore the computational procedure developed in this paper was used to solve an inverse problem, in order to extract appropriate properties of the interlayer between the two phases.

The application of the numerical procedure to solve this inverse problem for the (tentative) characterization of the properties of one phase (interphase) of the composite, provides a new analytical tool. Other methods for estimating composite moduli reviewed in the Introduction Section (Rule of Mixtures, self-consistent modelling, composite spheres assembly, Hashin-Shtrikman bounds, Takayanagi model) do not lend themselves easily to individual phase property determination. In the SBS example used for this study (Section VII), there was insufficient experimental data available on the composite to allow a complete, definitive deduction of the properties of the unknown phase (interlayer). However, with sufficiently refined time-temperature information on the composite, it should be possible with the numer-

ical procedure presented to determine the properties and domain size of the unknown phase completely.

It should be noted again that the model of the SBS composite material with a single phase interlayer of homogeneous properties is not likely to be physically correct. However, if this model provides a reasonable representation of the physical material, then the computational scheme yields precisely accurate results within finite element accuracy. In addition the numerical method is capable of supporting any number of other physical models, for SBS or other materials, with relative ease. It is this flexibility of the tool to adapt to known aspects of material structure that makes it especially beneficial.

That it was possible to match the sense of the experimental data by modelling the transition region as an interlayer of reasonable properties is of interest in and of itself. Moreover, the results obtained are physically appropriate: The composite moduli tend to follow the behavior of the matrix material (the continuous load-bearing phase) below the glass transition temperature of the included phases. The composite begins to exhibit thermorheologically complex behavior, signified by non-shifting of isothermal modulus curves to coincide with one another, at temperatures and frequencies when the included phases (the higher T_g phases) reach their glass-to-rubber transition. These results are also consistent in both the idealized material tests and the SBS composite material tests.

From results for the simplified composite without an interphase, the effect of different inclusion sizes and the difference in behavior between soft matrix/stiff inclusions and stiff matrix/soft inclusions was studied. The compos-

ite moduli are dominated by the matrix phase except for the high frequency loss modulus, for which the soft material controls dissipation nearly independently of volume fraction and phase orientation. Also, the composite properties are affected more when the inclusions are made of the stiff rather than the soft material. Comparison with results obtained by way of Rule of Mixtures clearly shows the inadequacy of that approach to determine multi-phase viscoelastic properties reliably; also the Rule of Mixtures estimates the properties of stiff inclusions in a softer matrix much more closely than the reverse case. The presentation of results in this work was primarily for Young's modulus and the in-plane shear modulus results discussed briefly in Section V are similar, except for a slightly smaller influence of the included phase on the composite properties than for the Young's modulus results.

From experimental results on multi-phase composite moduli one cannot predict moduli at every temperature from the short term experiments performed because of the inherent thermorheologically complex behavior of the material. It has been shown that the thermorheologically complex behavior results primarily from the fact that the glass-to-rubber transitions of the various phases occur at different frequencies and different temperatures and that the TRC behavior is accelerated by the marked change in properties of the included phases as their glass transition temperatures are approached. To use the computational procedure developed in this paper to solve the inverse problem in order to determine unknown properties of one phase of the composite, the experimental measurements of the composite are crucial. For better accuracy of the fine-tuning of property parameters for the unknown phase, the example on SBS has indicated that future measurements of the dynamic properties should provide a wider frequency range than is usually studied, for

comparison in a few of the the especially important TRC regions. Of course, it would also be best to have as much direct experimental information as possible on the size and structure of the phase in question to eliminate variables from the iterative property determination scheme. Finally, one should be careful not to use this tool at very high temperatures, above the microphase separation transition (MST) for block copolymers, because eventually (for SBS at about 140°C), the polymers begin to melt and there is global mixing of the phases.[50, 51]

There are great possibilities for future work both with this computational procedure and in further experimental work as suggested here. The current model is embedded in a two-dimensional finite element code; however, it is feasible that this analysis, in particular application of the correspondence principle to a finite element code to form a complex elasticity-like problem, could be programmed into a three-dimensional finite element procedure and enable analysis of materials that cannot be broken down into two-dimensional unit cells (spherical domains, for example). It would also be possible to use stochastic procedures to obtain moduli for materials with random size and distribution of inclusions. This result could be achieved, for example, by solving the unit cell problem of a regular array of inclusions for a variety of volume fractions of inclusions in the unit cell; then, considering the global composite to be a random distribution of these unit cells, the individual results could be combined with random variable analysis to model the effective global composite moduli as a function of the moduli of all the unit cells. Using a procedure of this kind, it would be possible to investigate the global properties of polymer blends. Polymer blends tend to have microstructures containing particles of one polymer in a random size and spatial distribution

within another polymer. These materials have one particular advantage for further study with the numerical analysis procedure developed here, in that polymer blends tend to have no, or very small, interlayers between the phases.

Some multi-phase materials have regions of regularity that are packed together in a random fashion similar to grains in metals. The microstructure of each grain is geometrically the same, but the orientation with respect to global axes is different for each grain. The current computational scheme can determine the moduli for a single grain. It would be possible to model the overall moduli of these materials by performing a "global ensemble average" of a random arrangement of grains knowing the properties in the three principle directions in any one grain.[52]

As mentioned in Section VII in connection with the interlayer, it is possible to replace the simple, initial model of a single interlayer with homogeneous properties. One sensible approach would be to consider several concentric interlayer regions each of systematically different properties, the innermost interlayer having properties quite close to those of polystyrene and the outermost interlayer having properties close to those of polybutadiene. (See Figure 7.11.) Another possible arrangement to extend this idea even further would be to examine not *rings* of an interlayer, but an interlayer region in which each element is allowed independently to have slightly varying properties from those of its neighbors. The variation of properties would have to be constrained such that the properties of neighboring elements still proceeded in an orderly manner from inclusion to matrix, but would avoid the restriction of discrete bands of distinct properties. A potential problem with both of these approaches depends on the actual size of the interlayer being

modelled; if the interlayer is on the order of 40Å and the size of the monomer units of the polymers in the composite are on the order of 10Å, then splitting the interlayer up into elements 5Å across and bestowing homogeneous polymer properties on them is not realistic. In this case, one is no longer dealing with a continuum.

Throughout the analysis it has been assumed that the boundary between phases is sharp and the phases are rigidly bonded together (no slipping or separation at the interface). It is possible to extend the current numerical procedure to account for imperfect bonding at an interface within finite element analysis and this might make another interesting pursuant study.

In terms of comparison with further experimental results it would be prudent to compare the computational procedure developed in this paper to results for 1,4-SBS materials, although their non-shift is not nearly as apparent as 1,2-SBS. With detailed thermorheological moduli data on unidirectional Kevlar-epoxy systems transverse to the fiber direction, this composite would make another good comparison.

Finally, it should be mentioned here that the computational procedure developed can be used to determine solutions for many kinds of boundary value problems on viscoelastic structures. Although the emphasis in this study has been purely on extracting global moduli of specific composites, one could just as well use this technique to examine the stress and strain fields within a complicated viscoelastic structure and determine regions and magnitudes of stress concentration. This potential use could have many applications in practical engineering analysis.

REFERENCES

1. A. V. Tobolsky and R. D. Andrews, *J. Chem. Phys.* **11,** 125 (1943).
2. H. Leaderman, *Elastic and Creep Properties of Filamentous Materials and Other High Polymers.* The Textile Foundation, Washington. (1943).
3. J. D. Ferry, *J. Am. Chem. Soc.* **72,** 3746 (1950).
4. J. D. Ferry, *Viscoelastic Properties of Polymers, 3rd Edition.* John Wiley and Sons, Inc., New York. 3rd Edition, 641pp. (1980).
5. F. W. J. Billmeyer, *Textbook of Polymer Science.* Interscience Publishers, a Division of John Wiley & Sons, Inc., New York. 601pp.pp. (1966).
6. D. J. Plazeck and V. M. O'Rourke, Viscoelastic behavior of low molecular weight polystyrene. *J. Polym Sci.: Part A-2,* **9,** 209-243 (1971).
7. Z. Hashin, Analysis of composite materials—A survey. *J. Applied Mech.* **50,** 481-505 (1983).
8. B. D. Agarwal and L. J. Broutman, *Analysis and Performance of Fiber Composites.* John Wiley & Sons, New York. 355pp. (1980).
9. R. Hill, A self-consistent mechanics of composites materials. *J. Mech. Phys. Solids* **13,** 213-222 (1965).
10. R. M. Christensen and K. H. Lo, Solutions for effective shear properties in three phase sphere and cylinder models. *J. Mech. Phys. Solids* **27,** 315-330 (1979).
11. J. D. Eshelby, The determination of the elastic field of an ellipsiodal inclusion, and related problems. *Proc. Royal Soc. London* **A:241,** 376-396 (1957).
12. Z. Hashin, Complex moduli of viscoelastic composites—I. General theory and application to particulate composites. *Int. J. Solids Structures* **6,** 539-552 (1970).
13. Z. Hashin, The elastic moduli of heterogeneous materials. *J. Appl. Mechanics* **29,** 143-150 (1962).
14. Z. Hashin and S. Shtrikman, A variational approach to the theory of the elastic behaviour of multiphase materials. *J. Mech. Phys. Solids* **11,** 127-140 (1963).
15. T. Horino, Y. Ogawa, T. Soen and H. Kawai, Tensile stress relaxation behavior of a mechanical mixture of two polymer components. *J. Appl. Polymer Sci.* **9,** 2261-2272 (1965).
16. A. Eisenburg and M. Navratil, Time-temperature superposition in styrene-based ionomers. *J. Polymer Sci.: Polymer Letters* **10,** 537-542 (1972).
17. D. G. Fesko and N. W. Tschoegl, Time-temperature superposition in styrene/butadiene/styrene block copolymers. *Intern. J. Polymeric Mater.* **3,** 51-79 (1974).
18. R. E. Cohen and N. W. Tschoegl, Comparison of the dynamic mechanical properties of two styrene-butadiene-styrene triblock copolymers with 1,2- and 1,4- polybutadiene center blocks. *Trans. Soc. Rheology* **20:1,** 153-169 (1976).

19. J. W. C. Child and J. D. Ferry, *J. Colloid Sci.* (1957).
20. D. G. Fesko and N. W. Tschoegl, Time-temperature superposition in thermorheologically complex materials. *J. Polymer Sci.: Part C* **35,** 51-69 (1971).
21. J. M. Caruthers and R. E. Cohen, Consequences of thermorheological complexity in viscoelastic materials. *Rheol. Acta* **19,** 606-613 (1980).
22. T. L. Cost, Approximate Laplace transform inversions in viscoelastic stress analysis. *AIAA Journal* **2:12,** 2157-2166 (1964).
23. Taylor, *FEAP—Finite Element Analysis Program.* University of California at Berkeley, (1982).
24. W. C. Zin and R. J. Roe, *Phase equilibria and transition in mixtures of a homopolymer and a block copolymer I. Small angle x-ray scattering study.* Office of Naval Research, Technical Report #8, task # NR356-655 (March 1983).
25. D. J. Meier, A theory of the interface in block copolymers. *Polym. Prepr., Am. Chem. Soc.* **15:1,** 171-176 (1974).
26. D. H. Kaelble, Interfacial morphology and mechanical properties of A-B-A triblock copolymers. *Trans. Soc. Rheol.* **15:2,** 235-260 (1971).
27. A. Todo, T. Hashimoto and H. Kawai, Small angle x-ray scattering from block copolymers as an ideal model system for a pseudo two-phase solid texture. *J. Appl. Chryst.* **11,** 558-563 (1978).
28. C. Jones Kiely, C.J., Wang, S.S., The Characterization of an SCS6/TI-6AL-4V MMC Interphase. *J. Materials Research* **4,** 327-335 (1989).
29. J. D. Achenbach and H. Zhu, Effect of interfacial zone on mechanical behavior and failure of fiber-reinforced composites. *J. Mech. Phys. Solids* **37,** 381-393 (1989).
30. G. C. Papanicolaou, G. J. Messinis and S. S. Karakatsanidis, The effect of interfacial conditions on the elastic-longitudinal modulus of fibre reinforced composites. *J. Mater. Sci.* **24,** 395-401 (1989).
31. J. Diamont, M. C. Williams and D. S. Soane, Microstructural diagnosis of block copolymer nonlinear mechanical properties. I. Uniaxial stress/strain. *Polym. Engr. Sci.* **28,** 207-220 (1988).
32. Y. C. Fung, *Foundations of Solid Mechanics.* Prentice-Hall, Inc., Englewood Cliffs, N. J. 525pp. (1965).
33. R. M. Christensen, *Theory of Viscoelasticity: An Introduction.* Academic Press, New York. 245pp. (1971).
34. O. C. Zienkiewicz, *The Finite Element Method.* McGraw Hill, London. Third Edition, 787pp. (1977).
35. J. N. Reddy, *An Introduction to the Finite Element Method.* McGraw-Hill Book Co., New York. (1984).
36. M. E. Gurtin and E. Sternberg, On the linear theory of viscoelasticity. *Arch. Rational Mech. Anal.* **11,** 291-356 (1962).
37. J. C. Nagtegaal, D. M. Parks and J. R. Rice, On numerically accurate finite element solutions in the fully plastic range. *Comp. Meths. Appl. Mech. Eng.* **4,** 153-177 (1974).

38. J. R. Rice, R. M. McMeeking, D. M. Parks and E. P. Sorensen, Recent finite element studies in placiticity and fracture mechanics. *Comp. Meths. Appl. Mech. Eng* **17/18,** 411-442 (1979).
39. R. D. Deanin, A. A. Deanin and T. Sjoblom, Practical Properties of Multi-Phase Polymer Systems. *Polym. Sci. Technol.* **4,** 63-91 (1974).
40. J. Dlugosz, A. Keller and E. Pedemonte, Electron microscope evidence of a macroscopic 'single crystal' from a three block coploymer. *Kolloid-Z. u. Z. Polymere* **242,** 1125-1130 (1970).
41. A. S. Argon, R. E. Cohen, O. S. Gebizlioglu and C. E. Schwier, Crazing in block copolymers and blends. *Advances in Polym. Sci.* **52,** 275-332 (1983).
42. K. C. Rusch, Time-temperature superposition and relaxational behavior in polymeric glasses. *J. Macromol. Sci.-Phys.* **B2:2,** 179-204 (1968).
43. J. F. Sanders, J. D. Ferry and R. H. Valentine, Viscoelastic properties of 1,2-polybutadiene—comparison with natural rubber and other elastomers. *J. Polymer Sci. Part A-2* **6,** 967-980 (1968).
44. R. G. C. Arridge and M. J. Folkes, The mechanical properties of a 'single crystal' of SBS copolymer—a novel composite material. *J. Phys. D: Appl. Phys.* **5,** 344-358 (1972).
45. E. Helfand, Block copolymer theory. III. Statistical mechanics of the microdomain structure. *Macromolocules* **8,** 552-556 (1975).
46. H. Hashimoto, M. Fujimura, T. Hashimoto and H. Kawai, Domain-boundary structure of styrene-isoprene block copolymer films cast from solutions. 7. Quantitative studies of solubilization of homopolymers in spherical domain systems. *Macromolocules* **14,** 844-851 (1981).
47. T. Hashimoto, A. Todo, H. Itoi and H. Kawai, Domain-boundary structure of styrene-isoprene block copolymer films cast from solutions. 2. Quantitative estimation of the interfacial thickness of lamellar microphase systems. *Macromolocules* **10:2,** 377-384 (1976).
48. G. Kraus and K. W. Rollmann, Dynamic viscoelastic behavior of ABA block copolymers and the nature of the domain boundary. *J. Polym. Sci.: Polym. Physics Edition* **14,** 1133-1148 (1976).
49. R. E. Cohen, *Dynamic mechanical properties of block copolymer blends — A study of the effect of terminal chains in elastomeric materials.* PhD Thesis, Caltech, (1972).
50. E. V. Gouinlock and R. S. Porter, Linear dynamic mechanical properties of an SBS block copolymer. *Polym. Engr. Sci.* **17:8,** 535-543 (1977).
51. F. S. Bates, Block copolymers near the microphase separation transition. 2. Linear dynamic mechanical properties. *Macromolocules* **17,** 2607-2613 (1984).
52. J. Sax and J. M. Ottino, Modeling of transport of small molecules in polymer blends: application of effective medium theory. *Polym. Eng. Sci.* **23:3,** 165-176 (1983).

APPENDIX: SIMPLE CHECKS ON PROCEDURE

Numerous checks were performed on the devised numerical procedure to ensure that all necessary changes had been made and that the code was indeed producing correct solutions. Two of the checks will be mentioned here. Both of these cases are simple enough that exact analytical solutions can be found and compared to the numerical results.

The first case covers the time dependent stress and strain field in a homogeneous rod of viscoelastic material subjected to unidirectional oscillatory displacement boundary conditions. The finite element model is a single element of the material subjected to a sinusoidal displacement boundary condition on one face. The time dependent response of the material is found by looping the program over time. Given a rod of viscoelastic material with the Young's modulus function expressed in a Prony series

$$E(t) = E_\infty + \sum_{j=1}^{N} E_j e^{-t/\xi_j} \tag{3.27}$$

subjected to uniaxial displacement at its ends

$$u_2(t) = u_0 sin(\omega t), \tag{3.28}$$

which in turn determines the homogeneous strain in the rod

$$\varepsilon_2(t) = \varepsilon_0 sin(\omega t), \tag{3.29}$$

the constitutive law can be used to determine the stress state in the rod

$$\sigma_2(t) = \int_{-\infty}^{t} E(t-\tau)\frac{d\varepsilon_2(t)}{d\tau}d\tau \tag{3.30}$$

The resulting homogeneous stress state upon substitution of (3.27) and (3.29) into (3.30) is found to be

$$\sigma_2(t) = \varepsilon_0 \sum_{j=1}^{N} \frac{E_j \omega}{\frac{1}{\xi_j^2} + \omega^2} [\frac{1}{\xi_j} cos(\omega t) + \omega sin(\omega t) - \frac{1}{\xi_j} e^{-t/\xi_j}] + E_\infty \varepsilon_0 sin(\omega t) \quad (3.31)$$

The finite element model of this simple problem, in the form of a single element, was run with the modified FEAP code in the axisymmetric mode and the results of the stress state over time were compared to the analytical results. If the transient term is neglected in the analytical solution, or after the initial cycles required for the transient term to die out, the results from the code are identical to the analytical results. This problem was also solved analytically using the correspondence principle, and those results match exactly the results of the program runs at all times.

The second check described here considers a rod composed of two different viscoelastic materials. One half of the rod is material A and the other half, perfectly bonded to the first half, is material B. This situation and the boundary conditions imposed are shown in Figure 3.3; oscillatory displacements $u_0 e^{i\omega t}$ were applied in the y-direction, perpendicular to the interface of the materials, and the vertical sides of the rod are completely constrained in the x-direction. This problem was solved analytically using the correspondence principle for the stress and strain states in materials A and B. Again, when the finite element model of this problem was solved using the modified FEAP code, the solutions obtained matched the analytical results exactly within plotting accuracy.

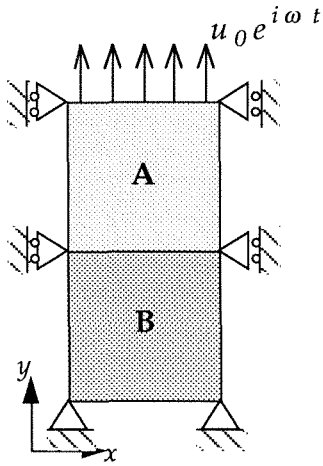

Figure 3.3: Simple example containing two materials for checking code.

One other very simple check on the procedure for obtaining $\bar{E}(\omega)$ was to examine an inclusion problem mesh, but where all of the elements possessed the same material properties. Then the boundary value problem (equation 3.25) was solved for this homogeneous unit cell by the same procedure described in Section III. For a single material, given the shear modulus and the bulk modulus, the Young's modulus was also determined analytically and checked with this numerical result.